



저작자표시-비영리-변경금지 2.0 대한민국

이용자는 아래의 조건을 따르는 경우에 한하여 자유롭게

- 이 저작물을 복제, 배포, 전송, 전시, 공연 및 방송할 수 있습니다.

다음과 같은 조건을 따라야 합니다:



저작자표시. 귀하는 원저작자를 표시하여야 합니다.



비영리. 귀하는 이 저작물을 영리 목적으로 이용할 수 없습니다.



변경금지. 귀하는 이 저작물을 개작, 변형 또는 가공할 수 없습니다.

- 귀하는, 이 저작물의 재이용이나 배포의 경우, 이 저작물에 적용된 이용허락조건을 명확하게 나타내어야 합니다.
- 저작권자로부터 별도의 허가를 받으면 이러한 조건들은 적용되지 않습니다.

저작권법에 따른 이용자의 권리는 위의 내용에 의하여 영향을 받지 않습니다.

이것은 [이용허락규약\(Legal Code\)](#)을 이해하기 쉽게 요약한 것입니다.

[Disclaimer](#)

공학박사학위논문

**기구학적 특성과 컴플라이언스 특성을
동시에 고려한 기구 위상 및 형상 통합
최적설계**

**Unified Topology and Shape Optimization of Linkage
Mechanisms Simultaneously Considering Kinematic
and Compliance Characteristics**

2020년 8월

서울대학교 대학원

기계항공공학부

한 상 민

기구학적 특성과 컴플라이언스 특성을 동시에 고려한 기구 위상 및 형상 통합 최적설계

Unified Topology and Shape Optimization of Linkage
Mechanisms Simultaneously Considering Kinematic
and Compliance Characteristics

지도교수 김 윤 영

이 논문을 공학박사 학위논문으로 제출함


2020 년 4 월


서울대학교 대학원
기계항공공학부
한 상 민


한상민의 공학박사 학위论문을 인준함


2020 년 6 월

위 원 장 : 박 종 우 

부위원장 : 김 윤 영 

위 원 : 윤 병 동 

위 원 : 김 도 년 

위 원 : 장 강 원 

ABSTRACT

Unified Topology and Shape Optimization of Linkage Mechanisms Simultaneously Considering Kinematic and Compliance Characteristics

Sangmin Han

School of Mechanical and Aerospace Engineering

The Graduate School

Seoul National University

Mechanism synthesis based on topology optimization has recently received much attention as an efficient design approach. The main thrust behind this trend is the capability of this method to determine automatically the topology and dimensions of linkage mechanisms. Towards this direction, there have been many investigations, but they have thus far focused mainly on mechanism synthesis considering kinematic characteristics describing a desired path or motion.

Here, we propose a new topology optimization method that synthesizes a linkage mechanism considering not only kinematic but also compliance (K&C) characteristics simultaneously, as compliance characteristics can also significantly affect the linkage mechanism performance; compliance characteristics dictate how

elastic components, such as bushings in a vehicle suspension, are deformed by external forces. To achieve our objective, we use the spring-connected rigid block model (SBM) developed earlier for mechanism synthesis considering only kinematic characteristics, but we make it suitable for the simultaneous consideration of K&C characteristics during mechanism synthesis by making its zero-length springs multifunctional. Variable-stiffness springs were used to identify the mechanism kinematic configuration only, but now in the proposed approach, they serve to determine not only the mechanism kinematic configuration but also the compliance element distribution. In particular, the ground-anchoring springs used to anchor a linkage mechanism to the ground are functionalized to simulate actual bushings as well as to identify the desired linkage kinematic chain.

After the proposed formulation and numerical implementation are presented, three case studies to synthesize planar linkage mechanisms were considered. Through these case studies, we verified the validation of the proposed approach and proved that the proposed methodology could solve problems when existing methods could not. After the effectiveness of the proposed method is demonstrated with a simplified two-dimensional vehicle suspension design problem, the proposed methodology is applied to design a three-dimensional suspension. To deal with three-dimensional mechanisms, a spatial SBM is newly developed because only planar SBMs have been developed. Furthermore, a set of design variables which can vary bushing stiffness are newly introduced. Using the proposed method, it was possible to

successfully synthesize two types of suspension mechanisms which have similar kinematic characteristics to each other but different compliance characteristics. By using the proposed method simultaneously considering kinematic and compliance characteristics, a unique suspension mechanism having an integral module which is known to improve R&H performances was synthesized.

In this study, although applications were made only to the design of vehicle suspensions, other practical design problems for which K&C characteristics must be considered simultaneously can be also effectively solved by the proposed approach. This study is expected to pave the way to advance the topology optimization method for general linkage mechanisms considering kinematic characteristics but also the other characteristics such as force-related characteristics.

**Keywords: Topology Optimization, Rigid-body Linkage Mechanism,
Kinematic Characteristics, Compliance Characteristics**

Student Number: 2013-23838

CONTENTS

ABSTRACT	i
CONTENTS.....	iv
LIST OF TABLES.....	viii
LIST OF FIGURES.....	ix
CHAPTER 1. Introduction.....	1
1.1 Motivation and related literatures	1
1.2 Research objectives	6
1.3 Background research	8
1.3.1 Linkage mechanism synthesis based on the spring-connected rigid block model (SBM)	8
1.3.2 Determination of the system's degree-of-freedom (DOF) based on the work transmittance efficiency function	10
1.4 Outline of thesis	12
CHAPTER 2. Unified topology and shape optimization method for the mechanism synthesis simultaneously considering kinematic and compliance (K&C) characteristics.....	18
2.1 Overview	18
2.2 Modeling and analysis.....	23
2.2.1 Modeling	23
2.2.2 Kinematic and compliance analyses with the SBM	26

2.3 Optimization Formulation	33
2.3.1 Design variable and interpolation.....	33
2.3.2 Objective and constraint functions	35
2.3.3 Sensitivity analysis	39
2.4 Case studies	43
2.4.1 Case study 1 - Validation of the proposed method	43
2.4.2 Case study 2 - Demonstration of the advantage of the proposed method.....	46
2.4.3 Case study 3 - Application to the design of a 2D vehicle suspension	50
2.5 Summary	57

**CHAPTER 3. Design of vehicle suspensions for rear using topology
optimization method considering K&C characteristics.....78**

3.1 Overview	78
3.2 Modeling and analysis based on the spatial SBM.....	81
3.2.1 The spatial SBM for the design of a vehicle suspension.....	81
3.2.2 Kinematic and compliance analyses by the spatial SBM.....	83
3.3 Optimization Formulation	90
3.3.1 Design variable and interpolation.....	90
3.3.2 Objective and constraint functions	93
3.3.3 Sensitivity analysis	95
3.4 Design of vehicle suspensions for rear using the proposed method.....	99

3.4.1 Definition of problem.....	99
3.4.2 Design Case 1 - Recovery of a double wishbone suspension	101
3.4.3 Design Case 2 - Suspension synthesis for improving ride and handling (R&H) performances.....	104
3.5 Summary	110
CHAPTER 4. Conclusions.....	133
APPENDIX A. Target cascading process for deriving K&C characteristics of a suspension to improve vehicle's R&H performances	138
A.1 Overview	138
A.2 Ride and handling (R&H) performances.....	139
A.3 Analysis procedure to evaluate R&H performances using a double wishbone suspension	140
A.4 Design optimization of a double wishbone suspension for deriving K&C characteristics to improve R&H performances	141
A.4.1 Design variable and interpolation.....	141
A.4.2 Metamodeling.....	142
A.4.3 Optimization formulation	144
A.4.4 Optimization result	145
APPENDIX B. Technique to suppress floating blocks.....	158
B.1 Overview	158
B.2 Explanation of techniques to suppress floating blocks.....	159
B.3 Revisit Case study 3 for applying the technique to suppress floating	

blocks	161
APPENDIX C. Investigation of mesh dependency issue.....	167
C.1 Overview	167
C.2 Re-consideration of Case study 1 with the more number of rigid blocks	168
REFERENCES.....	172
ABSTRACT (KOREAN).....	181
ACKNOWLEDTEMENTS.....	184

LIST OF TABLES

Table 2.1 Data of the eighteen points for target motion at the wheel center	59
Table 3.1 Values of the kinematic constraint functions at convergence for Design Case 1	112
Table 3.2 Values of the compliance constraint functions at convergence for Design Case 1	113
Table 3.3 Values of the kinematic constraint functions at convergence for Design Case 2	114
Table 3.4 Comparison between compliance characteristic values of the result suspension in Design Case 2 and the target values	115
Table A.1 R&H performance index used in this research.....	147
Table A.2 Explanation of objectives used for the optimization	148
Table A.3 Compliance characteristics of the initial and optimized layout.....	149

LIST OF FIGURES

Fig. 1.1 Overview of topology optimization of linkage mechanisms for generating the target path based on the SBM. (a) Problem definition and (b) the ground model using the SBM.....	14
Fig. 1.2 Representation of the connectivities depending on the spring stiffness. (a) Disconnected, (b) connected by a revolute joint, (c) rigidly-connected, and (d) rigidly-connected two blocks connected by an anchored revolute joint	15
Fig. 1.3 A four-bar mechanisms represented by a SBM	16
Fig. 1.4 Illustration of linkage mechanisms which have (a) DOF = 2, (b) DOF = 0, and (c) DOF = 1, respectively	17
Fig. 2.1 Example of a design process using the proposed method: (a) problem definition for a 2D vehicle suspension, (b) modeling with the SBM, and (c) layout of the SBM after optimization and the corresponding equivalent linkage mechanism	60
Fig. 2.2 The design domain discretized by 2x1 blocks connected by block-connecting and anchoring springs. The multi-functionality of the springs in the proposed method is compared with the mono-functionality in the existing method	61
Fig. 2.3 Representative cases with upper or lower bound stiffness values. Case A: disconnected, Case B: Connected by a revolute joint, Case C: Rigidly connected, and Case D: Hinged with a bushing.....	62
Fig. 2.4 A snapshot of two rigid blocks in a position after being moved by a given	

input motion or external force	63
Fig. 2.5 An example to validate the compliance analysis using the SBM with the suggested spring stiffness values: (a) linkage geometry and loading/boundary conditions, and (b) comparison of the analyses using the SBM model (left) and the original model with the ADAMS software package (right)	64
Fig. 2.6 Flow chart for topology optimization of linkage mechanisms simultaneously considering kinematic and compliance characteristics	65
Fig. 2.7 (a) Layout of the reference linkage mechanism for Case study 1 and (b) illustrations of the K&C characteristics used for the mechanism synthesis.....	66
Fig. 2.8 SBM to solve Case study 1: (a) design domain discretized by rigid blocks at the initial configuration and (b) illustration of how to prescribe the desired conditions using the SBM for the K&C analyses	67
Fig. 2.9 Optimization results for Case study 1: (a) final optimized layout of the SBM (left) and its equivalent mechanism (right), (b) design variables controlling the block-connecting spring stiffnesses at convergence, (c) design variables controlling the anchoring spring stiffnesses at convergence, and (d) iteration histories of the objective and the constraint functions	68
Fig. 2.10 (a) Layout of the reference linkage mechanism for Case study 2 and (b) analysis conditions for the K&C characteristics	69
Fig. 2.11 SBM to solve Case study 2: (a) design domain discretized by rigid blocks at its initial configuration and (b) illustration of the method used to prescribe the desired conditions using the SBM for K&C analyses	70

Fig. 2.12 Optimization results for Case study 2 obtained by the two-step sequential formulation (2.26) for the initial values for topology-controlling design variables ($\xi_{b_i}^T, \xi_{a_j}^T$) set to (a) 0.1 and (b) 0.5.....	71
Fig. 2.13 Optimization results for Case study 2 obtained by the proposed simultaneous formulation (2.21) for the initial values of topology-controlling design variables ($\xi_{b_i}^T, \xi_{a_j}^T$) set to (a) 0.1 and (b) 0.5	72
Fig. 2.14 Problem definition for Case study 3 dealing with the synthesis of a 2D vehicle suspension: (a) analysis domain discretized by rigid blocks where the leftmost 5×2 rigid blocks are used to synthesize linkages (the rightmost 5×1 rigid blocks represent a wheel carrier), and (b) sketches explaining how to evaluate the target K&C characteristics	73
Fig. 2.15 Optimization results for the 2D vehicle suspension design problem: (a) final optimized layout (thick lines represent the synthesized links), (b) identified linkage mechanism (right) from the optimized layout expressed by rigid blocks connected by block-connecting and anchoring springs having a lower bound stiffness value, (c) converged values of the design variables for block-connecting springs, and (d) converged values of design variables of the anchoring springs.....	74
Fig. 2.16 Iteration histories for Case study 3: (a) the mean value of the work transmittance efficiency function, (b) kinematic constraint functions, and (c) compliance constraint functions.....	75
Fig. 2.17 Intermediate and final layouts at different time steps of the synthesized linkage mechanism for the 2D vehicle suspension	76

Fig. 2.18 Comparison of the optimization results for Case study 3 obtained by the two-step sequential formulation (2.26) using the same initial values of the design variables	77
Fig. 3.1 Analysis conditions to define K&C characteristics of a vehicle suspension. (a) Wheel bump/rebound motion for kinematic characteristics, (b) lateral force for compliance characteristics, (c) longitudinal force for compliance characteristics, and (d) alinging moment for compliance characteristics	116
Fig. 3.2 Illustrations of the models used for topology optimization of linkage mechanisms. (a) The nonlinear bar based model and (b) the SBM.....	117
Fig. 3.3 Modeling with the spatial SBM for designing a vehicle suspension	118
Fig. 3.4 Explanation about spring connection of the two blocks connecting between chassis and wheel carrier.....	119
Fig. 3.5 Representative cases with upper or lower bound stiffness vlaues in a compliance analysis. Case A: disconnected, Case B: Connected by a spherical joint, Case C: Connected by a revolute joint, Case D: Rigdly connected, and Case E: Hinged with a bushing	120
Fig. 3.6 A snapshot of two rigid blocks in a moved position by a given input motion or an external force.....	121
Fig. 3.7 Spring stiffness for a cylindrical bushing	122
Fig. 3.8 Flow chart for topology optimization of vehicle suspensions considering both kinematic and compliance characteristics	123
Fig. 3.9 Problem definition for suspension linkage synthesis. (a) Design domain and	

the employed SBM, (b) analysis conditions for kinematic characteristic, and analysis conditions for compliance characteristics by (c) a lateral force, (d) a longitudinal force, and (e) an aligning moment 124

Fig. 3.10 Final optimization layout of the spatial SBM (left) and its equivalent linkage mechanism (right) for Design Case 1 125

Fig. 3.11 Design variables at convergence for Design Case 1: (a) topology controlling design variables related to the block-connecting springs, (b) topology controlling design variables related to the anchoring springs, (c) bushing stiffness design variables (the red bars indicates the design variables for bushing stiffness related to the mounting points to the chassis), and (d) shape design variables 126

Fig. 3.12 Convergence histories of Design Case 1: (a) objective, (b) kinematic constraints related to the displacement error, (c) kinematic constraints related to the angular error, (d) compliance constraints by a lateral force, (e) compliance constraints by a longitudinal force, and (f) compliance constraints by an aligning moment..... 127

Fig. 3.13 Comparison the K&C characteristics obtained from the SBM and ADAMS software to verify the validity of the proposed method using the result of Design Case 1. (a) The result suspension model using ADAMS software, (b) the comparison of kinematic curves, and (c) the comparison of compliance characteristic values 128

Fig. 3.14 Final optimization layout of the spatial SBM (left) and its equivalent linkage mechanism (right) for Design Case 2 129

Fig. 3.15 Design variables at convergence for Design Case 2: (a) topology

controlling design variables related to the block-connecting springs, (b) topology controlling design variables related to the anchoring springs, (c) bushing stiffness design variables (the red bars indicates the design variables for bushign stiffness related to the mounting points to the chassis), and (d) shape design variables130

Fig. 3.16 Identified the topology of the result linkage mechanism for Design Case 2 (left) from the optimized layout expressed by rigid blocks connected by the block-connecting and anchoring springs having the maximum stiffness value (right). (In this figure, the block is illustrated as the initial shape of them to decern easily.) .131

Fig. 3.17 Illustrations of suspension topology. (a) Double wishbone suspension, (b) integral link suspension, (c) the result suspension of Design Case 2 132

Fig. A.1 Sample graphs of full-car simulations considering in this research: (a) step steer, (b) double-lane change, (c) steady-circle simulation, and (d) rough road simulation 150

Fig. A.2 The overall analysis procedure automatically evaluating R&H performances from a configuration of a double wishbone suspension 151

Fig. A.3 The information for initial configuration of a double wishbone suspension to be used (P: bushing stiffness for radial direction, Q: bushing stiffness for the axial direction) 152

Fig. A.4 The comparison of analysis results when using a metamodel and using a simulation model (The function numbers denote the performance indices from 1 to 10 in Table A.1, respectively)..... 153

Fig. A.5 The result of correlation analysis between handling performance index

values using the data points obtained from OLHD: (a) The result sorting by the function number and (b) the result after rearranging with similar correlations	154
Fig. A.6 Pareto-optimal set obtained from the optimization problem in Appendix A. The Pareto-optimal set is plotted by two objective domain.	155
Fig. A.7 Rador chart for comparing the values of R&H performance index from the initial layout and optimized layout.....	156
Fig. A.8 Comparison of knematic curves obtained from the initial layout and optimized layout.....	157
Fig. B.1 Illustration of floating blocks existing in the result of Case study 3.....	164
Fig. B.2 Optimization results for the 2D vehicle suspension design problem with the technique of suppressing floating blocks: (a) final optimized layout (thick lines represent the synthesized links), (b) identified linkage mechanism (right) from the optimized layout expressed by rigid blocks connected by block-connecting and anchoring springs having a lower bound stiffness value, (c) converged values of the design variables for block-connecting springs, and (d) converged values of design variables of the anchoring springs.....	165
Fig. B.3 Iteration histories for Case study 3 with the technique of suppressing floating blocks: (a) the mean value of the work transmittance efficiency function, (b) kinematic constraint functions, and (c) compliance constraint functions	166
Fig. C.1 Problem definition for re-considering Case study 1 with (a) 5 by 5 rigid blocks and (b) 11 by 11 rigid blocks	170
Fig. C.2 Optimization results for re-considering Case study 1 with (a) 5 by 5 rigid	

blocks and (b) 11 by 11 rigid blocks	171
--	-----

CHAPTER 1.

Introduction

1.1 Motivation and related literatures

In a machine, mechanisms are used to convert a given driving force to the desired output motion and force. Linkage mechanisms are the mechanisms in which all the components are combined to form a closed chain, and they have been applied to many industrial applications where repetitive works are required such as vehicle suspensions, morphing mechanisms of airfoils, lifts and so on. Even though many linkage mechanism applications are replaced by robot systems, but they are still of great importance because of the advantages of simplicity, lightweight, and using fewer actuators compared to robot systems.

For the linkage mechanism design, there are mainly two types of conditions to be considered. The first is the conditions related to kinematic characteristics. Path generation and motion generation, which are the main problems of mechanism synthesis, fall into this type, and mechanical gain and transmission angle are also included. The other is the conditions related to the force. During linkage mechanisms

are working, external loads can be often applied to the mechanisms or inertial forces can be generated to the system. The conditions related to the force are such as minimizing the force acting on the components or minimizing input torque to generate the desired output force and so on.

Compliance characteristics dealt with in this thesis denote the change of mechanisms due to the deformation of elastic elements such as springs or bushings when external forces are applied, and they are one of the representative characteristics related to a force. A representative industrial application considering compliance characteristics is a vehicle suspension. Bushings are usually used to connect the vehicle chassis and suspension links in order to reduce the noise, vibration, and harshness (NVH), and external forces such as cornering forces or braking forces make the bushings deformed. Therefore, for good ride and handling (R&H) performances, the vehicle suspensions should be designed considering compliance characteristics such as these deformations as well as kinematic characteristics.

Traditionally, the design process of linkage mechanisms can be divided into two stages. The first is about concept design. In order to synthesize a linkage mechanism, the topology such as type and number should be determined. This process is usually carried out by the intuition of the engineer since no systematic method exists. After defining the topology of linkage mechanisms, the detailed design should be needed at the second stage. In the detailed design process, things such as the dimensions of

the links or bushing stiffness are defined to satisfy the desired design conditions. If failed to satisfy the design conditions in the detailed design stage, the engineer should start over from the first, to choose the topology of mechanism.

To avoid this iterative, time-consuming, and trial-error based design process, automatic synthesis method for linkage mechanisms have been researched since the early 2000s based on topology optimization method. The basic concept of this method is to find the topology of linkage mechanisms as well as the detailed design using the optimization method. In other words, the topology and shape of the linkage mechanisms which can satisfy the given design conditions are defined automatically by the optimization algorithm. The concept of mechanism synthesis based on topology optimization methodology was firstly implemented by Felter [1]. Then, Kawamoto and his colleagues [2-4] were succeeded in synthesizing non-Grashof type planar linkages which generated short-path based on a nonlinear bar based ground structure model, and also proposed the formulation for degree-of-freedom (DOF). The results that Kawamoto et al. were shown were the possibility to synthesize linkage mechanisms by using the gradient-based optimization because the DOF expression they proposed were able to be differentiable. After then, there have been some successful researches based on a nonlinear bar based model such as to synthesize large motion mechanism [5], to synthesize linkage mechanisms both the topology and geometry using two-stage optimization approach [6], and to synthesize practical linkage mechanisms like vehicle steering system [7] and suspensions [8].

Especially, the work transmittance function presented in [7] to deal with the DOF issue made it possible to be able to determine the DOF of the system by the ratio of the input and output energy.

In addition to the nonlinear bar based model, there have been many studies using the spring-connected rigid blocks. The concept of the spring-connected rigid block model (SBM) was firstly presented by Kim et al. [9]. In the SBM, the connectivity among the blocks is defined through the stiffness of the zero-length springs connecting the blocks, and the connectivity of the blocks can represent the linkage mechanisms. Nam et al. [10] dealt with numerical issues that could occur in the SBM and suggested some remedies. Then, the extended version of the SBM which can deal with more general joints such as prismatic or pin-in-slot was proposed in [11] because the earlier version was only able to represent revolute joints, and it was developed to be able to synthesize a finger rehabilitation robot device [12]. The SBM was developed to be able to deal with gear elements as well as links using additional design space consisted of gear blocks [13]. In addition to the improvement of the modeling, Fourier-based formulation for solving path generation without prescribed timing was proposed in [14], and linkage mechanism which can generate the human's gait trajectory path was successfully synthesized by Fourier-based formulation and by simultaneous topology and shape synthesis [15].

Besides the SBM, another modeling using rigid blocks were also presented in [16-

18], and another interesting approach for topology optimization of linkage mechanisms were also presented [19-23].

Although many studies about the automatic synthesis of linkage mechanisms have been researched so far, there is a limitation that only kinematic conditions such as path generation or motion generation have been dealt with in the previous studies. As mentioned in the beginning, there are other types of conditions to be considered when designing mechanisms as well as kinematic conditions. Therefore, even though linkage mechanisms are synthesized with the existing method for automatic synthesis, there should be an additional design process in order to consider the conditions related to a force. What if the mechanisms synthesized by the existing automatic synthesis method cannot satisfy the conditions related to the force at the additional design process? If so, the engineer would have to start over the design process like when using the traditional method.

1.2 Research objectives

In this dissertation, a new method of topology optimization for linkage mechanism synthesis which can consider two types of design conditions. Especially, this study aims to develop the topology optimization method which can consider kinematic and compliance (K&C) characteristics of linkage mechanisms simultaneously.

For topology optimization of linkage mechanisms considering K&C characteristics, there are several issues to be implemented. The first thing is to develop a modeling in which both kinematic and compliance analyses can be conducted. This is because when using the same modeling, the design variables for the optimization can be shared so that the design variables are updated to consider both characteristics. The second thing is that the modeling should be able to represent elastic elements. As mentioned in Chapter 1.1, compliance characteristics are determined by the deformation of the elastic elements. Especially, the elastic elements we employed in this research are elastic-behaving bushings because the main application in this research is focused on synthesizing a vehicle suspension.

To resolve these major issues, the modeling and formulation for topology optimization method simultaneously considering K&C characteristics of linkage mechanisms will be presented based on the spring-connected rigid block model (SBM) in this research. The idea is to utilize zero-length springs to represent bushing elements. In previous studies about the SBM, various joints or gear elements were

able to be represented through the zero-length springs, but the usage of the zero-length springs was still limited to be used only to represent the connectivity. Therefore, the problems which previous researches dealt with were related to kinematic characteristics. In order to overcome this problem, we will present the way how to make the zero-length springs had physical meaning for a compliance analysis.

And next, we will apply the proposed method to a vehicle suspension design for proving the validity and effectiveness. Vehicle suspensions have been synthesized by topology optimization method before [8], but at then, only kinematic characteristics like wheel center motion when wheel travels were considered. Therefore, the geometry of the vehicle suspensions could be obtained after the optimization, but additional design process should be needed for defining the bushing spec for compliance characteristics. However, since the proposed method can deal with both kinematic and compliance characteristics, we can present the spec of the bushing as well as geometry of the vehicle suspensions after the optimization. Thus, the modeling and formulation for designing a vehicle suspension considering K&C characteristics will be implemented.

1.3 Background research

1.3.1 Linkage mechanism synthesis based on the spring-connected rigid block model (SBM)

About the modeling for topology optimization of linkage mechanisms, there are two types of models that mainly have been used as mentioned in Chapter 1.1. One is the model consisted of nonlinear bars and the other is the model consisted of rigid blocks connected by zero-length springs called a SBM. Both models have been proved to be able to perform topology optimization of linkage mechanisms effectively through the previous studies. Spring-connected rigid block model (SBM) is employed in this research because of suitability for representing bushing stiffness and it will be explained in this section for better understanding. Especially, the simple version of a SBM [14, 15] is used to synthesize linkage mechanisms as the various joints or gear elements do not be needed to design vehicle suspension which is the main interest in this research.

Before explaining the modeling of a SBM, it is worth understanding the design process for automatic synthesis of linkage mechanisms based on a SBM. For an easy explanation, the problem is assumed to consider only with kinematic characteristics. Fig. 1.1 sketches a problem to synthesize a mechanism in a given design domain by topology optimization method for linkage mechanisms. Fig. 1.1(a) shows the problem definition that is to synthesize linkage mechanisms which can convert the given input motion to the target path at the end-effector in the design domain. For

the mechanisms synthesis, 3×3 rigid blocks connected each other by the zero-length variable-stiffness springs are employed as Fig. 1.1(b). The vertical and horizontal springs are to connect adjacent blocks while oblique springs, called anchoring springs, connect between the rigid blocks and the ground. The connectivity of the blocks are defined by the stiffness of the springs, and the stiffness of the springs are converged to minimum or maximum after optimization process.

The connectivity of the rigid blocks by the stiffness of springs is shown in Fig. 1.2. There are two block-connecting springs between two blocks and eight anchoring springs attached at every corner of the blocks. If the stiffness of all the springs have the minimum value as in Fig. 1.2(a), the two blocks can move separately. If only one block-connecting spring has the maximum value as in Fig. 1.2(b), the spring will bond rigidly the two points where the spring is attached, and this represents a revolute joint in 2D space. If the two block-connecting springs have the maximum stiffness as in Fig. 1.2(c), the two blocks will become one rigid body. In addition to the state of Fig. 1.2(c), if one anchoring spring has a maximum value, the rigid body consisted of the two blocks will be connected to the ground by an anchored revolute joint as in Fig. 1.2(d). If using this connectivity of the blocks, a four-bar mechanism can be presented by the SBM as in Fig. 1.3. We will make the SBM be able to consider compliance characteristics, and the detailed explanation will be given in Chapter 2.2.

1.3.2 Determination of the system's degree-of-freedom (DOF) based on the work transmittance efficiency function

The degree-of-freedom (DOF) of the system refers to the number of actuators required to define all the postures of the mechanism components, and when synthesizing mechanisms, the satisfaction of the correct DOF is a very important issue (typically 1 DOF). Normally, the DOF of the system can be calculated by Gruebler's equation using the number of links and joints if the mechanism is defined.

For the automatic synthesis method for linkage mechanism using gradient-based optimizer, dealing with integer-valued DOF's by using real-valued variables is important. While global optimizers can deal with integer values, gradient-based optimizers cannot handle integer directly because they require a sensitivity analysis. Some researches about dealing with the DOF as real-values were conducted [3, 24], but these methods had a limitation to solve the practical design problems because of the high-nonlinearity. However, the work transmittance efficiency function proposed in [7] could help to synthesize industrial applications through topology optimization method for linkage mechanisms based on gradient-based optimizers [7, 8, 12, 15].

Before presenting the form of the work transmittance efficiency function, it is worth knowing the states of the linkage mechanisms which have different DOF in detail. The states of the linkage mechanisms which have different DOF are shown in Fig. 1.4. According to Gruebler's equation, the DOF of the mechanisms in Fig. 1.4(a),

Fig. 1.4 (b), and Fig. 1.4 (c) are 2, 0, and 1, respectively. As in Fig. 1.4(a) and Fig. 1.4(b), when an input motion is given to the system, it can be seen that the 0-DOF system cannot move without deformation of the components and the 2-DOF system cannot resist the external force, respectively. By the way, the 1-DOF system can move without any deformation by resisting the external force. Based on this observations, the work transmittance energy function was presented, and the form is as follow:

$$\eta = W^{\text{out}} / W^{\text{inp}} \quad (1.1)$$

Where W^{inp} is the work done by an actuator, and W^{out} is the work done by the system against the resistance force through the movement of the loaded point. When the work transmittance function (η) is to be 1, it means that the system can move without any deformation by resisting the external force because all of the work done by an actuator is used to resist the external force not deforming the system. Because many studies successfully synthesized linkage mechanisms using this function already, we will also use this function as an objective to handle the DOF of the system. The specific form of the Eq. (1.1) will be given with the optimization formulation in Chapter 2.

1.4 Outline of thesis

The thesis is organized as follow.

In Chapter 2, we present a new topology optimization method to synthesize a linkage mechanism simultaneously considering not only kinematic but also compliance (K&C) characteristics. Especially, the way how we make the spring-connected rigid block model (SBM) suitable for the simultaneous consideration of K&C characteristics during mechanism synthesis is given. After the proposed formulation and numerical implementation are presented, three case studies are considered to synthesize planar linkage mechanisms.

In Chapter 3, a spatial vehicle suspension for rear is designed through the proposed methodology. For designing a vehicle suspension, we develop a spatial spring-connected rigid block model, and explanations about the analysis and formulation are presented. To verify the effectiveness of the developed methodology, two design cases are investigated.

In Chapter 4, the overall conclusion of this dissertation is presented.

In Appendix A, a target cascading process for deriving K&C characteristics to improve ride and handling (R&H) performances is given. For deriving K&C characteristics, a design optimization of a double wishbone to improve R&H

performances is conducted.

In Appendix B, the techniques to suppress floating blocks which do not affect K&C characteristics at convergence are explained. For confirming the effects of the floating blocks during optimization, Case study 3 in Chapter 2.4 is revisited with the technique to suppress floating blocks.

In Appendix C, a mesh dependency issue is investigated. For the investigation, Case study 1 in Chapter 2.4 is solved again with the more number of blocks, and the optimization results are presented.

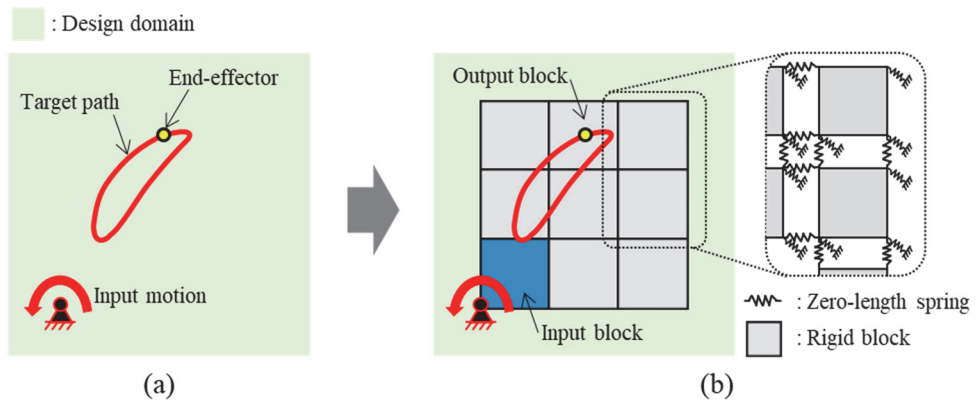


Fig. 1.1 Overview of topology optimization of linkage mechanisms for generating the target path based on the SBM. (a) Problem definition and (b) the ground model using the SBM

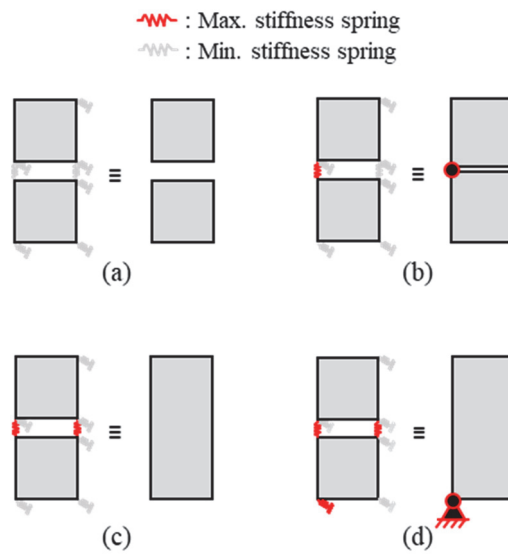


Fig. 1.2 Representation of the connectivities depending on the spring stiffness.
 (a) Disconnected, (b) connected by a revolute joint, (c) rigidly-connected, and
 (d) rigidly-connected two blocks connected by an anchored revolute joint

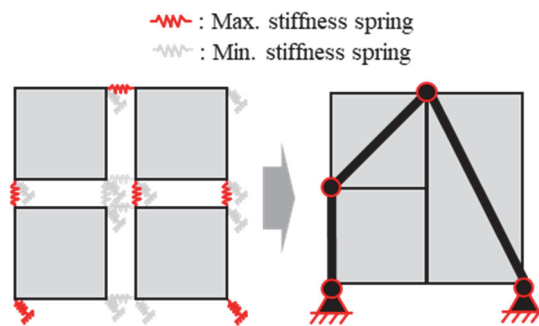


Fig. 1.3 A four-bar mechanisms represented by a SBM

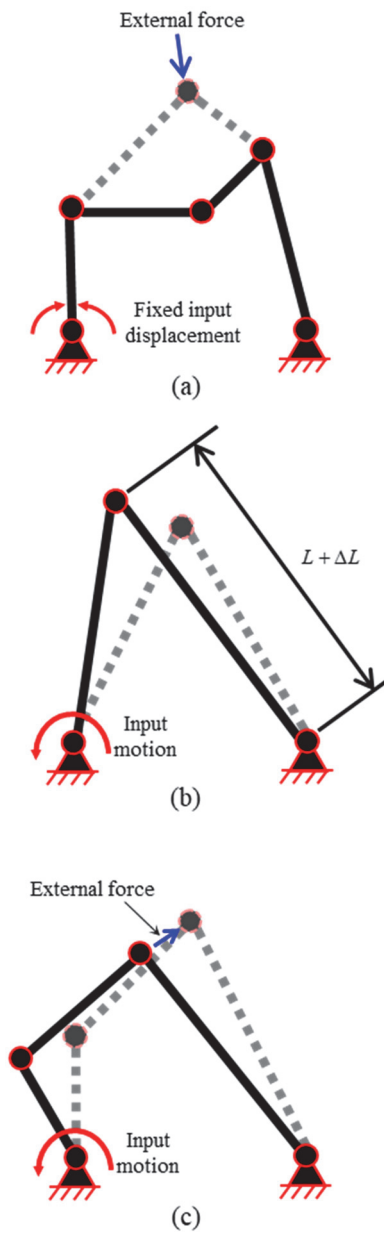


Fig. 1.4 Illustration of linkage mechanisms which have (a) $\text{DOF} = 2$, (b) $\text{DOF} = 0$, and (c) $\text{DOF} = 1$, respectively

CHAPTER 2.

Unified topology and shape optimization method for the mechanism synthesis simultaneously considering kinematic and compliance (K&C) characteristics

2.1 Overview

Mechanisms play an important role in machinery because they convert input drive into desired motion and force. Traditionally, mechanisms are synthesized in a sequential manner, during which engineers intuitively decide upon the basic topology of the linkage mechanisms. This process is followed by dimensional synthesis to meet design requirements precisely [25-30]. On the other hand, mechanism synthesis based on topology optimization has recently received much attention as an efficient alternative design approach. The main thrust behind this trend is the capability of this method automatically to determine the topology and dimensions of linkage mechanisms. Towards this direction, there have been many investigations [2-4, 6-18, 24]. After mechanism topology optimization based on the maximization of the work transmittance efficiency [7] was suggested, successful applications have been reported in the design of finger rehabilitation exoskeletons

[12] and vehicle suspensions [8]. However, these studies were limited in that they considered only kinematic characteristics, with which the generation of a desired motion or path is pursued. Kinematic characteristics are certainly the most important feature to consider in linkage mechanism synthesis, but compliance characteristics governing static deformations under applied forces are also important to consider in some applications [31-43]. However, no design method based on topology optimization that considers both kinematic and compliance characteristics is yet available.

Especially with regard to vehicle suspension design, not only kinematic but also compliance characteristics are known significantly to affect the behavior of a vehicle suspension, which in turn governs the ride and handling (R&H) performance of a vehicle [44-49]. The specific two-dimensional design example considered in this study is sketched in Fig. 2.1(a). As the desired kinematic characteristics, target wheel center motion is prescribed according to the vertical motion of the wheel. As the desired compliance characteristics, the displacement of the contact patch should be within a certain range when lateral force is applied at the initial position. (It is known that large displacement of the contact patch can degrade the R&H performance of a vehicle [45, 49].) As indicated in Fig. 2.1(a), the compliance characteristics can be evaluated by measuring the movement of a suspension mechanism due to the elastic deformation of its bushings when external force is applied. Because currently available topology optimization methods for mechanism synthesis are limited in that

they only consider kinematic characteristics, it is necessary to develop a new topology optimization method that can handle both kinematic and compliance (K&C) requirements.

In developing the proposed method, we employ the spring-connected rigid block model (SBM) [9, 10, 14, 15], as illustrated in Fig. 2.1(b). In this model, the design domain is discretized by a set of rigid blocks which are connected to each other by zero-length block-connecting springs and to the ground by zero-length ground-anchoring springs. This SBM can configure a desired mechanism if the stiffness values of the springs, which vary as functions of design variables, are appropriately assigned or optimized. While more detailed accounts of the SBM can be found in the literature [9, 10, 14, 15], it is commonly known that when the stiffness of a spring reaches its maximum or minimum value, two blocks (or a block and the ground) can be considered as one rigid body or links connected by a revolute joint or as two rigid bodies disconnected from each other. Because the current SBM has thus far been developed for the synthesis of a mechanism that generates a target path only without considering the compliance characteristics, it is necessary to resolve major modeling and topology optimization formulation issues in order to achieve mechanism synthesis considering K&C characteristics simultaneously. First, both kinematic and compliance analyses should be performed within a single SBM framework to ensure a streamlined optimization process. Otherwise, different mechanism models should be used depending on the type of analysis, i.e., a kinematic or compliance analysis.

Second, the SBM to be used for synthesis considering K&C characteristics simultaneously should be able to represent bushings with elastic properties. This is not considered in the existing SBM.

Before we present the proposed techniques to resolve the aforementioned issues, it should be noted that bushings (elastic elements) are typically installed only at the grounding joints. Accordingly, we allow the ground-anchoring springs to be conceptually multifunctional, implying that they serve both rigidly to connect a synthesized mechanism to the ground (or a chassis frame) for a kinematic analysis and to simulate elastically deforming bushings for a compliance analysis. Thereby, we use different spring stiffness values for the same block-connecting or anchoring spring to conduct the kinematic and compliance analyses needed during the topology optimization iterations. Specifically, the stiffness of an anchoring spring of an SBM representing a mechanism being synthesized is set to vary from zero to some finite value (k_{\max}^k) for a kinematic analysis and to vary from zero to another value (k_{bushing}) for a compliance analysis, where k_{bushing} denotes the actual stiffness of the candidate bushings and k_{\max}^k is a chosen value to allow a stable kinematic analysis for mechanism synthesis. For the compliance analysis, the value of k_{rigid} is assigned to the block-connecting spring, while the value of k_{\max}^k (upper bound) is assigned for the kinematic analysis to the same spring if the design variable controlling the spring stiffness reaches its upper bound value. (More details will be

given in the main part of this paper.)

Fig. 2.1(c) shows a converged SBM state after the proposed topology optimization is successfully completed. The anchoring springs with the maximum stiffness value (k_{bushing}) serve to represent actual bushings, while blocks connected by the springs of the maximum stiffness (k_{rigid}) represent a rigid link. The illustration on the right side of Fig. 2.1(c) shows that the synthesized mechanism in the design domain specified in Fig. 2.1(a) is the desired one-degree-of-freedom (DOF) linkage mechanism which satisfies the desired K&C characteristics.

This chapter proceeds as follows. Chapter 2.2 presents a brief overview of the SBM and the K&C analyses with the SBM. In Chapter 2.3, the formulation for topology optimization of the mechanism synthesis considering K&C characteristics simultaneously and the sensitivity analysis will be presented. As the design variables control continuously varying spring stiffness values, a numerically efficient gradient-based method for which a sensitivity analysis is necessary is used to update the design variables. To confirm the validity of the proposed method, three carefully selected case studies, including the design of a two-dimensional simplified vehicle suspension, will be conducted in Chapter 2.4. Concluding remarks are given in Chapter 2.5.

2.2 Modeling and analysis

2.2.1 Modeling

To perform topology optimization for mechanism synthesis, a ground model capable of representing various mechanism topologies should be used. In this study, we employ the spring-connected rigid block model (SBM) [9, 10, 14, 15] originally proposed for mechanism synthesis only considering kinematic characteristics and extend it to be able to perform mechanism topology optimization while considering both kinematic and compliance (K&C) characteristics. While a representative discretization of a design domain with SBs (spring-connected rigid block) is shown in Fig. 2.1, we will use the simplest case, shown in Fig. 2.2, to explain our new modeling approach that allows consideration of K&C characteristics simultaneously.

In Fig. 2.2, the design domain is discretized by two SBs, with the two blocks interconnected by zero-length block-connecting springs (k_{b_i} , where i is the spring index) and zero-length ground-anchoring springs (k_{a_j} , where j is the spring index).

The stiffness of each and every spring is varied as a continuous function of the design variable $\xi_{b_i}^T$ (for block-connecting spring) or $\xi_{a_j}^T$ (for anchoring spring) with

$10^{-6} \leq \xi_{b_i}^T, \xi_{a_j}^T \leq 1$. The spring stiffness is treated as a monotonically increasing

function of the corresponding design variable (detailed form given in the next section), and it should reach its maximum or minimum stiffness value at the convergence of the mechanism topology optimization. As indicated on the right side

of Fig. 2.2, the same design variables are used in the existing method (considering only kinematic characteristics) and in the proposed method (considering both kinematic and compliance characteristics). Among two sets of springs k_{b_i} and k_{a_j} , we will mainly consider the anchoring spring k_{a_j} in the subsequent discussion because the discussion pertaining to k_{a_j} is also valid for k_{b_i} .

In the existing method, only the spring stiffness $k_{a_j}^k$ is assigned to the anchoring spring k_{a_j} and is interpolated as a function of the design variable $\xi_{a_j}^T$, where $k_{a_j}^k$ denotes the stiffness of the spring used to calculate the kinematic behavior of a synthesized mechanism represented by the SBM. In the proposed method, on the other hand, the two sets of spring stiffnesses ($k_{a_j}^k$ and $k_{a_j}^c$) are assigned to k_{a_j} and are interpolated as a function of the same design variable $\xi_{a_j}^T$, where $k_{a_j}^k$ and $k_{a_j}^c$ denote the stiffnesses of the springs used to calculate the kinematic and compliance behaviors, respectively. This means that in the proposed method, the spring is considered to be multifunctional, with its functionality appropriately determined depending on the type of analysis.

To be more specific, four cases are illustrated in Fig. 2.3, where all design variables are assumed to reach their minimum (ξ_{\min}^T) or maximum (ξ_{\max}^T) values. In Case A, all stiffness values reach their minimum and the two blocks are assumed to be

disconnected and thus do not represent a specific layout as a whole. Cases B and C present a two-link system connected by a revolute joint and a single link as a whole, respectively. To represent these systems, the stiffnesses of some block-connecting springs (as indicated by the thick red springs) have their maximum value while other stiffness values reach their minimum. As the right side of Fig. 2.3 indicates, different stiffness values are assigned depending on the types of analyses, either kinematic or compliance in the present approach. Specifically, $k_{b_i}^k(\xi_{\max}^T) = k_{\max}^k$ and $k_{b_i}^c(\xi_{\max}^T) = k_{\text{rigid}}$. Because stable kinematic and compliance analyses generally require different stiffness values, an adjustment of the maximum stiffness values for different analyses is necessary. The situation for Case D better represents why two different stiffnesses should be used for the simultaneous K&C analysis. First, we note that Case D represents a single link connected to the ground by a hinge joint with a bushing element. Clearly, the block-connecting springs should have corresponding maximum values to ensure that the two blocks represent a single link. In order to represent a hinged joint with a bushing element having a specific stiffness value, the bushing element having the given stiffness should appear during the mechanism synthesis step. Therefore, the corresponding anchoring spring should behave multi-functionally to represent a revolute joint with $k_{a_j}^k(\xi_{\max}^T) = k_{\max}^k$ and a bushing having the specific stiffness value (k_{bushing}) with $k_{a_j}^c(\xi_{\max}^T) = k_{\text{bushing}}$. Because multi-functionality of the block-connecting and anchoring springs is critical for mechanism synthesis considering both kinematic and compliance characteristics,

topology optimization should be formulated so as to accommodate this requirement. Several related techniques will be presented in the section on the formulation.

2.2.2 Kinematic and compliance analyses with the SBM

To understand how kinematic and compliance analyses are performed with an SBM in an arbitrary configuration (corresponding to a set of design variables with any value between its minimum and maximum value), the principle of minimizing the strain energy stored by zero-length elastically behaving springs can be used. If an input motion or external force acts on an SBM, the positions of the rigid blocks of the SBM can be determined in such a way that the strain energy stored in the zero-length springs is minimized. For a kinematic analysis, the position of the blocks when changed by a given input motion is calculated, while for a compliance analysis, the position of the blocks when changed by an external force is calculated. Therefore, it is necessary to evaluate the strain energy stored in the system of zero-length springs when the blocks of an SBM are moved by an external disturbance. Fig. 2.4 presents a snapshot of two rigid blocks in a position after being moved by a given input motion or external force. The current configurations of the two blocks are illustrated as gray quadrangles with their edges indicated by solid lines, while the edges of the corresponding original configurations are denoted by dotted lines. The two blocks are connected to each other by the i th block-connecting spring (k_{b_i}), and the right block is also connected to the ground by the j th anchoring spring (k_{a_j}). As noted earlier in Chapter 2.1, the block-connecting springs serve to define the connectivity

between two blocks and the anchoring springs serve to define the connectivity between a block and the ground. Note that these springs only couple the translational motions (in the X and Y directions).

For the sake of convenience, the left block in Fig. 2.4 is denoted by the symbol “1” and the right block is denoted by the symbol “2”. The symbols $\mathbf{r}_{b_i,1}$ and $\mathbf{r}_{b_i,2}$ are the position vectors from the origin O of the global coordinate system (X, Y) to the initial center points of Blocks 1 and 2, respectively. The transformation matrices between the global coordinate system and the block-fixed local coordinate system of Blocks 1 and 2 are correspondingly denoted by $\mathbf{T}_{b_i,1}$ and $\mathbf{T}_{b_i,2}$, defined as

$$\mathbf{T}_{b_i,1} = \begin{bmatrix} \cos \phi_{b_i,1} & \sin \phi_{b_i,1} \\ -\sin \phi_{b_i,1} & \cos \phi_{b_i,1} \end{bmatrix}; \quad \mathbf{T}_{b_i,2} = \begin{bmatrix} \cos \phi_{b_i,2} & \sin \phi_{b_i,2} \\ -\sin \phi_{b_i,2} & \cos \phi_{b_i,2} \end{bmatrix} \quad (2.1)$$

where $\phi_{b_i,1}$ and $\phi_{b_i,2}$ are the angles between the global coordinate system and the local block-coordinate systems of Blocks 1 and 2, respectively. Using $\mathbf{T}_{b_i,1}$ and $\mathbf{T}_{b_i,2}$, the displacement between the corners of the two blocks at which the i th block-connecting spring is attached can be calculated as

$$\mathbf{u}_{b_i} = \left\{ \mathbf{r}_{b_i,1} + (\mathbf{T}_{b_i,1})^t \mathbf{s}_{b_i,1} \right\} - \left\{ \mathbf{r}_{b_i,2} + (\mathbf{T}_{b_i,2})^t \mathbf{s}_{b_i,2} \right\} \quad (2.2)$$

where $\mathbf{s}_{b_i,1}$ ($\mathbf{s}_{b_i,2}$) is the position vector from $\mathbf{r}_{b_i,1}$ ($\mathbf{r}_{b_i,2}$) to the k_{b_i} -attached corner in the local block-fixed coordinate system of Block 1 (Block 2). Likewise, the displacement of the j th anchoring spring can be defined as

$$\mathbf{u}_{a_j} = \left\{ \mathbf{r}_{b_i,2} + (\mathbf{T}_{b_i,2})^t \mathbf{s}_{a_j} \right\} - \mathbf{r}_{a_j} \quad (2.3)$$

Here, \mathbf{s}_{a_j} is the position vector from $\mathbf{r}_{b_i,2}$ to the k_{a_j} -attached corner in the local block-fixed coordinate system of Block 2 and \mathbf{r}_{a_j} is the position vector from the origin O of the global coordinate system (X, Y) to the k_{a_j} -attached corner of Block 2 at the initial position.

Using Eqs. (2.2) and (2.3), the strain energy stored in the i th block-connecting spring and the j th anchoring spring can be expressed as

$$U_{b_i} = \frac{1}{2} k_{b_i} (\mathbf{u}_{b_i})^t (\mathbf{u}_{b_i}); \quad U_{a_j} = \frac{1}{2} k_{a_j} (\mathbf{u}_{a_j})^t (\mathbf{u}_{a_j}) \quad (2.4)$$

The total strain energy stored in all of the springs can be then calculated as

$$U(\mathbf{q}) = \sum_{i=1}^{N_b} \frac{1}{2} k_{b_i} (\mathbf{u}_{b_i})^t (\mathbf{u}_{b_i}) + \sum_{j=1}^{N_a} \frac{1}{2} k_{a_j} (\mathbf{u}_{a_j})^t (\mathbf{u}_{a_j}) \quad (2.5)$$

where N_b and N_a correspondingly represent the number of block-connecting and anchoring springs. The symbol \mathbf{q} representing the state variable vector of the blocks is defined as

$$\mathbf{q} = \left\{ \mathbf{q}_1^t, \mathbf{q}_2^t, \dots, \mathbf{q}_{N_B}^t \right\}^t \quad (2.6)$$

with

$$\mathbf{q}_l = \left\{ \mathbf{r}_l^t, \phi_l \right\}^t = \{x_l, y_l, \phi_l\}^t \quad (l=1, 2, \dots, N_B) \quad (2.7)$$

(N_B : the total number of rigid blocks)

In the subsequent discussions, it is convenient to redefine $\mathbf{r}_{b_i,1}$ and $\mathbf{r}_{b_i,2}$ as \mathbf{r}_l , the

position vector of the l th block with proper renumbering.

In the kinematic analysis, the motion of a block is generated by a given input motion in terms of the prescribed state variable of the input block. For example, if the input motion corresponds to the rotation of the l th block, ϕ_l will be prescribed at all time steps. In addition, the input motion is fixed at zero for the compliance analysis because the compliance characteristics are defined at the initial position in this research. Therefore, the state variable of the input motion is given in both analyses and the total strain energy can therefore be considered as a function of the remaining state variables, defined as

$$\mathbf{v} = \left\{ \mathbf{q}_1^t, \mathbf{q}_2^t, \dots, \tilde{\mathbf{q}}_l^t, \dots, \mathbf{q}_{N_B}^t \right\}^t \quad (2.8)$$

where

$$\tilde{\mathbf{q}}_l = \{x_l, y_l\}^t \quad \text{if } \phi_l \text{ is the input DOF} \quad (2.9)$$

To determine \mathbf{v} at any time instance, the total potential energy $E(\mathbf{v})$ is minimized, as in earlier work (see Refs. [10, 11, 14]):

$$\text{Minimize } E(\mathbf{v}) = U(\mathbf{v}) - W^{out}(\mathbf{v}) \quad (2.10)$$

As the result of Eq. (2.10), the following force equilibrium is obtained:

$$\mathbf{F}^{int}(\mathbf{v}) - \mathbf{F}^{ext}(\mathbf{v}) = 0 \quad \text{for given } \phi_l \quad (2.11)$$

where

$$\mathbf{F}^{int} = dU/d\mathbf{v}; \quad \mathbf{F}^{ext} = dW^{out}/d\mathbf{v} \quad (2.12)$$

In Eq. (2.12), \mathbf{F}^{int} denotes the internal force generated by the springs and \mathbf{F}^{ext} is the external force applied to the system. In the kinematic analysis, Eq. (2.11) is solved at every time step t^* ($t^* = 1, 2, \dots, t_{\max}$) under the given input motion ϕ_{l,t^*} . Typically, external force acts on the motion of the end-effector of a synthesized mechanism for a kinematic analysis. This force should be known to define the work transmittance efficiency function [7], which is critical when determining whether or not the synthesized mechanism has the correct DOF. We explain how the external force is applied later in the paper. In the compliance analysis, Eq. (2.11) is solved at the initial position with the given external force. The explicit formulas for the terms in Eq. (2.11) are omitted because they can be found in previous studies [10-15].

As discussed in Chapter 2.1 and as shown in Fig. 2.1, the block-connecting and anchoring springs used to identify the configuration of a synthesized mechanism are multifunctional; hence, their stiffness values are defined differently depending on the analysis type, i.e., kinematic or compliance. For anchoring spring k_{a_j} , its stiffness value becomes $k_{a_j} = k_{a_j}^k$ with a maximum value of k_{\max}^k for a kinematic analysis, and for a compliance analysis, $k_{a_j} = k_{a_j}^c$ with a maximum value of k_{bushing} , where k_{bushing} is the actual stiffness of the used bushing. For the block-connecting spring k_{b_i} , its stiffness value becomes $k_{b_i} = k_{b_i}^k$ with a maximum value of k_{\max}^k for a kinematic analysis, and for a compliance analysis $k_{b_i} = k_{b_i}^c$ with its

maximum value of k_{rigid} . Because the proper value of k_{max}^k needed for a stable kinematic analysis was given in an earlier study [15], here we show that if k_{rigid} has a sufficiently large value, approximately 2×10^3 larger than k_{bushing} in this study, the blocks connected by block-connecting springs with $k_{b_i}^c = k_{\text{rigid}}$ behave practically as a single rigid body for a compliance analysis. Thereby, the deformation of an SBM in which the blocks are connected by these types of springs should occur mostly in the anchoring springs. Considering that the stiffness value $k_{b_i}^c$ will vary between 0 and k_{rigid} , and the stiffness value $k_{a_j}^c$ will vary between 0 and k_{bushing} during the topology optimization iterations, here we examine if the suggested choice of k_{rigid} provides accurate compliance results using $k_{a_j}^c = k_{\text{bushing}}$ and $k_{b_i}^c = k_{\text{rigid}}$ with the example shown in Fig. 2.5.

Fig. 2.5(a) shows a four-bar linkage mechanism connected to the ground by bushings the stiffness of which is 2000 N/m. It is loaded by an external force acting on its end-effector (Q). The input angle is fixed at zero for the compliance analysis and the magnitude of the load is set to 200 N. For the compliance analysis, the horizontal and vertical stiffnesses of the anchoring spring simulating a bushing are set to $k_{\text{bushing}} = 2 \times 10^3$ N/m and the block-connecting spring is set to $k_{\text{rigid}} = 4 \times 10^6$ N/m. When modeling the four-bar linkage mechanism with ADAMS for the verification purpose of the SBM, revolute joints are modeled using the ‘revolute joint’ element

and bushings are modeled with the ‘bushing’ element. To ensure that the input actuator does not rotate, a ‘planar joint’ element is attached to the input actuator. The compliance analysis results give the displacement of the end-effector, which is given in Fig. 2.5(b). The results indicate that the analysis using the SBM with the suggested value k_{rigid} is nearly as accurate as the ADAMS analysis using the original four-bar linkage model. Based on this test example, k_{rigid} will establish $k_{\text{rigid}} = 2 \times 10^3 k_{\text{bushing}}$ for all case studies considered here.

2.3 Optimization Formulation

In this section, we discuss the method used to set the design variables of the SBM for the K&C analysis and present a topology optimization formulation for linkage mechanism synthesis considering both kinematic and compliance characteristics. A sensitivity analysis is also conducted because we use the method of moving asymptotes (MMA) [50], a gradient-based optimizer, in this research.

2.3.1 Design variable and interpolation

As explained in Chapter 2.1, the spring stiffness and the shape of the blocks of an SBM should be determined to configure the desired mechanism. While the spring stiffnesses are used to determine the topology of the synthesized mechanism, the coordinates of the grid points used to discretize the design domain into a set of rigid blocks (equivalently, the block edge coordinates) determine its shape. For simultaneous topology and shape optimization, we introduce two set of design variables, the topology-controlling design variable ξ^T and the shape-controlling design variable ξ^X , defined as

$$\xi^T = \left\{ \left(\xi_b^T \right)^t, \left(\xi_a^T \right)^t \right\} = \left\{ \xi_{b_1}^T, \xi_{b_2}^T, \dots, \xi_{b_{N_b}}^T, \xi_{a_1}^T, \xi_{a_2}^T, \dots, \xi_{a_{N_a}}^T \right\}^t \quad (2.13)$$

$$\xi^X = \left\{ \xi_1^X, \xi_2^X, \dots, \xi_{2N_N}^X \right\}^t \quad (2.14)$$

with

$$\xi = \left\{ \left(\xi^T \right)^t, \left(\xi^X \right)^t \right\} \quad (2.15)$$

In Eq. (2.13), the total number of block-connecting springs is N_b and the total number of the anchoring springs is N_a . The total number of design variables for the shape of the blocks is $2N_N$ because these variables are related to the coordinates of the block grid points (N_N : the total number of the block grid points). Once these design variables are introduced, the spring stiffness vectors for the kinematic analysis (\mathbf{k}^k) and the compliance analysis (\mathbf{k}^c) are interpolated as functions of the design variables to carry out topology optimization:

$$\mathbf{k}^k = \left\{ \left(\mathbf{k}_b^k \right)^t, \left(\mathbf{k}_a^k \right)^t \right\} = \left\{ k_{b_1}^k, k_{b_2}^k, \dots, k_{b_{N_b}}^k, k_{a_1}^k, k_{a_2}^k, \dots, k_{a_{N_a}}^k \right\}^t \quad (2.16a)$$

$$k_{b_i}^k = k_{\max}^k \times (\xi_{b_i}^T)^p; \quad k_{a_j}^k = k_{\max}^k \times (\xi_{a_j}^T)^p \quad (2.16b)$$

$$\mathbf{k}^c = \left\{ \left(\mathbf{k}_b^c \right)^t, \left(\mathbf{k}_a^c \right)^t \right\} = \left\{ k_{b_1}^c, k_{b_2}^c, \dots, k_{b_{N_b}}^c, k_{a_1}^c, k_{a_2}^c, \dots, k_{a_{N_a}}^c \right\}^t \quad (2.17a)$$

$$k_{b_i}^c = k_{\text{rigid}} \times (\xi_{b_i}^T)^p; \quad k_{a_j}^c = k_{\text{bushing}} \times (\xi_{a_j}^T)^p \quad (2.17b)$$

where

$$10^{-6} \leq \xi_{b_i}^T, \quad \xi_{a_j}^T \leq 1 \quad (i=1,2,\dots,N_b, \quad j=1,2,\dots,N_a) \quad (2.18)$$

In Eqs. (2.16b) and (2.17b), p is the penalty parameter. Its value is set to 3, as in earlier works [11-15]. Note that different maximum spring stiffness values are used for the kinematic analysis and compliance analysis. Because the same design variables are used in the two analyses, however, the mechanism layout status represented by a set of design variables is identical for both the kinematic and compliance analyses. The Cartesian coordinates (X_i and Y_i) of the i th grid point,

which determine the shape of the blocks, are treated as functions of the design variables (ξ_{2i-1}^X and ξ_{2i}^X) as

$$\mathbf{X} = \{X_1, Y_1, X_2, Y_2, \dots, X_{N_N}, Y_{N_N}\}^t \quad (2.19a)$$

$$X_i = X_{\max} \xi_{2i-1}^X + X_{\min} (1 - \xi_{2i-1}^X); \quad Y_i = Y_{\max} \xi_{2i}^X + Y_{\min} (1 - \xi_{2i}^X) \quad (2.19a)$$

where

$$10^{-6} \leq \xi_l^X \leq 1 \quad (l=1, 2, 3, \dots, 2N_N) \quad (2.20)$$

and X_{\max} (Y_{\max}) and X_{\min} (Y_{\min}) are correspondingly the maximum and minimum values of the X (Y) coordinate of the design domain boundary.

2.3.2 Objective and constraint functions

Our proposed formulation for topology optimization of linkage mechanisms considering K&C characteristics is as follow:

**Proposed simultaneous formulation:
Considering K&C characteristics simultaneously**

$$\begin{aligned} &\text{Find } \xi^T \text{ and } \xi^X \\ &\text{to minimize } 1 - \bar{\eta} \end{aligned} \quad (2.21a)$$

Subject to 1) Kinematic condition under the given input motion

$$\psi_{t^*}^{k(i)}(\mathbf{v}_{t^*}) \leq \varepsilon^{k(i)} \quad (t^* = 1, 2, 3, \dots, t_{\max}) \quad (2.21b)$$

2) Compliance constraints for the given external load

$$\psi^{c(j)}(\mathbf{v}_0) \leq \varepsilon^{c(j)} \quad (0: \text{initial position}) \quad (2.21c)$$

3) Constraint on the maximum number of bushings

$$\sum_{m=1}^{N_a} \xi_{a_m}^T \leq n \quad (2.21d)$$

where

$$\bar{\eta} = \frac{1}{t_{\max}} \sum_{t=1}^{t_{\max}} \eta_t \quad (\eta_t : \text{Work transmittance efficiency at time } t) \quad (2.22)$$

In Eq. (2.21a), the mean value of the work transmittance efficiency function ($\bar{\eta}$) [7] is used as an objective here. It has been proven that if $\bar{\eta}$ is maximized or $1-\bar{\eta}$ is minimized, the correct DOF for a desired mechanism can be guaranteed in the system [7, 8, 11-15]. The work transmittance efficiency function at each time step (η_{t^*}) can be calculated according to the ratio of the work done by the system against the external force to the work done by the input motion, as

$$\eta_{t^*}(\mathbf{v}_{t^*}) = \frac{W_{t^*}^{out}}{W_{t^*}^{in}} = \frac{W_{t^*}^{out}}{W_{t^*}^{out} + U_{t^*}} \quad (t^* = 1, 2, \dots, t_{\max}) \quad (2.23)$$

where

$$W_{t^*}^{out}(\mathbf{v}_{t^*}) = \sum_{t=1}^{t^*} \mathbf{F}_t^{ext} \cdot (\mathbf{r}_{t-1}^Q - \mathbf{r}_t^Q) \quad (2.24)$$

Additionally, the external force at time step t (\mathbf{F}_t^{ext}) is defined as

$$\mathbf{F}_t^{ext}(\mathbf{v}_t) = F_t \frac{\mathbf{r}_{t-1}^Q - \mathbf{r}_t^Q}{\|\mathbf{r}_{t-1}^Q - \mathbf{r}_t^Q\|} \quad (2.25)$$

where \mathbf{r}_t^Q is the current location of the end-effector. The external force is applied against the motion of the end-effector, expressed as Eq. (2.25), and the magnitude (F_t) is set to one. The output work and the external force are functions of the state variable vector at time t (\mathbf{v}_t) because the location of the end-effector is derived from the state variables of the output block.

The constraint functions in Eqs. (2.21b) and (2.21c) are related to the K&C characteristics. The symbol $\psi_t^{k(i)}$ represents the i th kinematic constraint and $\psi^{c(j)}$ is the j th compliance constraint. For example, if the kinematic requirement is to synthesize a linkage mechanism capable of generating a given target path, one kinematic constraint will be given ($i=1$) by $\psi_t^{k(1)} = \|\mathbf{r}_t^Q - \hat{\mathbf{r}}_t^Q\|$, which represents the Euclidean error, where \mathbf{r}_t^Q denotes the position of the end-effector at time step t^* and $\hat{\mathbf{r}}_t^Q$ is the position of the target path at time step t^* . In contrast, if the target compliance characteristics are to hold the x -coordinate displacement and the angular displacement of the end-effector by external force within the error bounds, two compliance constraints will be necessary ($j = 1, 2$). These are defined as $\psi^{c(1)} = |\Delta x_0^Q|$ and $\psi^{c(2)} = |\Delta \theta_0^Q|$.

The last constraint function, Eq. (2.21d), is employed to restrict the number of used bushings, as a specific number of bushings is usually used in the actual design process. In addition, this constraint can avoid the creation of unnecessary bushings that do not contribute to governing the linkage motion but that instead adversely affect the system stiffness at the end of the mechanism topology optimization iterations. If unnecessary redundant bushings appear at the end, the resulting mechanism may not satisfy the requirements of the target compliance characteristics considering the bushing stiffness value used. In this study, the number of bushings is set to $n = 2$, which is the minimum number of bushings needed to compose a planar

linkage mechanism. A flowchart of the topology optimization process of linkage mechanisms considering the kinematic and the compliance characteristics is presented in Fig. 2.6.

If the proposed method is not used for mechanism synthesis considering kinematic and compliance characteristics, one may need to utilize an existing method developed for problems considering kinematic characteristics only and then consider design optimization to consider compliance characteristics using the topological layout obtained from the previous step. Therefore, two optimization process is needed to synthesize a linkage mechanism which can satisfy the given kinematic and compliance characteristics. This sequential optimization procedure is expressed as shown below.

Two-step sequential formulation

- First step: Topology optimization only considering kinematic condition

Find ξ^T and ξ^X
to minimize $1 - \bar{\eta}$

Subject to 1) Kinematic condition under the given input motion

$$\psi_{t^*}^{k(i)}(\mathbf{v}_{t^*}) \leq \varepsilon^{k(i)} \quad (t^* = 1, 2, \dots, t_{\max})$$

- Second step: Shape optimization considering K&C constraints

Find ξ^X (2.26)
to minimize $1 - \bar{\eta}$

Subject to 1) Kinematic condition under the given input motion

$$\psi_{t^*}^{k(i)}(\mathbf{v}_{t^*}) \leq \varepsilon^{k(i)} \quad (t^* = 1, 2, \dots, t_{\max})$$

2) Compliance constraints for given external load

$$\psi^{c(j)}(\mathbf{v}_0) \leq \varepsilon^{c(j)} \quad (0: \text{initial position})$$

Contrary to the simultaneous formulation proposed in this research, this formulation is inevitably sequential due to the lack of a method to consider both kinematic and compliance characteristics within a single topology optimization formulation. Therefore, the use of the second step in Eq. (2.26) for shape optimization is inevitable. With regard to this step, the bushing stiffness values are applied to the fixed pivots, and the dimensions of the linkage mechanism synthesized during the previous step are determined to satisfy the K&C constraints. The critical limitation of this sequential approach is that if the desired K&C constraints cannot be satisfied during the second step, it becomes necessary to use another mechanism topology; this necessitates repeating the first step with different initial guesses. This process may be repeated multiple times until the topology of a mechanism can be used to satisfy the K&C constraints during the second step of the optimization. In Case study 2, we will demonstrate that this undesirable situation can actually occur. At the same time, we will show that a desired optimal mechanism can be found in a single step if the proposed method is employed.

2.3.3 Sensitivity analysis

For an efficient mechanism synthesis, the method of moving asymptotes (MMA) [50], a gradient-based optimizer, is used in this research. To use a gradient-based optimizer, the sensitivities of the objective and constraint functions with respect to the design variables are required. First, the sensitivity of the objective function is calculated via

$$\frac{d\eta_{t^*}}{d\boldsymbol{\xi}} = \begin{bmatrix} \frac{d\eta_{t^*}}{d\boldsymbol{\xi}^T} \\ \frac{d\eta_{t^*}}{d\boldsymbol{\xi}^X} \end{bmatrix} = \begin{bmatrix} \frac{d\mathbf{k}^k}{d\boldsymbol{\xi}^T} \left(\frac{\partial \eta_{t^*}}{\partial \mathbf{k}^k} + \frac{d\mathbf{v}_{t^*}}{d\mathbf{k}^k} \frac{\partial \eta_{t^*}}{\partial \mathbf{v}_{t^*}} \right) \\ \frac{d\mathbf{X}}{d\boldsymbol{\xi}^X} \left(\frac{\partial \eta_{t^*}}{\partial \mathbf{X}} + \frac{d\mathbf{v}_{t^*}}{d\mathbf{X}} \frac{\partial \eta_{t^*}}{\partial \mathbf{v}_{t^*}} \right) \end{bmatrix} = \begin{bmatrix} \frac{d\mathbf{k}^k}{d\boldsymbol{\xi}^T} \left(\frac{d\mathbf{v}_{t^*}}{d\mathbf{k}^k} \frac{\partial \eta_{t^*}}{\partial \mathbf{v}_{t^*}} \right) \\ \frac{d\mathbf{X}}{d\boldsymbol{\xi}^X} \left(\frac{d\mathbf{v}_{t^*}}{d\mathbf{X}} \frac{\partial \eta_{t^*}}{\partial \mathbf{v}_{t^*}} \right) \end{bmatrix} \quad (2.27)$$

Because the objective function is derived from the kinematic analysis, \mathbf{k}^k is used in Eq. (2.27). In addition, $\partial \eta_{t^*} / \partial \mathbf{k}^k$ and $\partial \eta_{t^*} / \partial \mathbf{X}$ will become zero because η_{t^*} is a function of the state variable vector \mathbf{v}_{t^*} . The sensitivities $d\mathbf{k}^k / d\boldsymbol{\xi}^T$ and $d\mathbf{k}^k / d\boldsymbol{\xi}^X$ are calculated as follows:

$$\frac{d\mathbf{k}^k}{d\boldsymbol{\xi}^T} = \text{diag} \left(3k_{\max}^k (\xi_{b_1}^T)^2, \dots, 3k_{\max}^k (\xi_{b_{N_b}}^T)^2, 3k_{\max}^k (\xi_{a_1}^T)^2, \dots, 3k_{\max}^k (\xi_{a_{N_a}}^T)^2 \right) \quad (2.28)$$

$$\frac{d\mathbf{X}}{d\boldsymbol{\xi}^X} = \text{diag} (X_{\max} - X_{\min}, Y_{\max} - Y_{\min}, \dots, X_{\max} - X_{\min}, Y_{\max} - Y_{\min}) \quad (2.29)$$

To find $d\mathbf{v}_{t^*} / d\mathbf{k}^k$ and $d\mathbf{v}_{t^*} / d\mathbf{X}$, Eq. (2.11) is differentiated with respect to \mathbf{k}^k and \mathbf{X} to obtain

$$\frac{d(\mathbf{F}_{t^*}^{int}(\mathbf{v}_{t^*}) - \mathbf{F}_{t^*}^{ext})}{d\mathbf{k}^k} = \frac{d\mathbf{F}_{t^*}^{int}(\mathbf{v}_{t^*})}{d\mathbf{k}^k} = \frac{d}{d\mathbf{k}^k} \left(\frac{\partial \mathbf{F}_{t^*}^{int}}{\partial \mathbf{k}^k} + \frac{d\mathbf{v}_{t^*}}{d\mathbf{k}^k} \frac{\partial \mathbf{F}_{t^*}^{int}}{\partial \mathbf{v}_{t^*}} \right) = 0 \quad (2.30a)$$

$$\frac{d\mathbf{v}_{t^*}}{d\mathbf{k}^k} = -\frac{\partial \mathbf{F}_{t^*}^{int}}{\partial \mathbf{k}^k} \left(\frac{\partial \mathbf{F}_{t^*}^{int}}{\partial \mathbf{v}_{t^*}} \right)^{-1} = -\frac{\partial^2 U_{t^*}}{\partial \mathbf{v}_{t^*} \partial \mathbf{k}^k} \left(\frac{\partial^2 U_{t^*}}{\partial \mathbf{v}_{t^*}^2} \right)^{-1} = -\frac{\partial^2 U_{t^*}}{\partial \mathbf{v}_{t^*} \partial \mathbf{k}^k} (\mathbf{J}_{t^*})^{-1} \quad (2.30b)$$

$$\frac{d(\mathbf{F}_{t^*}^{int}(\mathbf{v}_{t^*}) - \mathbf{F}_{t^*}^{ext})}{d\mathbf{X}} = \frac{d\mathbf{F}_{t^*}^{int}(\mathbf{v}_{t^*})}{d\mathbf{X}} = \frac{d}{d\mathbf{X}} \left(\frac{\partial \mathbf{F}_{t^*}^{int}}{\partial \mathbf{X}} + \frac{d\mathbf{v}_{t^*}}{d\mathbf{X}} \frac{\partial \mathbf{F}_{t^*}^{int}}{\partial \mathbf{v}_{t^*}} \right) = 0 \quad (2.31a)$$

$$\frac{d\mathbf{v}_{t^*}}{d\mathbf{X}} = -\frac{\partial \mathbf{F}_{t^*}^{int}}{\partial \mathbf{X}} \left(\frac{\partial \mathbf{F}_{t^*}^{int}}{\partial \mathbf{v}_{t^*}} \right)^{-1} = -\frac{\partial^2 U_{t^*}}{\partial \mathbf{v}_{t^*} \partial \mathbf{X}} \left(\frac{\partial^2 U_{t^*}}{\partial \mathbf{v}_{t^*}^2} \right)^{-1} = -\frac{\partial^2 U_{t^*}}{\partial \mathbf{v}_{t^*} \partial \mathbf{X}} (\mathbf{J}_{t^*})^{-1} \quad (2.31b)$$

If Eq. (2.23) is used, $\partial \eta_{t^*} / \partial \mathbf{v}_{t^*}$ can be calculated as

$$\frac{\partial \eta_{t^*}}{\partial \mathbf{v}_{t^*}} = \frac{\partial}{\partial \mathbf{v}_{t^*}} \left(\frac{W_{t^*}^{out}}{W_{t^*}^{out} + U_{t^*}} \right) = \frac{1}{(W_{t^*}^{out} + U_{t^*})} \frac{\partial W_{t^*}^{out}}{\partial \mathbf{v}_{t^*}} - \frac{W_{t^*}^{out}}{(W_{t^*}^{out} + U_{t^*})^2} \left(\frac{\partial W_{t^*}^{out}}{\partial \mathbf{v}_{t^*}} + \frac{\partial U_{t^*}}{\partial \mathbf{v}_{t^*}} \right) \quad (2.32)$$

The sensitivity of the kinematic constraint function is calculated as follows:

$$\frac{d\psi_{t^*}^{k(i)}}{d\xi} = \begin{bmatrix} \frac{d\psi_{t^*}^{k(i)}}{d\xi^T} \\ \frac{d\psi_{t^*}^{k(i)}}{d\xi^X} \end{bmatrix} = \begin{bmatrix} \frac{d\mathbf{k}^k}{d\xi^T} \left(\frac{\partial \psi_{t^*}^{k(i)}}{\partial \mathbf{k}^k} + \frac{d\mathbf{v}_{t^*}}{d\mathbf{k}^k} \frac{\partial \psi_{t^*}^{k(i)}}{\partial \mathbf{v}_{t^*}} \right) \\ \frac{d\mathbf{X}}{d\xi^X} \left(\frac{\partial \psi_{t^*}^{k(i)}}{\partial \mathbf{X}} + \frac{d\mathbf{v}_{t^*}}{d\mathbf{X}} \frac{\partial \psi_{t^*}^{k(i)}}{\partial \mathbf{v}_{t^*}} \right) \end{bmatrix} = \begin{bmatrix} \frac{d\mathbf{k}^k}{d\xi^T} \left(\frac{d\mathbf{v}_{t^*}}{d\mathbf{k}^k} \frac{\partial \psi_{t^*}^{k(i)}}{\partial \mathbf{v}_{t^*}} \right) \\ \frac{d\mathbf{X}}{d\xi^X} \left(\frac{d\mathbf{v}_{t^*}}{d\mathbf{X}} \frac{\partial \psi_{t^*}^{k(i)}}{\partial \mathbf{v}_{t^*}} \right) \end{bmatrix} \quad (2.33)$$

The first and second terms in Eq. (2.33) were calculated using Eqs. (2.28) to (2.31),

and the last term can be calculated easily because $\psi_{t^*}^{k(i)}$ is an explicit function of the state variable vector \mathbf{v}_{t^*} in all case studies considered in this study. The

sensitivity of the compliance constraint function is calculated as follows:

$$\frac{d\psi^{c(j)}}{d\xi} = \begin{bmatrix} \frac{d\psi^{c(j)}}{d\xi^T} \\ \frac{d\psi^{c(j)}}{d\xi^X} \end{bmatrix} = \begin{bmatrix} \frac{d\mathbf{k}^c}{d\xi^T} \left(\frac{\partial \psi^{c(j)}}{\partial \mathbf{k}^c} + \frac{d\mathbf{v}_0}{d\mathbf{k}^c} \frac{\partial \psi^{c(j)}}{\partial \mathbf{v}_0} \right) \\ \frac{d\mathbf{X}}{d\xi^X} \left(\frac{\partial \psi^{c(j)}}{\partial \mathbf{X}} + \frac{d\mathbf{v}_0}{d\mathbf{X}} \frac{\partial \psi^{c(j)}}{\partial \mathbf{v}_0} \right) \end{bmatrix} = \begin{bmatrix} \frac{d\mathbf{k}^c}{d\xi^T} \left(\frac{d\mathbf{v}_0}{d\mathbf{k}^c} \frac{\partial \psi^{c(j)}}{\partial \mathbf{v}_0} \right) \\ \frac{d\mathbf{X}}{d\xi^X} \left(\frac{d\mathbf{v}_0}{d\mathbf{X}} \frac{\partial \psi^{c(j)}}{\partial \mathbf{v}_0} \right) \end{bmatrix} \quad (2.34)$$

Because the compliance constraint function is derived from the compliance analysis,

\mathbf{k}^c is used in Eq. (2.34). $d\mathbf{k}^c/d\xi^T$ is calculated as

$$\frac{d\mathbf{k}^c}{d\xi^T} = \text{diag}\left(3k_{\text{rigid}}(\xi_{b_1}^T)^2, \dots, 3k_{\text{rigid}}(\xi_{b_{N_b}}^T)^2, 3k_{\text{bushing}}(\xi_{a_1}^T)^2, \dots, 3k_{\text{bushing}}(\xi_{a_{N_a}}^T)^2\right) \quad (2.35)$$

and $d\mathbf{v}_0/d\mathbf{k}^c$ can be derived from Eq. (2.11) as

$$\frac{d(\mathbf{F}_0^{\text{int}}(\mathbf{v}_0) - \mathbf{F}_0^{\text{ext}})}{d\mathbf{k}^c} = \frac{d\mathbf{F}_0^{\text{int}}(\mathbf{v}_0)}{d\mathbf{k}^c} = \frac{d}{d\mathbf{k}^c} \left(\frac{\partial \mathbf{F}_0^{\text{int}}}{\partial \mathbf{k}^c} + \frac{d\mathbf{v}_0}{d\mathbf{k}^c} \frac{\partial \mathbf{F}_0^{\text{int}}}{\partial \mathbf{v}_0} \right) = 0 \quad (2.36a)$$

$$\frac{d\mathbf{v}_0}{d\mathbf{k}^c} = -\frac{\partial \mathbf{F}_0^{\text{int}}}{\partial \mathbf{k}^c} \left(\frac{\partial \mathbf{F}_0^{\text{int}}}{\partial \mathbf{v}_0} \right)^{-1} = -\frac{\partial^2 U_0}{\partial \mathbf{v}_0 \partial \mathbf{k}^c} \left(\frac{\partial^2 U_0}{\partial \mathbf{v}_0^2} \right)^{-1} = -\frac{\partial^2 U_0}{\partial \mathbf{v}_0 \partial \mathbf{k}^c} (\mathbf{J}_0)^{-1} \quad (2.36b)$$

Although the last term in Eq. (2.34) depends on the specific problems, it can be calculated easily in this study because $\psi^{c(j)}$ is an explicit function of the state variable vector \mathbf{v}_0 in all case studies in the next chapter.

The sensitivity of Eq. (2.21d) is very simple to calculate because Eq. (2.21d) is the sum of the design variables associated with bushings modeled by anchoring springs. Therefore, the value of the component of the sensitivity related to the design variable for the anchoring springs is 1, and the other values are 0.

2.4 Case studies

In this section, three case studies are solved to demonstrate the validity and effectiveness of the proposed method. First, we verify the proposed method by synthesizing linkage mechanisms considering K&C characteristic simultaneously. The second case study is considered to demonstrate the critical advantage of the proposed method over a sequential method based on existing techniques. To this end, we consider the synthesis of a two-dimensional vehicle suspension, which can be regarded as a simplified version of a three-dimensional vehicle suspension as the third example. In all case studies, the units of the length, force, moment, and spring stiffness are the meter (m), newton (N), newton-meter (Nm), and newton per meter (N/m), respectively. Note that when using the optimized result in Case study 3, dealing with a realistic design problem, we explain in some detail how to interpret a linkage mechanism from rigid blocks connected by block-connecting and anchoring springs. (Accordingly, no detailed procedure by which to extract a specific linkage mechanism layout from the SBM is presented in the details of Case Studies 1 and 2.)

2.4.1 Case study 1 - Validation of the proposed method

Here, the validity of the proposed method is checked; i.e., we assess whether a known reference mechanism layout configuration can be recovered if its kinematic and compliance characteristics are given. The specific mechanism considered for this test is shown in Fig. 2.7(a). The target K&C characteristics used to synthesize the mechanism are described in Fig. 2.7(b). With regard to the kinematic characteristics,

the target path $\hat{\mathbf{r}}_i^Q$ at its end-effector location Q is a banana-shaped path which is generated by the rotating input motion of link AB of the reference linkage. Specifically, the input motion to generate the reference path is given by the rotation angle as a function of time t^* :

$$\phi_i^{Input} = \frac{\pi}{18} t^* \quad (t^* = 1, 2, \dots, 36) \quad (2.37)$$

As the desired compliance characteristics, the angular displacement of the end-effector is used in the initial configuration of the reference mechanism ($t^* = 0$) under the applied external force, as indicated in Fig. 2.7(b).

Fig. 2.8 shows the design domain discretized into 3×3 rigid blocks to be used for the synthesis of the mechanism for Case study 1. The rigid blocks are connected to each other by block-connecting springs and are connected to the ground by anchoring springs attached to all corners of the rigid blocks. In total, there are 24 block-connecting springs (controlled by 24 corresponding design variables) and 36 anchoring springs (controlled by 36 corresponding design variables.) To allow the input block to rotate around the bottom left corner, the design variable values for the anchoring springs attached to the input block are kept such that the maximum design variable value is allocated to the lower left anchoring spring and the minimum design variable value to the other anchoring springs. The end-effector is located at the center of the output block, which is the top middle block in the initial layout. Thus, the prescribed kinematic and the compliance conditions in Fig. 2.8(b) are identical to

those given in Fig. 2.7(b). These conditions are explicitly written as

$$\psi_{t^*}^k(\mathbf{v}_{t^*}) = \|\mathbf{r}_{t^*}^Q - \hat{\mathbf{r}}_{t^*}^Q\| \leq \varepsilon^k \quad (t^* = 1, 2, \dots, 36) \quad (2.38a)$$

$$\psi^c(\mathbf{v}_0) = |\Delta\theta_0^Q| - |\Delta\hat{\theta}_0^Q| \leq \varepsilon^c \quad (2.38b)$$

In Eq. (2.38a), the Euclidean error is used to estimate the distance between the position ($\mathbf{r}_{t^*}^Q$) of the end-effector and the position ($\hat{\mathbf{r}}_{t^*}^Q$) of the target path at time step t^* . Eq. (2.38b) states that the absolute value of the angular displacement is less than the target value. For the numerical calculations, the following values are used:

$$k_{\max}^k = 1 \times 10^4; \quad \varepsilon^k = 0.05; \\ k_{\text{bushing}} = 3 \times 10^5; k_{\text{rigid}} = 2 \times 10^3 k_{\text{bushing}}; \quad |\Delta\hat{\theta}_0^Q| = 0.0032^\circ; \quad \varepsilon^c = 0$$

The results obtained for Case study 1 using the proposed formulation are presented in Fig. 2.9. First, Fig. 2.9(a) shows the optimized mechanism layout represented by rigid blocks along with the actual four-bar linkage mechanism interpreted from the rigid blocks and the states of the block-connecting and anchoring springs. Fig. 2.9(b) and Fig. 2.9(c) respectively show the converged design variables for the block-connecting springs and those for the anchoring springs, which are used to determine the topology of the synthesized mechanism. These figures show good convergence of the design variables to their lower bound value of 0 or upper bound value of 1. As shown in Fig. 2.9(c), only two bushings (modeled by anchoring springs) are identified in the final mechanism among the 36 anchoring springs due to the constraint expressed by Eq. (2.21d). Fig. 2.9(d) shows the iteration histories of the

objective and constraint functions. After convergence, the mean value of the work transmittance efficiency function (black line) goes nearly to 1, indicating that the converged linkage mechanism has 1 DOF. (It was shown in an earlier study (Ref. [7]) that if $\bar{\eta} = 1$, the corresponding mechanism has exactly 1 DOF.) The red and blue lines indicate the maximum value of the kinematic constraint functions and the value of the compliance constraint function, respectively. Clearly, all constraints are within the error bound, as shaded in green, at convergence.

From the results presented in Fig. 2.9, the proposed method is shown to find the topology and dimension of the target linkage mechanism successfully if the corresponding kinematic and compliance characteristics are given. Similar behaviors were observed in other tested problems. In the next case study, we aim to demonstrate why the simultaneous consideration of kinematic and compliance characteristics for mechanism synthesis is crucial.

2.4.2 Case study 2 - Demonstration of the advantage of the proposed method

The aim of Case study 2 is to demonstrate the critical advantage of the proposed method that considers the K&C characteristics simultaneously during mechanism synthesis over a method that considers K&C characteristics sequentially. The known reference linkage mechanism is shown in Fig. 2.10(a). We will investigate how effective the proposed method is when used to synthesize the mechanism back with

the given target path $\hat{\mathbf{r}}_i^Q$ at its end effector location Q and the specified compliance expressed as $\Delta\hat{\mathbf{x}}_0^Q$ under external vertical load \mathbf{F}_0^{ext} , as sketched in Fig. 2.10(b). Specifically, the desired (target) path is a path including a crunode, which is to be generated by the input rotation motion of link AB of the reference linkage, given by

$$\phi_{t^*}^{Input} = \frac{\pi}{18} t^* \quad (t^* = 1, 2, \dots, 36) \quad (2.39)$$

Here, a path including a crunode is selected because the mechanism used to generate a path overlapping a path curve is generally regarded as difficult to synthesize by a numerical method [7]. For the compliance characteristics, the displacement in the x -coordinate of the end-effector when external force is applied at the initial position is used, as shown in Fig. 2.10(b).

Fig. 2.11 illustrates the problem definition of Case study 2. Fig. 2.11(a) shows the design domain and the initial layout of the SBM employed for the mechanism synthesis. All statuses of the design domain and the SBM are identical to those used in case Study 1 without the locations of the end-effector and the output block. The output block in Case study 2 is the bottom-middle block and the end-effector is located at the center of the output block in the initial layout. The conditions for the kinematic and compliance analyses for optimization are identical to those in Fig. 2.10(b), and the kinematic and compliance constraint functions are as follows:

$$\psi_{t^*}^k(\mathbf{v}_{t^*}) = \|\mathbf{r}_{t^*}^Q - \hat{\mathbf{r}}_{t^*}^Q\| \leq \varepsilon^k \quad (t^* = 1, 2, \dots, 36) \quad (2.40a)$$

$$\psi^c(\mathbf{v}_0) = -\left(\left|\Delta x_0^{\mathcal{O}}\right| - \left|\Delta \hat{x}_0^{\mathcal{O}}\right|\right) \leq \varepsilon^c \quad (2.40b)$$

Unlike in Case study 1, the compliance constraint equation (2.40b) requires the absolute value $\left|\Delta x_0^{\mathcal{O}}\right|$ of the x -directional displacement to exceed the target value $\left|\Delta \hat{x}_0^{\mathcal{O}}\right|$. The values of the parameters used for this case are $k_{\text{bushing}} = 2 \times 10^3$ and $\left|\Delta \hat{x}_0^{\mathcal{O}}\right| = 0.005$, while the unlisted parameter values are identical to those given in Case study 1.

Before presenting the result by the proposed method, we initially solve this problem using a two-step sequential method which combines existing approaches, as depicted in Eq. (2.26). The first step is to perform topology optimization to determine the topological layout of a synthesized mechanism considering only the kinematic condition that requires the synthesized linkage mechanism to generate the target path which includes a crunode. This step is followed by the second step of shape optimization using the linkage mechanism synthesized in the first step. During the second step, the dimensions of the linkage that satisfy the prescribed K&C characteristics are determined.

The optimization results according to the two-step sequential method with different initial design variables or configurations are presented in Fig. 2.12(a) and (b). Note that in these figures, blocks of the same color form a single rigid body or link as a whole. Apparently, mechanisms to generate the target path may not be unique (within

the tolerance error) in general, and in this case, two mechanisms with different topologies are obtained after the first step of topology-optimization-based synthesis depending on the initial design variables. Specifically, a six-bar linkage mechanism is synthesized (see the middle figure of Fig. 2.12(a)) if all design variables ($\xi_{b_i}^T, \xi_{a_j}^T$) controlling the mechanism topology are set to 0.1 while a four-bar linkage mechanism (see the middle figure of Fig. 2.12(b)) is synthesized if they ($\xi_{b_i}^T, \xi_{a_j}^T$) are set to 0.5. (Note that the design variables for anchoring springs attached to the input block are excluded from this setting, as they should retain their values to allow the input block to rotate around the bottom left corner during the optimization process.)

Using the synthesized mechanisms with the topologies identified in the first step, shape optimization is performed to satisfy both the target K&C constraints. These results are presented as the final figures in Fig. 2.12(a) and (b). Clearly, the six-bar mechanism among two synthesized mechanisms in the first step fails to satisfy all of the required K&C characteristics. Although the use of initial ($\xi_{b_i}^T, \xi_{a_j}^T$) values equal to 0.5 happens to satisfy the target K&C constraints, the message from this example is clear. The overall design process consisting of two steps of sequential optimization may be repeated iteratively, which overshadows the use of an automated optimization-based design method. This situation requires the proposed method that undertakes an optimization for mechanism synthesis considering the K&C

characteristics simultaneously. Note that when using the proposed optimization method, both the topology and shape optimization steps are integrated into a single formulation.

Fig. 2.13 shows the optimization results according to the proposed approach Eq. (2.21), as obtained with different initial topology-controlling design variables. Irrespective of the initial design variables, the proposed method yields a mechanism with the same topology, i.e., a four-bar linkage mechanism. Although the states of block connections are not equivalent in the two synthesized mechanisms, the geometries of the identified mechanisms resulting from the final SB layouts are virtually identical. Because the proposed method is not so sensitive to the initial guesses when both K&C characteristics are considered and successfully yield the desired mechanism, the advantage of the proposed single-step unified approach over the two-step sequential approach is readily apparent. In the next case study, we will demonstrate how effective the proposed method can be in more realistic design problem, in which there is no reference mechanism available.

2.4.3 Case study 3 - Application to the design of a 2D vehicle suspension

This case study presents the application of the developed optimization-based mechanism synthesis method to the design of a more realistic mechanism, in this case a two-dimensional simplified version of a vehicle's suspension mechanism.

The motivation of this Case study is to determine if we can design a suspension mechanism as an alternative to the commonly used double-wishbone suspension (the 2D version of which is modeled as a four-bar linkage mechanism) using the developed method. Specifically, we would like to find a suspension mechanism that maintains kinematic characteristics nearly identical to those of the double-wishbone suspension (a four-bar linkage in the 2D case) while the lateral stiffness of a vehicle equipped with the suspension is improved. Because smaller deformation of the contact patch of a wheel subjected to a certain set of resultant forces to the wheel helps improve the vehicle response onto the steering input [45, 49], we aim to find a new suspension, the deformation of which is smaller than that by the double-wishbone suspension. The specific target values will be given below.

With this motivation in mind, Fig. 2.14(a) illustrates the entire analysis domain discretized by 5×3 rigid blocks in which the design and non-design domains are discretized by the left 5×2 and rightmost 5×1 rigid blocks (darkly shaded), respectively. While the non-design domain represents a wheel carrier, the design domain is the area where a 2D version of a vehicle suspension is to be synthesized by the proposed method. An explanation is necessary of the modeling technique based on the SBM. First, the rightmost 5×1 rigid blocks are rigidly connected to each other and the wheel center is located at the center of the middle block among the five blocks. Second, the suspension mechanism to be synthesized in the design domain should be connected not only to the wheel carrier but also to the vehicle chassis (this

is not explicitly shown in Fig. 2.14(a), but see Fig. 2.1 for more details) lying next to the left side of the design domain. Note that the vehicle chassis for the K&C analysis can be considered as the ground because only the relative motion between the chassis and wheel carrier is of primary concern with regard to suspension design. While the motion between the wheel carrier and the vehicle suspension can be fully governed by the kinematic characteristics, the motion between the chassis and the vehicle suspension is governed by both the kinematic and the compliance characteristics. Therefore, the use of elastically acting bushings must be considered when connecting the chassis and the vehicle suspension. Accordingly, the proposed multifunction anchoring springs can play a pivotal role in representing both the kinematic and compliance characteristics, as explained in Chapter 2.1. Specifically, all left corners of the leftmost blocks in the design domain are connected to the chassis (ground) by anchoring springs.

As the target kinematic characteristics, the motion of the wheel center is specified as the wheel goes up and down. This can be expressed as

$$\psi_{t^*}^{k(1)} = \left| x_{t^*}^Q - \hat{x}_{t^*}^Q \right| \leq \varepsilon^{k(1)}; \quad \psi_{t^*}^{k(2)} = \left| \theta_{t^*}^Q - \hat{\theta}_{t^*}^Q \right| \leq \varepsilon^{k(2)} \quad (2.41)$$

where $\varepsilon^{k(1)} = 0.0015$ and $\varepsilon^{k(2)} = 0.015^\circ$. The target values, the spatial location ($\hat{x}_{t^*}^Q$ and $\hat{y}_{t^*}^Q$) of the wheel center and its orientation ($\hat{\theta}_{t^*}^Q$), are given in the form of discrete data at 18 time steps in Table 2.1. The specific values in Table 2.1 are taken from the motion of the wheel center of a two-dimensional version of a typical double-

wishbone suspension (which is a four-bar linkage). For the kinematic analysis during the mechanism synthesis step, a value of $k_{\max}^k = 2 \times 10^3$ is used.

As the target compliance characteristics, the horizontal displacement (Δx_0^Q) and rotation ($\Delta \theta_0^Q$) at the wheel center point Q at time step $t^* = 0$ are required not to vary more than the corresponding specified values when external loads are applied to the wheel center. As illustrated in Fig. 2.14(b), external horizontal force $\mathbf{F}_0^{ext} = -1000\mathbf{e}_x$ and external moment $\mathbf{M}_0^{ext} = -270\mathbf{e}_x \times \mathbf{e}_y$ ($\mathbf{e}_x, \mathbf{e}_y$: unit vectors in the horizontal and vertical directions) are applied to center point Q while its vertical displacement at $t^* = 0$ is not allowed to move; i.e., $y_0^Q = 0$. The constraints imposed on the displacement of the center point can be written as

$$\psi^{c(1)} = |\Delta x_0^Q| \leq \varepsilon^{c(1)}; \quad \psi^{c(2)} = |\Delta \theta_0^Q| \leq \varepsilon^{c(2)} \quad (2.42)$$

where $\varepsilon^{c(1)} = 2 \times 10^{-6}$ and $\varepsilon^{c(2)} = 0.0015^\circ$. It should be noted that the set value of $\varepsilon^{c(1)}$ is smaller than the typical values ($\varepsilon^{c(1)} = 3 \times 10^{-6}$) used for a double-wishbone suspension to improve the lateral stiffness of a vehicle equipped with the suspension mechanism to be designed. The k_{bushing} value is so chosen to represent the stiffness of commonly used bushing elements, $k_{\text{bushing}} = 2 \times 10^8$. As in the previous case studies, k_{rigid} is set to $k_{\text{rigid}} = 2 \times 10^3 k_{\text{bushing}}$. The results related to this case study are presented in Fig. 2.15 to Fig. 2.17.

Fig. 2.15(a) shows the final optimized layout represented by the SBM, showing a six-bar linkage mechanism, as indicated by the thick blue lines in the figure. Fig. 2.15(b) explains how the six-bar linkage mechanism is represented in the SBM. On the left-hand side figure of Fig. 2.15(b), only block-connecting and anchoring springs having the upper bound stiffness value are sketched. Using these springs, the following linkage layout interpretations are possible. First, block-connecting springs 1 and 2 make Blocks 1 and 2 behave as a single link. Blocks 9 and 10 also behave as a single link due to the presence of block-connecting springs 17 and 18. Because Blocks 7 and 8 are connected only at a single corner by block-connecting spring 14, they behave as two links connected by a revolute joint. Likewise, block-connecting spring 34 connects Blocks 7 and 9 by a revolute joint. Block-connecting springs 4, 16, and 20 connect Blocks 2, 8, and 10 to the wheel carrier by revolute joints, respectively. With regard to the anchoring springs, Blocks 1 and 7 are connected to the chassis (ground) by bushings, as represented by anchoring springs 1 and 7. Note that these springs serve to connect these blocks to the chassis by a revolute joint in the kinematic analysis. Blocks 3, 4, 5, and 6 are floating blocks not affecting the configuration of the optimized layout even though they are connected to the skeletal blocks by not converged springs. (The K&C characteristics of the result mechanism do not change even if the floating blocks are detached and the more explanation about floating blocks is given in Appendix B.) Based on these analyses, the optimized layout represented in the SBM can be identified as a six-bar linkage mechanism (four rigid bodies represented by a set of blocks, the wheel carrier, and

the chassis). The converged values of the topology design variables (ξ^T) controlling the stiffnesses of the block-connecting and anchoring springs are shown in Fig. 2.15(c) and (d), respectively. Fig. 2.15(c) shows that several design variables did not reach either the upper or lower bound values. However, the spring stiffnesses, which are controlled by these design variables, do not affect the actual kinematic and compliance characteristics of the resulting mechanism; no block-connecting spring connecting any two of the floating blocks (Blocks 3, 4, 5, and 6) affects the layout of the final optimized mechanism. On the other hand, the stiffnesses of all anchoring springs reached their upper or lower bound value, as demonstrated in Fig. 2.15(d). Owing to constraint equation Fig. 2.15(d) (with $n = 2$), only two anchoring springs attained the maximum stiffness value.

The iteration histories of the objective and the constraint functions are plotted in Fig. 2.16. Fig. 2.16(a) shows that the mean value of the work transmittance efficiency function $\bar{\eta}$ converges to 1, implying that the synthesized mechanism has the correct DOF, which is 1. This is an important convergence criterion of the proposed synthesis algorithm. Fig. 2.16(b) and Fig. 2.16(c) show the convergence histories of the kinematic and the compliance constraints, respectively. At convergence, the convergence criteria imposed on the constraints are satisfied because $\max(\psi_t^{k(1)}) = 0.0015$, $\max(\psi_t^{k(2)}) = 0.015^\circ$, $\psi^{c(1)} = 1.99 \times 10^{-6}$, and $\psi^{c(2)} = 0.0011^\circ$.

Several snapshots of the intermediate and final layouts of the SBM at different wheel center locations ($y_i^Q = 0.05, 0, \text{ and } -0.05$) are shown in Fig. 2.17. The block-connecting and anchoring springs are not shown in this figure, but the evolution of the block shapes, governed by design variable ξ^X , is clearly shown. After the 150th iteration, the synthesized mechanism starts to become identifiable.

It is worthwhile to compare the performance of the proposed simultaneous formulation and that of the two-step sequential formulation for this case. These results are compared in Fig. 2.18, which shows that unlike the proposed method, yielding a six-bar linkage mechanism that successfully satisfies all of the required K&C characteristics, the sequential method yields a four-bar linkage that cannot satisfy the required compliance characteristics, instead only satisfying the kinematic characteristics. As noted in the caption of Fig. 2.18, the same initial guesses of the design variables are used for both formulations. It would be possible to find the same six-bar linkage as yielded by the proposed method if many different initial guesses were attempted for the two-step sequential formulation, but such a process is not feasible for use for streamlined optimization-based mechanism synthesis.

2.5 Summary

All previous studies on the topic of topology optimization of rigid-body linkage mechanisms were limited to the synthesis of mechanisms considering only kinematic characteristics. Here, we developed a new topology-optimization-based linkage mechanism synthesis method that considers both kinematic and compliance characteristics simultaneously during the iteration of the optimization process. Its effectiveness was demonstrated through case studies. As the ground model for the synthesis, the SBM (spring-connected rigid block model), as developed for synthesis considering kinematic characteristics, is used in this study, but the proposed approach to make block-connecting and anchoring springs multifunctional depending on the analysis type, kinematic or compliance, was found to be critically useful. Accordingly, the SBM framework using rigid blocks and stiffness-varying springs was also found to be useful for when simultaneously considering the K&C formulation, and an appropriate simultaneous formulation was proposed. Some findings from the case studies considered can be summarized as follows.

1. It was difficult or required repeated optimization runs using different initial guesses to find successfully optimized results if the two-step sequential formulation based on conventional approaches is used.
2. For the considered design problems, including the synthesis of a 2D suspension mechanism, the proposed simultaneous formulation yielded successfully optimized mechanisms satisfying all of the required K&C characteristics.

3. Especially during the design of a 2D suspension mechanism, the proposed simultaneous formulation yielded an unconventional six-bar linkage mechanism. For the synthesis, the wheel motion of a reference four-bar linkage mechanism was used as the target kinematic characteristics, but tighter constraints imposed on the target compliance characteristics were responsible for synthesizing the six-bar linkage mechanism, in contrast to the reference mechanism.

As future studies or practical applications, the proposed method can be extended to deal with the synthesis of three-dimensional mechanisms. While the bushing stiffness is fixed in the present work, it will be more practical if the value of the bushing stiffness is also simultaneously designed within the proposed formulation. In spite of some remaining tasks and issues that require further consideration, this study is expected to contribute to the advancement of our knowledge of topology optimization methods for linkage mechanisms.

Table 2.1 Data of the eighteen points for target motion at the wheel center

t^*	0	1	2	3	4	5	6	7	8	9
y_t^Q	0	0.01	0.02	0.03	0.04	0.05	0.06	0.07	0.08	0.09
\hat{x}_t^Q	0	0.00012	0.00006	-0.00033	-0.00098	-0.0019	-0.0031	-0.0045	-0.0062	-0.0082
$\hat{\theta}_t^Q$	0	0.37	0.77	1.20	1.60	2.10	2.59	3.10	3.64	4.20

t^*	10	11	12	13	14	15	16	17	18
y_t^Q	-0.01	-0.02	-0.03	-0.04	-0.05	-0.06	-0.07	-0.08	-0.09
\hat{x}_t^Q	-0.00039	-0.0011	-0.0021	-0.0034	-0.0049	-0.0068	-0.0090	-0.012	-0.015
$\hat{\theta}_t^Q$	-0.34	-0.67	-0.97	-1.25	-1.50	-1.72	-1.91	-2.06	-2.17

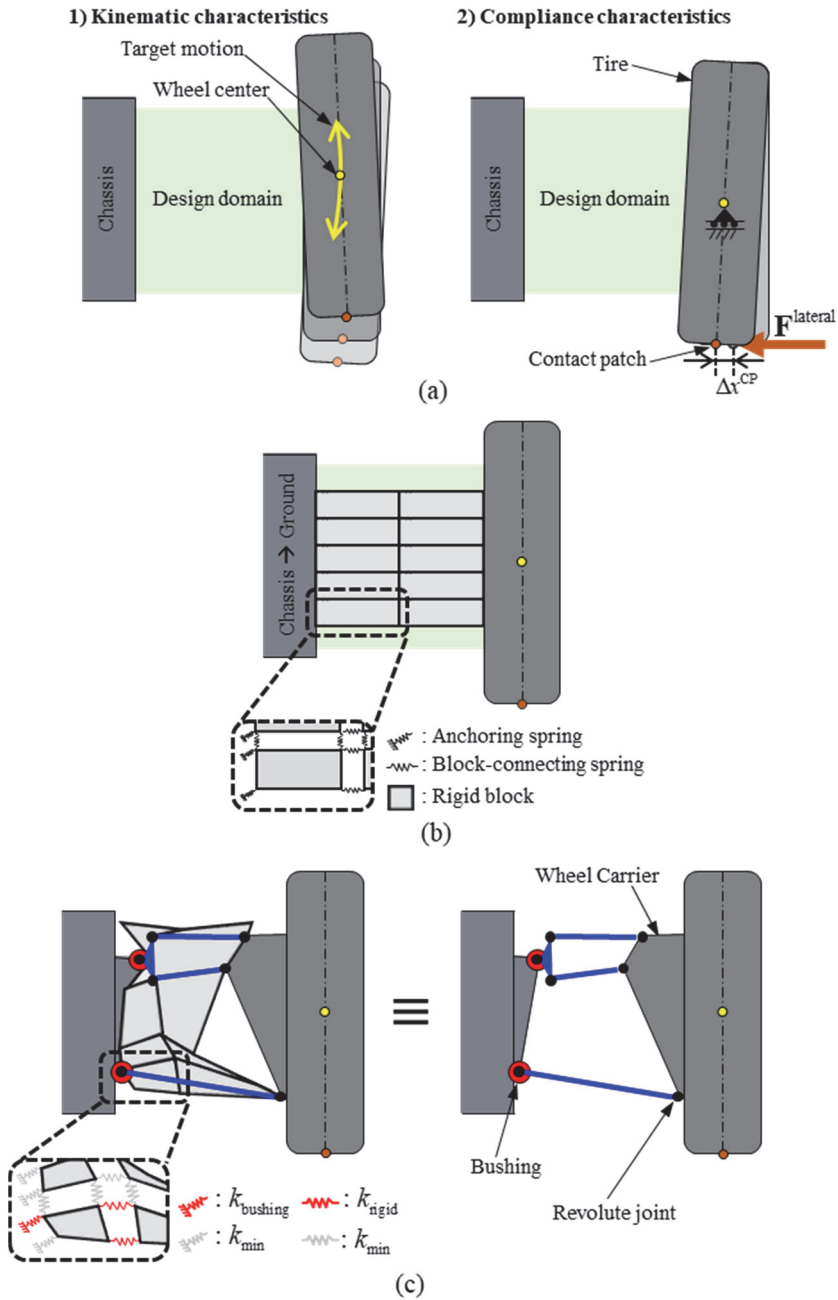
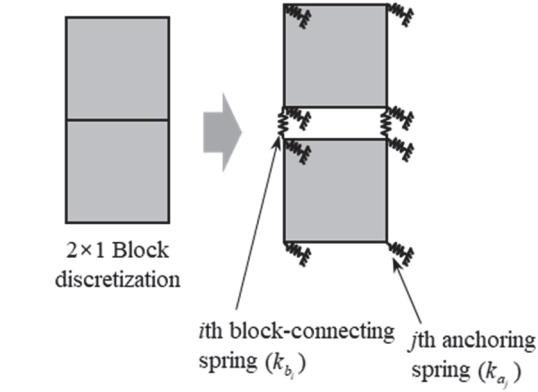


Fig. 2.1 Example of a design process using the proposed method: (a) problem definition for a 2D vehicle suspension, (b) modeling with the SBM, and (c) layout of the SBM after optimization and the corresponding equivalent linkage mechanism



- Existing method

(only for kinematic characteristics)

$$\text{---}\text{w}\text{---} : k_{b_i} \rightarrow k_{b_i}^k(\zeta_{b_i}^T)$$

$$\text{---}\text{w}\text{---} : k_{a_j} \rightarrow k_{a_j}^k(\zeta_{a_j}^T)$$

- Proposed method

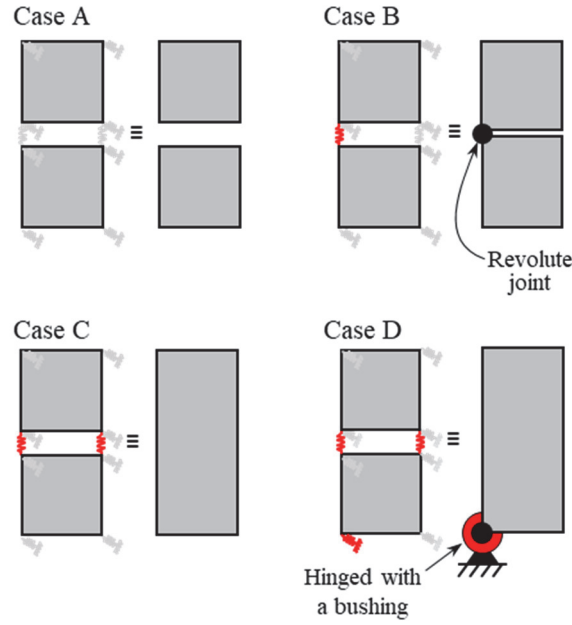
(both for kinematic and compliance characteristics)

$$\text{---}\text{w}\text{---} : k_{b_i} \rightarrow k_{b_i}^k(\zeta_{b_i}^T) \ \& \ k_{b_i}^c(\zeta_{b_i}^T)$$

$$\text{---}\text{w}\text{---} : k_{a_j} \rightarrow k_{a_j}^k(\zeta_{a_j}^T) \ \& \ k_{a_j}^c(\zeta_{a_j}^T)$$

$\zeta_{b_i}^T$: design variable for the i th block-connecting spring stiffness
 $\zeta_{a_j}^T$: design variable for the j th anchoring spring stiffness

Fig. 2.2 The design domain discretized by 2x1 blocks connected by block-connecting and anchoring springs. The multi-functionality of the springs in the proposed method is compared with the mono-functionality in the existing method







Spring type		Existing method	Proposed method
Block-connecting spring (k_b)		$k_b^k(\xi_{\max}^T) = k_{\max}^k$	$k_b^k(\xi_{\max}^T) = k_{\max}^k, k_b^c(\xi_{\max}^T) = k_{\text{rigid}}$
		$k_b^k(\xi_{\min}^T) \approx 0$	$k_b^k(\xi_{\min}^T) \approx 0, k_b^c(\xi_{\min}^T) \approx 0$
Anchoring spring (k_a)		$k_a^k(\xi_{\max}^T) = k_{\max}^k$	$k_a^k(\xi_{\max}^T) = k_{\max}^k, k_a^c(\xi_{\max}^T) = k_{\text{bushing}}$
		$k_a^k(\xi_{\min}^T) \approx 0$	$k_a^k(\xi_{\min}^T) \approx 0, k_a^c(\xi_{\min}^T) \approx 0$
$\xi_{\min}^T \leq \xi_b^T, \xi_a^T \leq \xi_{\max}^T$ ($\xi_{\min}^T = 10^{-6}, \xi_{\max}^T = 1$)			

Fig. 2.3 Representative cases with upper or lower bound stiffness values. Case A: disconnected, Case B: Connected by a revolute joint, Case C: Rigidly connected, and Case D: Hinged with a bushing

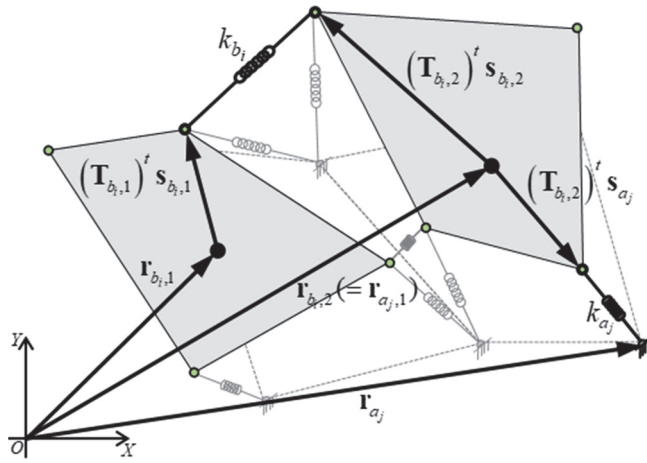


Fig. 2.4 A snapshot of two rigid blocks in a position after being moved by a given input motion or external force

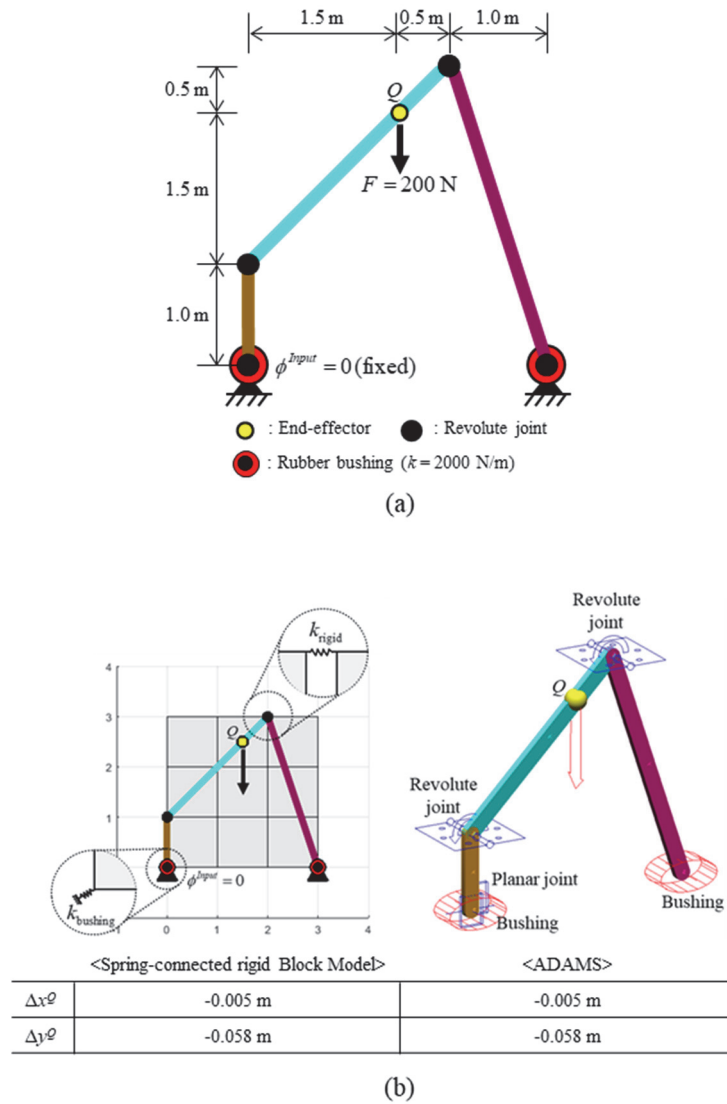


Fig. 2.5 An example to validate the compliance analysis using the SBM with the suggested spring stiffness values: (a) linkage geometry and loading/boundary conditions, and (b) comparison of the analyses using the SBM model (left) and the original model with the ADAMS software package (right)

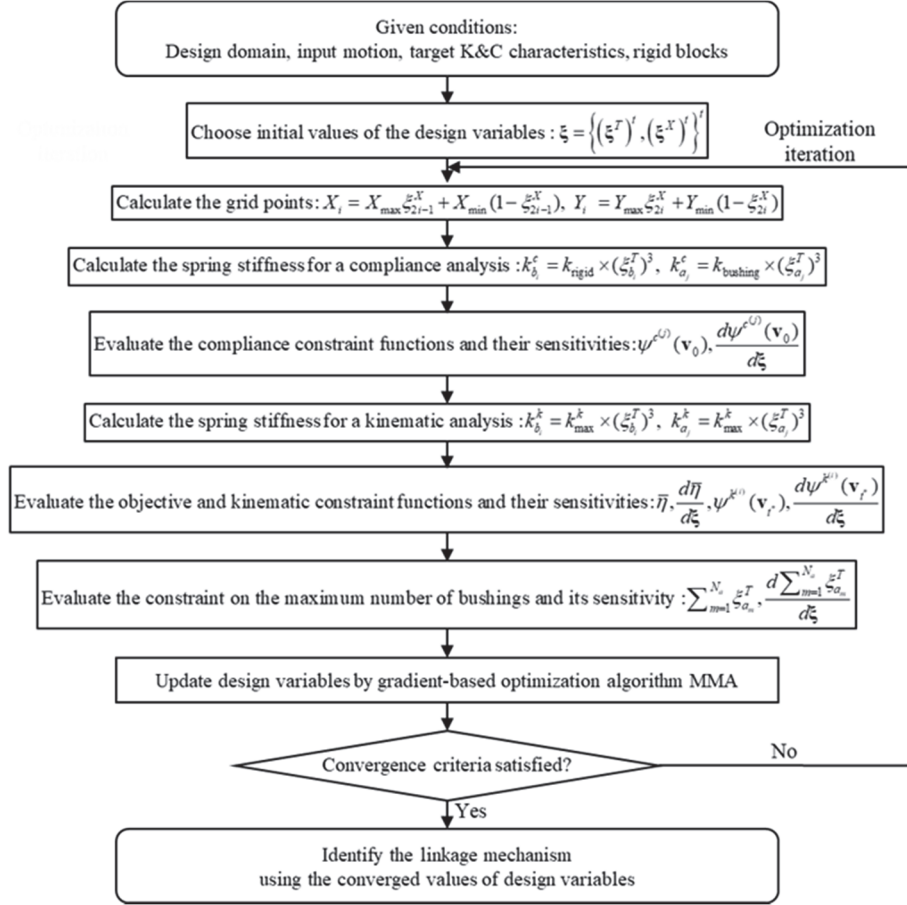


Fig. 2.6 Flow chart for topology optimization of linkage mechanisms simultaneously considering kinematic and compliance characteristics

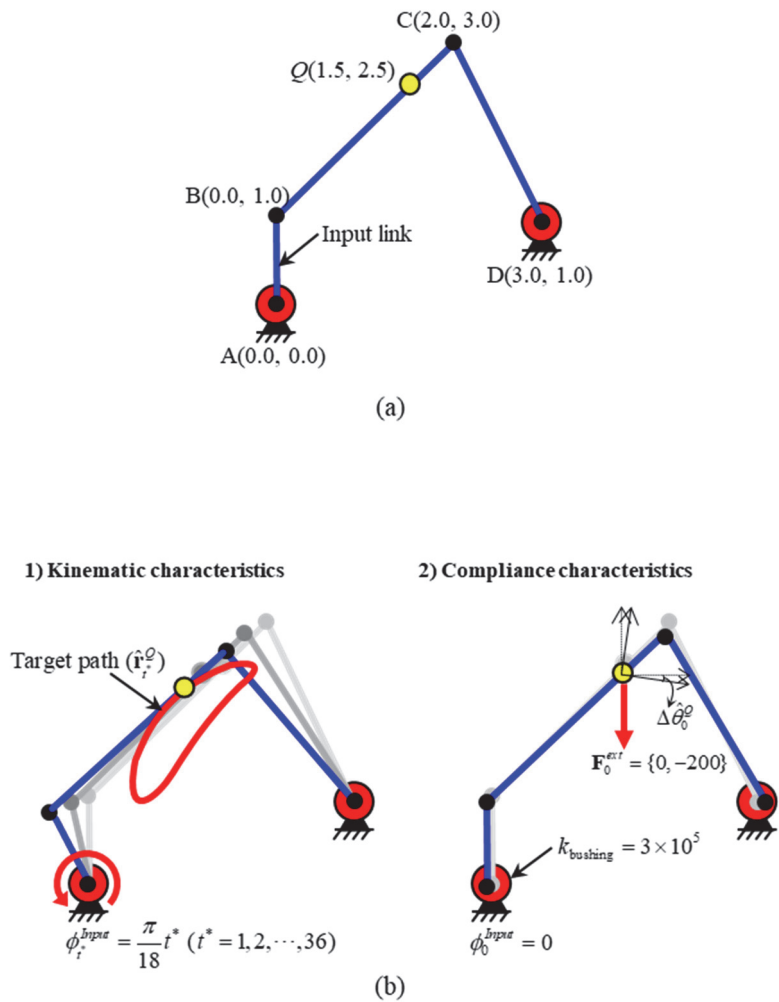


Fig. 2.7 (a) Layout of the reference linkage mechanism for Case study 1 and (b) illustrations of the K&C characteristics used for the mechanism synthesis

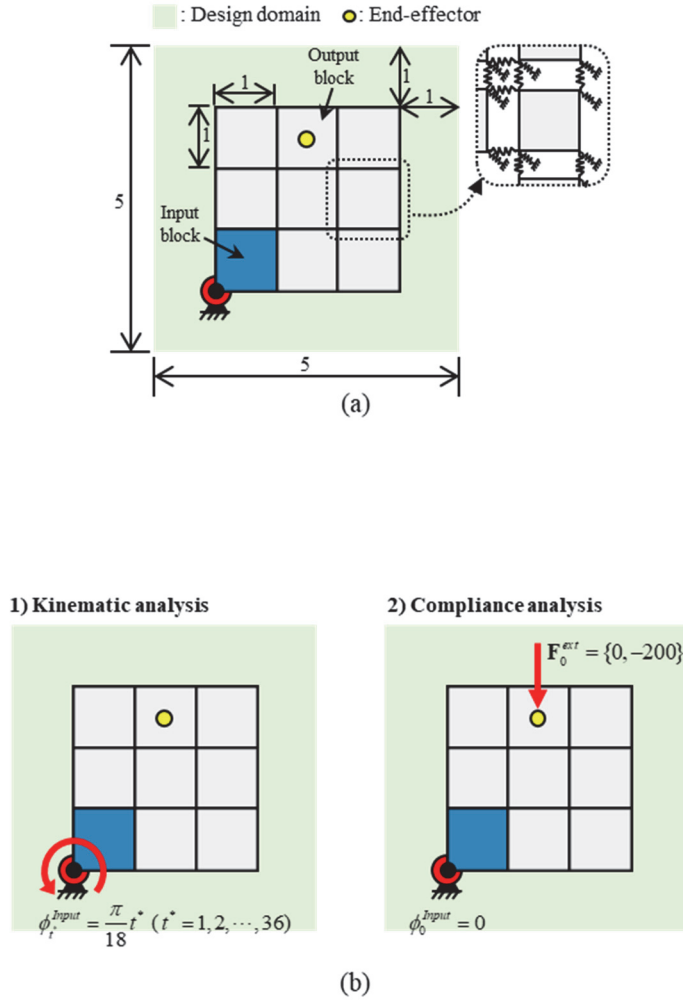


Fig. 2.8 SBM to solve Case study 1: (a) design domain discretized by rigid blocks at the initial configuration and (b) illustration of how to prescribe the desired conditions using the SBM for the K&C analyses

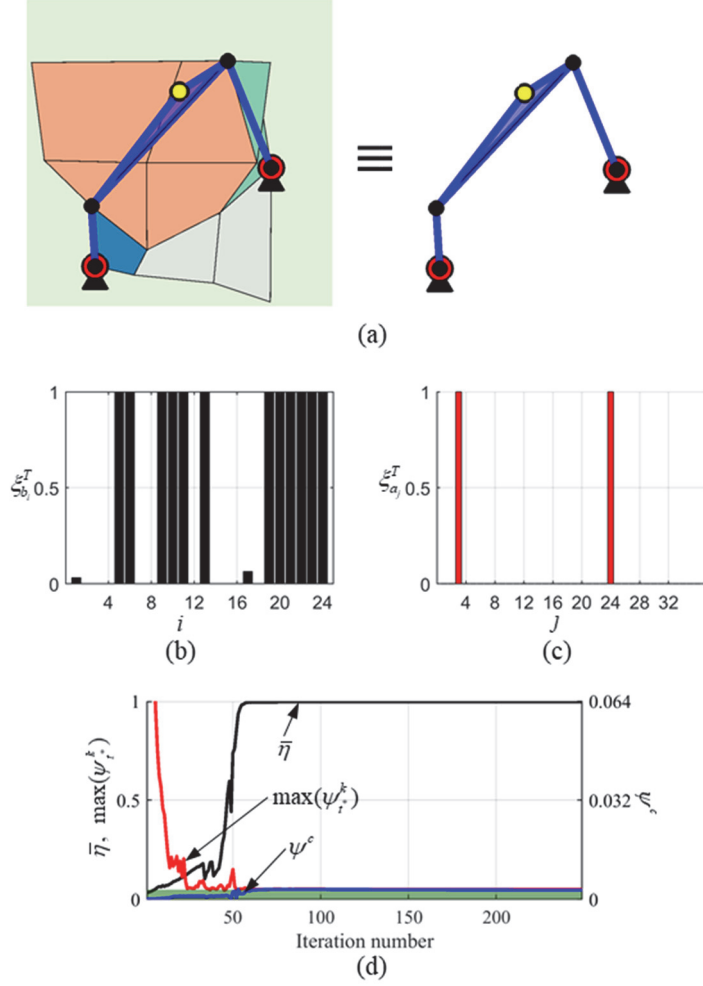


Fig. 2.9 Optimization results for Case study 1: (a) final optimized layout of the SBM (left) and its equivalent mechanism (right), (b) design variables controlling the block-connecting spring stiffnesses at convergence, (c) design variables controlling the anchoring spring stiffnesses at convergence, and (d) iteration histories of the objective and the constraint functions

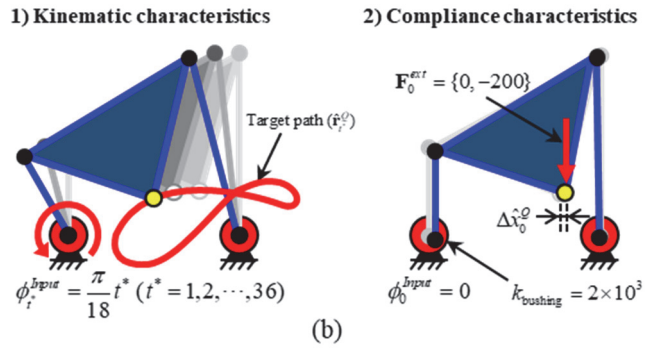
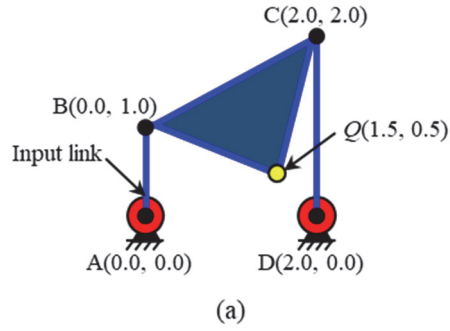


Fig. 2.10 (a) Layout of the reference linkage mechanism for Case study 2 and (b) analysis conditions for the K&C characteristics

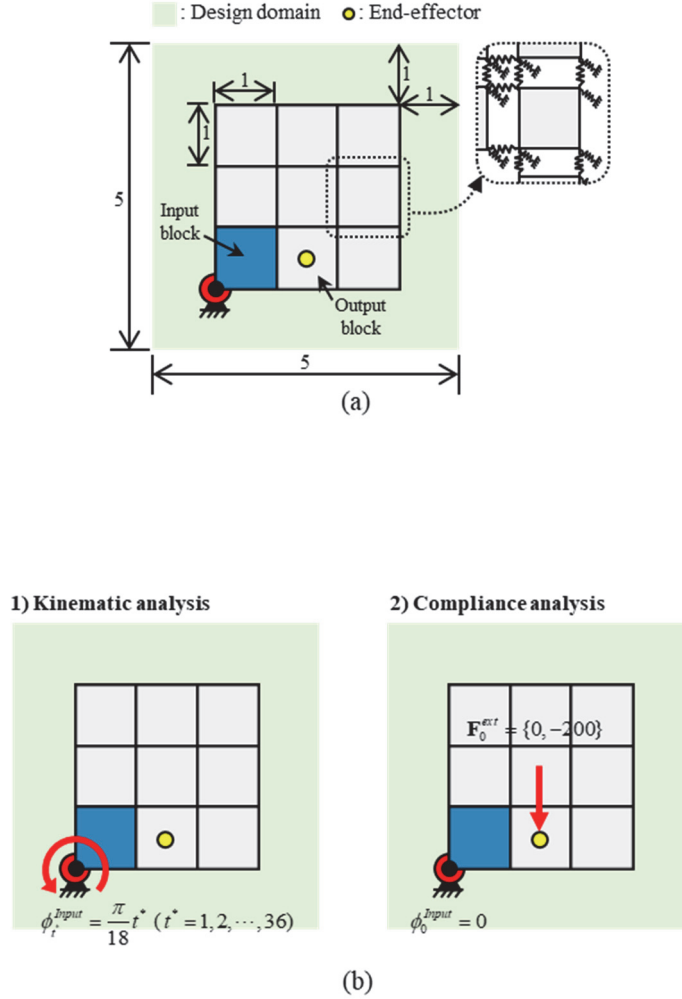
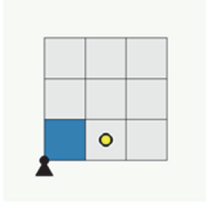
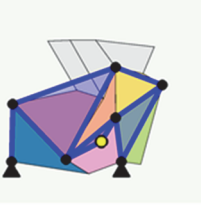
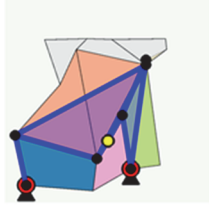
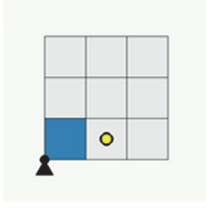
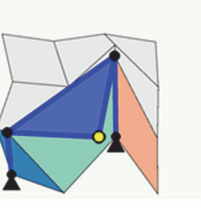
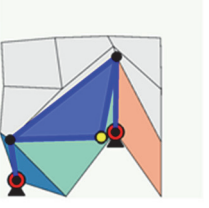


Fig. 2.11 SBM to solve Case study 2: (a) design domain discretized by rigid blocks at its initial configuration and (b) illustration of the method used to prescribe the desired conditions using the SBM for K&C analyses

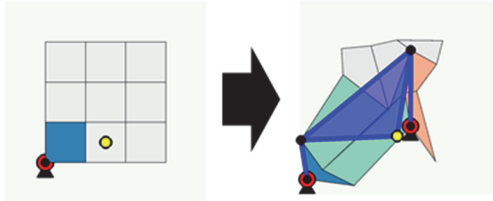
State	Initial configuration ($\xi_{b_i}^T, \xi_{a_j}^T = 0.1$)	After topology optimization considering kinematic constraints	After shape optimization considering K&C constraints
Layout			
$\max(\psi_i^k)$	-	0.0482 (satisfied)	0.0883 (failed)
ψ^c	-	-	0.0031 (failed)

(a)

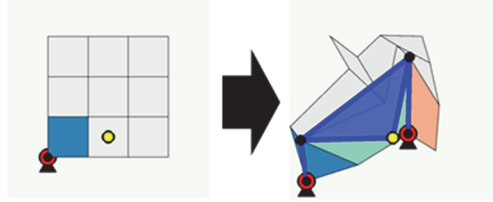
State	Initial configuration ($\xi_{b_i}^T, \xi_{a_j}^T = 0.5$)	After topology optimization considering kinematic constraints	After shape optimization considering K&C constraints
Layout			
$\max(\psi_i^k)$	-	0.0478 (satisfied)	0.0480 (satisfied)
ψ^c	-	-	0.0053 (satisfied)

(b)

Fig. 2.12 Optimization results for Case study 2 obtained by the two-step sequential formulation (2.26) for the initial values for topology-controlling design variables ($\xi_{b_i}^T, \xi_{a_j}^T$) set to (a) 0.1 and (b) 0.5

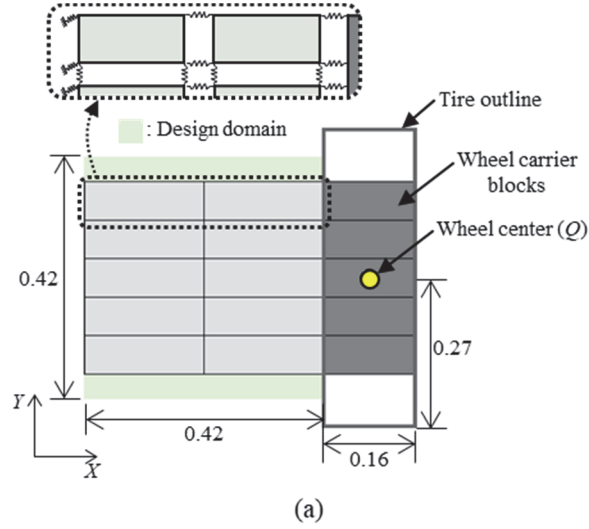
State	Initial configuration ($\xi_{b_i}^T, \xi_{a_j}^T = 0.1$)	After topology optimization considering K&C characteristics
Layout		
$\max(\psi_i^k)$	-	0.0493 (satisfied)
ψ^e	-	0.0054 (satisfied)

(a)

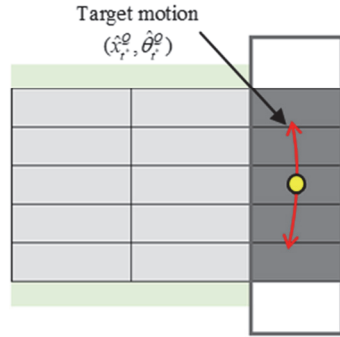
State	Initial configuration ($\xi_{b_i}^T, \xi_{a_j}^T = 0.5$)	After topology optimization considering K&C characteristics
Layout		
$\max(\psi_i^k)$	-	0.0481 (satisfied)
ψ^e	-	0.0053 (satisfied)

(b)

Fig. 2.13 Optimization results for Case study 2 obtained by the proposed simultaneous formulation (2.21) for the initial values of topology-controlling design variables ($\xi_{b_i}^T, \xi_{a_j}^T$) set to (a) 0.1 and (b) 0.5

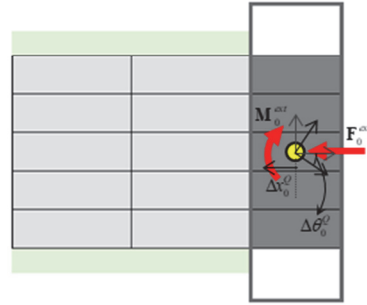


1) Kinematic analysis



Input motion : y_r^Q ($r^* = 1, 2, \dots, 18$)

2) Compliance analysis



(b)

Fig. 2.14 Problem definition for Case study 3 dealing with the synthesis of a 2D vehicle suspension: (a) analysis domain discretized by rigid blocks where the leftmost 5×2 rigid blocks are used to synthesize linkages (the rightmost 5×1 rigid blocks represent a wheel carrier), and (b) sketches explaining how to evaluate the target K&C characteristics

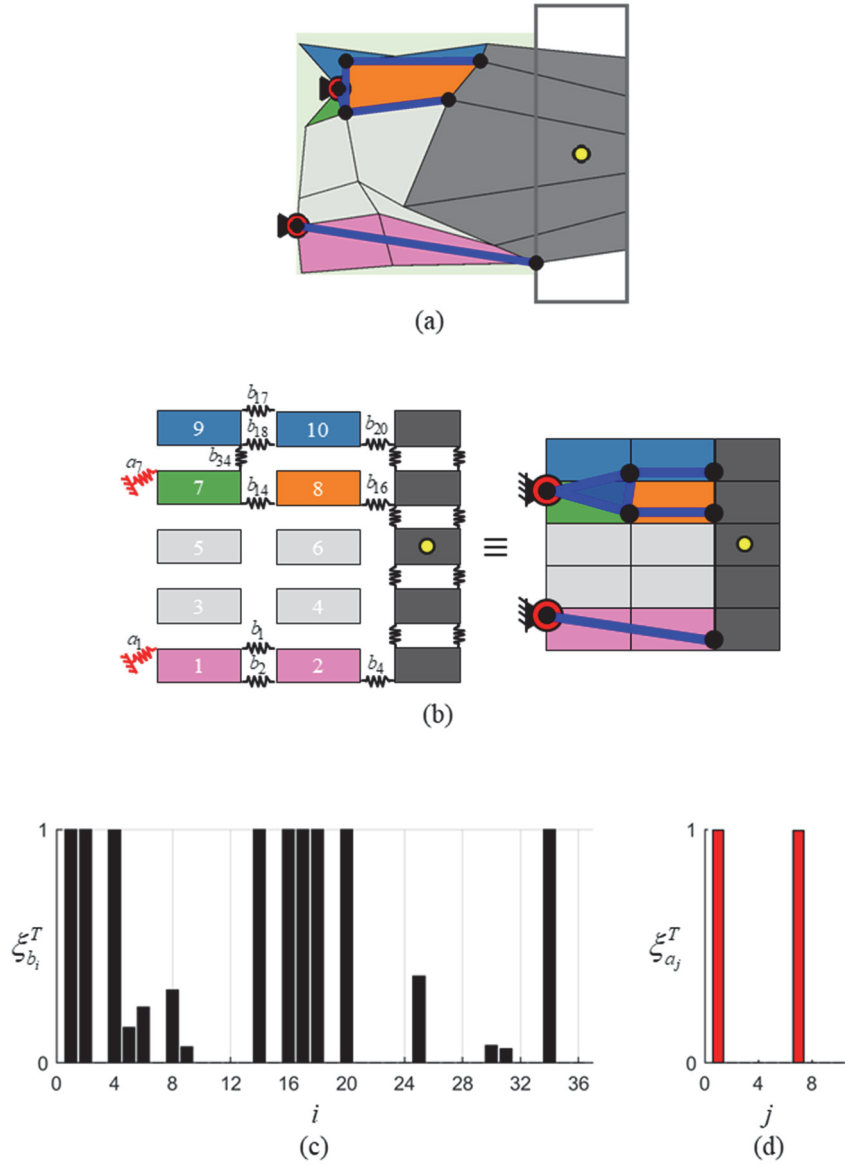
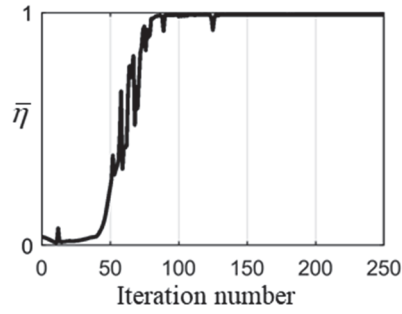
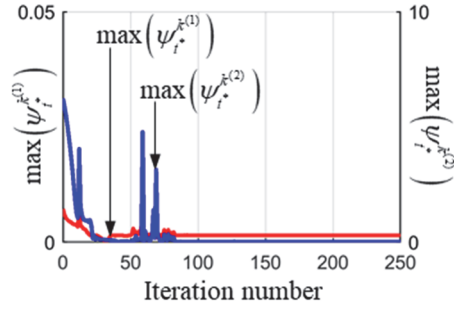


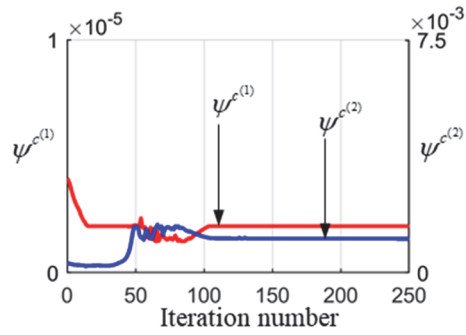
Fig. 2.15 Optimization results for the 2D vehicle suspension design problem:
 (a) final optimized layout (thick lines represent the synthesized links), (b) identified linkage mechanism (right) from the optimized layout expressed by rigid blocks connected by block-connecting and anchoring springs having a lower bound stiffness value, (c) converged values of the design variables for block-connecting springs, and (d) converged values of design variables of the anchoring springs



(a)



(b)



(c)

Fig. 2.16 Iteration histories for Case study 3: (a) the mean value of the work transmittance efficiency function, (b) kinematic constraint functions, and (c) compliance constraint functions

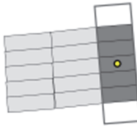
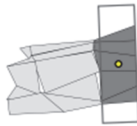
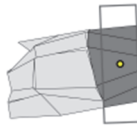
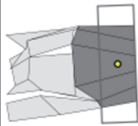
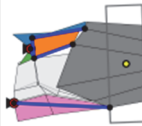
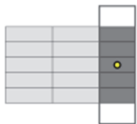
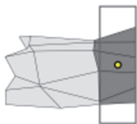
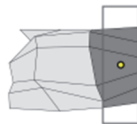
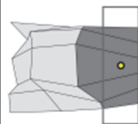
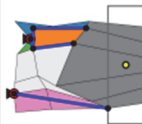
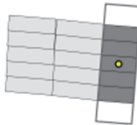
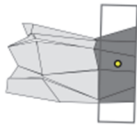
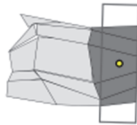
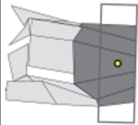
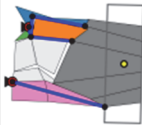
Iteration number	0 (Initial)	50	100	150	250 (Converged)
$y_i^Q = 0.05$					
$y_i^Q = 0.05$					
$y_i^Q = -0.05$					

Fig. 2.17 Intermediate and final layouts at different time steps of the synthesized linkage mechanism for the 2D vehicle suspension

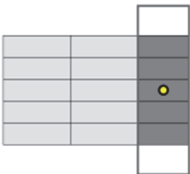
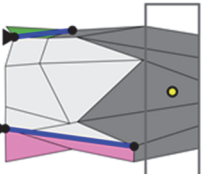
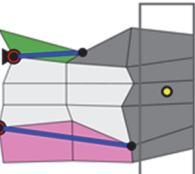
State	Initial configuration	After topology optimization considering kinematic constraints	After shape optimization considering K&C constraints
Layout			
$\max(\psi_t^{k(1)})$	-	0.0015 (satisfied)	0.0014 (satisfied)
$\max(\psi_t^{k(2)})$	-	0.0150 (satisfied)	0.0138 (satisfied)
$\psi^{e(1)}$	-	-	2.03×10^{-6} (failed)
$\psi^{e(2)}$	-	-	0.0016 (failed)

Fig. 2.18 Comparison of the optimization results for Case study 3 obtained by the two-step sequential formulation (2.26) using the same initial values of the design variables

CHAPTER 3.

Design of vehicle suspensions for rear using topology optimization method considering K&C characteristics

3.1 Overview

Vehicle suspension is a key part of whole vehicle systems since ride and handling (R&H) performances of a vehicle can differ how the vehicle suspension is designed. Especially, K&C characteristics of the vehicle suspensions are key parameters by which many R&H performances of the vehicles can be affected [8, 45, 46, 48, 51, 52]. Kinematic characteristics of a vehicle suspension are related to the wheel motion when the wheel goes up and down, and it is defined by the geometry of the suspension. Compliance characteristics are mainly defined by the geometry of the suspension and stiffnesses of bushings [45, 46, 52]. Especially, compliance characteristics can be defined by the wheel movement arisen from the deformation of bushings by the external forces such as lateral force, longitudinal force or aligning torque [46, 47, 53] shown in Fig. 3.1.

Traditionally, vehicle suspensions were sequentially synthesized like the way to synthesize any other types of linkage mechanisms. First, the engineer decides intuitively the basic concept of a vehicle suspension such as a topology. Second, the dimensions are synthesized and the stiffnesses of bushings are defined to meet the design requirements such as K&C characteristics [46, 49]. Many studies about design optimization of suspensions were conducted thus far, but only geometric parameters or bushing stiffness were mainly concerned [8, 46-48, 52-56]. On the other hand, some studies tried to investigate the atlas of the independent suspensions using number synthesis [51, 57], and topology optimization method only considering kinematic characteristics has been used to synthesize a vehicle suspension [8].

In this Chapter, we apply the topology optimization method for linkage mechanisms considering K&C characteristics to the design of spatial vehicle suspensions for rear. For doing that, there are two main issues to be addressed. First, the model suitable for the synthesize vehicle suspensions is needed. Second, stiffnesses of the bushings as well as the geometry of the suspension should be designed because compliance characteristics are defined by the geometry of the suspension as well as the stiffnesses of bushings. To resolve this, we develop a spatial spring-connected rigid block model for vehicle suspensions in contrary to the previous study [8] in which nonlinear bar based model was used. That is because the 3D SBM is more effective to represent linkage mechanisms with bushings. Fig. 3.2 is prepared to compare the differences between a nonlinear bar based model and a SBM. As shown in Fig. 3.2,

anchoring springs are used in both models to connect a rigid body to the ground. As the key idea for topology optimization considering K&C characteristics proposed in Chapter 2 is to utilize anchoring springs as bushings in a compliance analysis, the nonlinear bar based model also may be used for the proposed method. However, since many nonlinear bars share one anchoring spring, two more rigid bodies can be generated on the same anchoring spring at convergence. Since this result is not possible to implement in actual, post-processing should be needed [7, 8]. However, after the post-processing, the number of anchoring springs could increase because the rigid links should have their own fixed pivots, and it can make compliance characteristics changed. In contrary to the nonlinear bar based model, since a rigid block does not share anchoring springs to the other block in the SBM, the possibility to increase the number of bushings represented by anchoring springs does not exist in the SBM. The overview of the 3D SBM for synthesizing a vehicle suspension is shown in Fig. 3.3.

The outline of this Chapter is as follow. In Chapter 3.2, an explanation of a modeling and analysis of a spatial SBM will be given. In Chapter 3.3, the optimization formulation for designing a vehicle suspension will be presented, and also an explanation about the design variables will be given. In addition, since a gradient-based optimizer is used, sensitivity analysis will be also presented. To confirm the validity of the proposed method, two carefully selected design cases will be considered in Chapter 3.4. Concluding remarks are given in Chapter 3.5.

3.2 Modeling and analysis based on the spatial SBM

3.2.1 The spatial SBM for the design of a vehicle suspension

For designing a vehicle suspension with a spatial SBM, the spatial SBM should be represented the various types of the vehicle suspensions such as a double wishbone type or multilink type. (MacPherson strut type is not considered in this research because it is usually not used to vehicle suspension for the rear.) In addition, the components of vehicle suspensions such as spherical joints, revolute joints, rigid links, rigid arm, and elastically-behaving bushings should be able to be included in the SBM.

Fig. 3.4 shows the two blocks between the chassis and the wheel carrier. As shown in Fig. 3.4, block-connecting springs are attached to the adjacent corners of the blocks and anchoring springs are attached to the block corners. For synthesizing a vehicle suspension, the chassis of the car can be regarded as the ground because K&C characteristics are defined as relative motions of a vehicle suspension against the chassis. Therefore, the anchoring springs are only attached to the chassis-side corners of the chassis-side blocks.

As explained in Chapter 2, the spring stiffness is used in a multifunctional way, in which an anchoring spring at its maximum stiffness represents a rigid connection to the ground in a kinematic analysis while it represents the ground-anchored bushings in a compliance analysis. Therefore, the spring stiffness set to be different in two

analyses as shown in Fig. 3.4. Unlike the 2D, stiffness of the springs in a compliance analysis is presented as a vector form because stiffnesses of cylindrical bushings is varies in each direction. By the way, as stiffness of block-connecting springs only represents the connection between two points, only topology controlling design variable ($\xi_{b_i}^T$) is used to interpolate the stiffness of block-connecting springs. In contrary, as an anchoring spring represent a cylindrical bushing, design variable for bushing stiffness (ξ_j^B) is used as well as topology controlling design variable ($\xi_{a_j}^T$) to interpolate. The way how to interpolate spring stiffness by the design variables will be given in Chapter 3.3.

Fig. 3.5 shows relationships of two blocks depending on the spring stiffness. Four block-connecting springs are attached to the adjacent corners of the blocks and four anchoring springs are attached to the chassis-side corners of the chassis-side block. As shown in Fig. 3.5(a), if all the topology controlling design variables of the block-connecting springs are at their minimum, two blocks can move separately. If only one topology controlling design variable of block-connecting springs has the maximum value, two blocks will be connected by a spherical joint and if two have the maximum value, two blocks will be connected by a revolute joint that rotates around the axis connecting two points as shown in Fig. 3.5(b) and Fig. 3.5(c), respectively. In addition, if three or four topology controlling design variables of block-connecting springs have the maximum value, two blocks act as one rigid as shown in Fig. 3.5(d). At last, if one topology controlling design variable for

anchoring springs has the maximum value, the point where the anchoring spring is attached is anchored by a bushing in a compliance analysis regardless of the value of the design variable for bushing stiffness as shown in Fig. 3.5(e). (Note that, however, the point is anchored by a spherical joint in a kinematic analysis.)

3.2.2 Kinematic and compliance analyses by the spatial SBM

Before giving an explanation about how to perform kinematic and compliance analyses, defining the state variables for a rigid block in a three-dimensional space is needed. In this research, in order to depict the translational motion of the i th rigid blocks, $\mathbf{r}_i = \{x_i, y_i, z_i\}^t$, which is the position vector from the origin O of the global coordinate system (X, Y, Z) to the initial center points of the i th block is used. To represent the roll, pitch, and yaw angles of the blocks, we employ the Tait-Bryan angles $\boldsymbol{\theta}_i = \{\phi_i, \theta_i, \psi_i\}^t$ that are defined in a coordinate system fixed at the i th block. Therefore, the state variable vector of the i th rigid block becomes $\mathbf{q}_i = \{x_i, y_i, z_i, \phi_i, \theta_i, \psi_i\}^t$.

The way to perform kinematic analysis of the spatial SBM is not different from the 2D SBM because the principle to minimize the strain energy stored by zero-length springs can be used for 3D SBM. To calculate the total strain energy stored in the zero-length springs when the blocks of an SBM are moved by a given input motion, a snapshot of two rigid blocks in a moved position by a given input motion is

prepared in Fig. 3.6. The moved positions of the two blocks are illustrated as gray cubes with their edges in solid lines, while the edges of their initial positions are denoted by dotted lines. The two blocks are connected to each other by the i th block-connecting spring and the left block is also connected to the ground by the j th anchoring spring. Note that these springs only couple the translational motions (in the X , Y , and Z directions) because the spring at its maximum only plays a role as a rigid connection where the spring is attached.

For a kinematic analysis, the strain energy stored in zero-length springs is needed to be calculated. With the state variable vector, the displacement between the corners of the two blocks at which the i th block-connecting springs are attached can be calculated as

$$\mathbf{u}_{b_i} = \left\{ \mathbf{r}_{b_i,1} + \mathbf{A}_{b_i,1} \mathbf{s}_{b_i,1} \right\} - \left\{ \mathbf{r}_{b_i,2} + \mathbf{A}_{b_i,2} \mathbf{s}_{b_i,2} \right\} \quad (3.1)$$

where

$$\begin{aligned} \mathbf{A}_{b_i,1} &= \begin{bmatrix} 1 & 0 & 0 \\ 0 & \cos \phi_{b_i,1} & -\sin \phi_{b_i,1} \\ 0 & \sin \phi_{b_i,1} & \cos \phi_{b_i,1} \end{bmatrix} \begin{bmatrix} \cos \theta_{b_i,1} & 0 & \sin \theta_{b_i,1} \\ 0 & 1 & 0 \\ -\sin \theta_{b_i,1} & 0 & \cos \theta_{b_i,1} \end{bmatrix} \begin{bmatrix} \cos \psi_{b_i,1} & -\sin \psi_{b_i,1} & 0 \\ \sin \psi_{b_i,1} & \cos \psi_{b_i,1} & 0 \\ 0 & 0 & 1 \end{bmatrix}; \\ \mathbf{A}_{b_i,2} &= \begin{bmatrix} 1 & 0 & 0 \\ 0 & \cos \phi_{b_i,2} & -\sin \phi_{b_i,2} \\ 0 & \sin \phi_{b_i,2} & \cos \phi_{b_i,2} \end{bmatrix} \begin{bmatrix} \cos \theta_{b_i,2} & 0 & \sin \theta_{b_i,2} \\ 0 & 1 & 0 \\ -\sin \theta_{b_i,2} & 0 & \cos \theta_{b_i,2} \end{bmatrix} \begin{bmatrix} \cos \psi_{b_i,2} & -\sin \psi_{b_i,2} & 0 \\ \sin \psi_{b_i,2} & \cos \psi_{b_i,2} & 0 \\ 0 & 0 & 1 \end{bmatrix} \end{aligned} \quad (3.2)$$

For the sake of convenience, the left block in Fig. 3.6 is denoted by symbol “1” and the right block is denoted by symbol “2”. The symbols $\mathbf{r}_{b_i,1}$ and $\mathbf{r}_{b_i,2}$ are the position vectors from the origin O of the global coordinate system (X, Y, Z) to the initial center points of Blocks 1 and 2, respectively. (Note that the initial center points remain unchanged when the shape of the blocks are changed.) The symbols $\mathbf{s}_{b_i,1}$ ($\mathbf{s}_{b_i,2}$) is the position vector from the $\mathbf{r}_{b_i,1}$ ($\mathbf{r}_{b_i,2}$) to the k_{b_i} -attached corner in a coordinate system fixed at Block 1 (Block 2). The matrices $\mathbf{A}_{b_i,1}$ and $\mathbf{A}_{b_i,2}$ denote the rotation matrices for Blocks 1 and 2, respectively.

Likewise, the displacement of the j th anchoring spring can be defined as

$$\mathbf{u}_{a_j} = \left\{ \mathbf{r}_{b_i,1} + \mathbf{A}_{b_i,1} \mathbf{s}_{a_j} \right\} - \mathbf{r}_{a_j} \quad (3.3)$$

Here, $\mathbf{s}_{b_i,1}$ is the position vector from the $\mathbf{r}_{b_i,1}$ to the k_{a_j} -attached corner in the local block-fixed coordinate system of Block 1 and \mathbf{r}_{a_j} is the position vector from the origin O of the global coordinate system (X, Y, Z) to the k_{a_j} -attached corner of Block 1 at the initial position

Using Eqs. (3.2) and (3.3), the strain energy stored in the i th block-connecting spring and the j th anchoring spring can be expressed as

$$U_{b_i} = \frac{1}{2} k_{b_i} (\mathbf{u}_{b_i})^t (\mathbf{u}_{b_i}); \quad U_{a_j} = \frac{1}{2} k_{a_j} (\mathbf{u}_{a_j})^t (\mathbf{u}_{a_j}) \quad (3.4)$$

and the total strain energy stored in all of the springs can be then calculated as

$$U(\mathbf{q}) = \sum_{i=1}^{N_b} \frac{1}{2} k_{b_i} (\mathbf{u}_{b_i})^t (\mathbf{u}_{b_i}) + \sum_{j=1}^{N_a} \frac{1}{2} k_{a_j} (\mathbf{u}_{a_j})^t (\mathbf{u}_{a_j}) \quad (3.5)$$

The total number of the block-connecting springs and anchoring springs are denote as N_b and N_a . The symbol \mathbf{q} represents the state variable vector of all blocks, which is defined as

$$\mathbf{q} = \{\mathbf{q}_1^t, \mathbf{q}_2^t, \dots, \mathbf{q}_{N_B}^t\}^t \quad (3.6)$$

with

$$\mathbf{q}_m = \{\mathbf{r}_m^t, \boldsymbol{\theta}_m^t\}^t = \{x_m, y_m, z_m, \phi_m, \theta_m, \psi_m\}^t \quad (m=1, 2, \dots, N_B) \quad (3.7)$$

(N_B : the total number of rigid blocks)

In a kinematic analysis for the 3D vehicle suspension design problem, the vertical motion of the wheel center ($z_{w/C}$) is prescribed at all time steps. Therefore, the strain energy can be considered as a function of the remaining state variables, defined as

$$\mathbf{v} = \{\mathbf{q}_1^t, \mathbf{q}_2^t, \dots, \tilde{\mathbf{q}}_{w/C}^t, \dots, \mathbf{q}_{N_B}^t\}^t \quad (3.8)$$

where

$$\tilde{\mathbf{q}}_{w/C} = \{x_{w/C}, y_{w/C}, \phi_{w/C}, \theta_{w/C}, \psi_{w/C}\}^t \quad (3.9)$$

Since the remained process to define \mathbf{v} at any time instance is the same as when doing in 2D SBM through Eqs. (2.10) and (2.12), they are not presented here.

For a compliance analysis of vehicle suspensions using the spatial SBM, a linear equation is used here because the behavior of the wheel motion by the external forces

is nearly proportional to the magnitude of the force [47]. Therefore, linear equation to calculate the displacement of blocks by the external forces is needed. The state variable for the small linearized motion can be

$$\Delta \mathbf{q} = \left\{ \Delta \mathbf{q}_1^t, \Delta \mathbf{q}_2^t, \dots, \Delta \mathbf{q}_{N_B}^t \right\}^t \quad (3.10)$$

with

$$\Delta \mathbf{q}_m = \left\{ \Delta \mathbf{r}_m^t, \Delta \boldsymbol{\theta}_m^t \right\}^t = \left\{ \Delta x_m, \Delta y_m, \Delta z_m, \Delta \phi_m, \Delta \theta_m, \Delta \psi_m \right\}^t \quad (3.11)$$

$(m=1, 2, \dots, N_B)$

To derive the governing equation of the compliance analysis, we can assume that positions of two blocks in Fig. 3.6 are changed by an external force. Then, the elastic joint forces applied to the left and right blocks through the i th block-connecting spring are given as below.

$$\mathbf{F}_{b_i}^e = \begin{Bmatrix} \mathbf{F}_{b_i,1}^e \\ \mathbf{T}_{b_i,1}^e \\ \mathbf{F}_{b_i,2}^e \\ \mathbf{T}_{b_i,2}^e \end{Bmatrix} = \mathbf{K}_{b_i}^c \begin{Bmatrix} \Delta \mathbf{r}_{b_i,1} \\ \Delta \boldsymbol{\theta}_{b_i,1} \\ \Delta \mathbf{r}_{b_i,2} \\ \Delta \boldsymbol{\theta}_{b_i,2} \end{Bmatrix} = \mathbf{K}_{b_i}^c \begin{Bmatrix} \Delta \mathbf{q}_{b_i,1} \\ \Delta \mathbf{q}_{b_i,2} \end{Bmatrix} \quad (3.12)$$

$$\mathbf{K}_{b_i}^c = \begin{bmatrix} \mathbf{K}_{b_i,Tr}^c & -\mathbf{K}_{b_i,Tr}^c \tilde{\mathbf{s}}_{b_i,1} & -\mathbf{K}_{b_i,Tr}^c & \mathbf{K}_{b_i,Tr}^c \tilde{\mathbf{s}}_{b_i,2} \\ \tilde{\mathbf{s}}_{b_i,1} \mathbf{K}_{b_i,Tr}^c & -\tilde{\mathbf{s}}_{b_i,1} \mathbf{K}_{b_i,Tr}^c \tilde{\mathbf{s}}_{b_i,1} + \mathbf{K}_{b_i,Ro}^c & -\tilde{\mathbf{s}}_{b_i,1} \mathbf{K}_{b_i,Tr}^c & \tilde{\mathbf{s}}_{b_i,1} \mathbf{K}_{b_i,Tr}^c \tilde{\mathbf{s}}_{b_i,2} - \mathbf{K}_{b_i,Ro}^c \\ -\mathbf{K}_{b_i,Tr}^c & \mathbf{K}_{b_i,Tr}^c \tilde{\mathbf{s}}_{b_i,1} & \mathbf{K}_{b_i,Tr}^c & -\mathbf{K}_{b_i,Tr}^c \tilde{\mathbf{s}}_{b_i,2} \\ -\tilde{\mathbf{s}}_{b_i,2} \mathbf{K}_{b_i,Tr}^c & \tilde{\mathbf{s}}_{b_i,2} \mathbf{K}_{b_i,Tr}^c \tilde{\mathbf{s}}_{b_i,1} - \mathbf{K}_{b_i,Ro}^c & \tilde{\mathbf{s}}_{b_i,2} \mathbf{K}_{b_i,Tr}^c & -\tilde{\mathbf{s}}_{b_i,2} \mathbf{K}_{b_i,Tr}^c \tilde{\mathbf{s}}_{b_i,2} + \mathbf{K}_{b_i,Ro}^c \end{bmatrix} \quad (3.13)$$

$$\mathbf{K}_{b_i,Tr}^c = \mathbf{T}^t \begin{bmatrix} k_{b_i,x}^c & 0 & 0 \\ 0 & k_{b_i,y}^c & 0 \\ 0 & 0 & k_{b_i,z}^c \end{bmatrix} \mathbf{T}; \quad \mathbf{K}_{b_i,Ro}^c = \mathbf{T}^t \begin{bmatrix} k_{b_i,\phi}^c & 0 & 0 \\ 0 & k_{b_i,\theta}^c & 0 \\ 0 & 0 & k_{b_i,\psi}^c \end{bmatrix} \mathbf{T} \quad (3.14)$$

Here, the symbols “ Tr ” and “ Ro ” denote translational stiffness and rotational stiffness, respectively. The symbol $\mathbf{s}_{b_i,1}$ ($\mathbf{s}_{b_i,2}$) is already defined in a kinematic analysis, and $\tilde{\mathbf{s}}_{b_i,1}$ ($\tilde{\mathbf{s}}_{b_i,2}$) is the skew-symmetric matrix of it. In addition, the stiffness values for each direction in 3D can be different, six values are introduced to represent them. The matrix \mathbf{T} is a matrix which converts a coordinate attached to the bushing into a global coordinate, but it is the same as the identity matrix \mathbf{I} because the bushing direction is fixed to a global coordinate in this research. Similarly, the elastic joint force applied to the left block through the j th anchoring spring is given as below.

$$\mathbf{F}_{a_j}^e = \begin{Bmatrix} \mathbf{F}_{a_j,1}^e \\ \mathbf{T}_{a_j,1}^e \end{Bmatrix} \mathbf{K}_{a_j}^c \begin{Bmatrix} \Delta \mathbf{r}_{b_i,1} \\ \Delta \boldsymbol{\theta}_{b_i,1} \end{Bmatrix} = \mathbf{K}_{a_j}^c \Delta \mathbf{q}_{b_i,1} \quad (3.15)$$

$$\mathbf{K}_{a_j}^c = \begin{bmatrix} \mathbf{K}_{a_j,Tr}^c & -\mathbf{K}_{a_j,Tr}^c \tilde{\mathbf{s}}_{a_j} \\ \tilde{\mathbf{s}}_{a_j} \mathbf{K}_{a_j,Tr}^c & -\tilde{\mathbf{s}}_{a_j} \mathbf{K}_{a_j,Tr}^c \tilde{\mathbf{s}}_{a_j} + \mathbf{K}_{a_j,Ro}^c \end{bmatrix} \quad (3.16)$$

$$\mathbf{K}_{a_j,Tr}^c = \mathbf{T}^t \begin{bmatrix} k_{a_j,x}^c & 0 & 0 \\ 0 & k_{a_j,y}^c & 0 \\ 0 & 0 & k_{a_j,z}^c \end{bmatrix} \mathbf{T}; \quad \mathbf{K}_{a_j,Ro}^c = \mathbf{T}^t \begin{bmatrix} k_{a_j,\phi}^c & 0 & 0 \\ 0 & k_{a_j,\theta}^c & 0 \\ 0 & 0 & k_{a_j,\psi}^c \end{bmatrix} \mathbf{T} \quad (3.17)$$

In Eq. (3.15), as the counterpart of Block 1 with the l th anchoring spring is the ground, the elastic joint force to Block 1 is only used to the governing static equation. The

governing static equation for compliance analysis using the SBM can be written as

$$\mathbf{K}^c \Delta \mathbf{q} = \mathbf{F}^{ext} \quad (3.18)$$

Here, \mathbf{K}^c denotes the global stiffness matrix by assembling all the local stiffness matrices in Eqs. (3.13) and (3.16). In addition, \mathbf{F}^{ext} stands for a global external force vector applied to the system.

By the way, since the interested compliance characteristics in this research are calculated at the initial position of the wheel, the z -coordinate of the wheel center is fixed to the initial position of it for a compliance analysis, the governing equation in Eq. (3.18) can be changed to obtain the remaining state variables as follow:

$$\mathbf{K}^c \Delta \mathbf{v} = \mathbf{F}^{ext} \quad (3.19)$$

and the remaining state variable vector for the small linearized motion ($\Delta \mathbf{v}$) is as below.

$$\Delta \mathbf{v} = \left\{ \Delta \mathbf{q}_1^t, \Delta \mathbf{q}_2^t, \dots, \Delta \tilde{\mathbf{q}}_{W/C}^t, \dots, \Delta \mathbf{q}_{N_B}^t \right\}^t \quad (3.20)$$

where

$$\Delta \tilde{\mathbf{q}}_{W/C} = \left\{ \Delta x_{W/C}, \Delta y_{W/C}, 0, \Delta \phi_{W/C}, \Delta \theta_{W/C}, \Delta \psi_{W/C} \right\}^t \quad (3.21)$$

(W/C : Wheel center)

and Eq. (3.19) can be solved by using any linear solving method to obtain $\Delta \mathbf{v}$ for compliance analysis [47].

3.3 Optimization Formulation

3.3.1 Design variable and interpolation

For designing a vehicle suspension considering K&C characteristics, three types of design variables are introduced. The first is for defining a topology, the second is for determining dimensions, and the last is for adjusting bushing stiffness. These three types of design variables are as follow:

$$\xi = \left\{ \left(\xi^T \right)^t, \left(\xi^X \right)^t, \left(\xi^B \right)^t \right\} \quad (3.22)$$

where

$$\xi^T = \left\{ \left(\xi_b^T \right)^t, \left(\xi_a^T \right)^t \right\} = \left\{ \xi_{b_1}^T, \xi_{b_2}^T, \dots, \xi_{b_{N_b}}^T, \xi_{a_1}^T, \xi_{a_2}^T, \dots, \xi_{a_{N_a}}^T \right\} \quad (3.23)$$

$$\xi^X = \left\{ \xi_1^X, \xi_2^X, \dots, \xi_{3N_N}^X \right\} \quad (3.24)$$

$$\xi^B = \left\{ \xi_1^B, \xi_2^B, \dots, \xi_{N_a}^B \right\} \quad (3.25)$$

Here, ξ^T , ξ^X , and ξ^B denote the design variables of the topology, dimension, and bushing stiffness, respectively. In Eq. (3.23), subscripts “ b ” and “ a ” denote block-connecting springs and anchoring springs, respectively. The total number of block-connecting springs is N_b and the total number of the anchoring springs is N_a . The total number of design variables for the shape of the blocks is $3N_N$ because these variables are related to the coordinates of the block grid points (N_N : the total number of the block grid points). The total number of the design variable for bushing stiffness is N_a because bushings are only attached to the anchoring springs.

The spring stiffness vector is derived from the design variables using the equations below.

$$\mathbf{k}^k = \left\{ k_{b_1}^k, k_{b_2}^k, \dots, k_{b_{N_b}}^k, k_{a_1}^k, k_{a_2}^k, \dots, k_{a_{N_a}}^k \right\}^t \quad (3.26a)$$

$$k_{b_i}^k = (\xi_{b_i}^T)^p \times k_{\max}^k; \quad k_{a_j}^k = (\xi_{a_j}^T)^p \times k_{\max}^k \quad (3.26b)$$

$$\mathbf{k}^c = \left\{ \left(\mathbf{k}_{b_1}^c \right)^t, \left(\mathbf{k}_{b_2}^c \right)^t, \dots, \left(\mathbf{k}_{b_{N_b}}^c \right)^t, \left(\mathbf{k}_{a_1}^c \right)^t, \left(\mathbf{k}_{a_2}^c \right)^t, \dots, \left(\mathbf{k}_{a_{N_a}}^c \right)^t \right\}^t \quad (3.27a)$$

$$\mathbf{k}_{b_i}^c = (\xi_{b_i}^T)^p \times \mathbf{k}_{\text{rigid}} \quad (3.27b)$$

$$\mathbf{k}_{a_j}^c = (\xi_{a_j}^T)^p \times \left\{ (1 - \xi_j^B) \mathbf{k}_{\text{bushing,min}} + \xi_j^B \mathbf{k}_{\text{bushing,max}} \right\} \quad (3.27c)$$

where

$$10^{-6} \leq \xi_l^T \leq 1 \quad (l=1, 2, \dots, N_b + N_a), \quad 0 \leq \xi_m^B \leq 1 \quad (m=1, 2, \dots, N_a) \quad (3.28)$$

Here, p is the penalty parameter, the value of which is set to three, as in earlier works [11-15]. In Eqs. (3.26) and (3.27), the superscripts k and c denote the kinematic analysis and the compliance analysis, respectively. As in Eqs. (3.26) and (3.27), spring stiffness vector is defined differently in the kinematic and compliance analyses. Since the anchoring springs in a kinematic analysis only represent the connection between the two points where the springs are attached, but the anchoring springs in a compliance analysis represent cylindrical bushings. Stiffness of a cylindrical bushing can be specified as 3 translational springs and 3 rotational springs as shown in Fig. 3.7. In addition, the stiffness of anchoring springs is linearly interpolated by the design variable for bushing stiffness from the values at their minimum to the values at their maximum in each direction as in Eq. (3.27c).

The stiffness vector for a compliance analysis is defined as below.

$$\mathbf{k}_{\text{rigid}} = \{k_{\text{rigid}}, k_{\text{rigid}}, k_{\text{rigid}}, 0, 0, 0\}^t \quad (3.29a)$$

$$\mathbf{k}_{\text{bushing,min}} = \{k_{x,\text{min}}^c, k_{y,\text{min}}^c, k_{z,\text{min}}^c, 0, 0, 0\}^t \quad (3.29b)$$

$$\mathbf{k}_{\text{bushing,max}} = \{k_{x,\text{max}}^c, k_{y,\text{max}}^c, k_{z,\text{max}}^c, 0, 0, 0\}^t \quad (3.29c)$$

Bushings used in this research are modeled following the assumption that translational stiffness of the radial direction (y and z axes) is 20 times than the translational stiffness of the axial direction (x axis), and the rotational stiffnesses are assumed to be zero because they are relatively small compared to the values of the translational stiffness. Additionally, the maximum stiffness value of translational direction in block-connecting springs k_{rigid} is set to be a sufficiently large value, about 2×10^3 larger than $k_{y,\text{max}}^c$ for representing a rigid connection.

The design variables for dimensions determine the lengths of the linkage mechanism by changing the grid points of rigid blocks. The interpolation between the grid points and design variables are as follow:

$$\mathbf{X} = \{X_1, Y_1, Z_1, X_2, Y_2, Z_2, \dots, X_{N_N}, Y_{N_N}, Z_{N_N}\}^t \quad (3.30)$$

$$\begin{aligned} X_i &= X_{\text{max}} \xi_{3i-2}^X + X_{\text{min}} (1 - \xi_{3i-2}^X); \quad Y_i = Y_{\text{max}} \xi_{3i-1}^X + Y_{\text{min}} (1 - \xi_{3i-1}^X); \\ Z_i &= Z_{\text{max}} \xi_{3i}^X + Z_{\text{min}} (1 - \xi_{3i}^X) \end{aligned} \quad (3.31)$$

where

$$10^{-6} \leq \xi_n^X \leq 1 \quad (l=1, 2, \dots, 3N_N) \quad (3.32)$$

The symbols X_i , Y_i , and Z_i represent the global Cartesian coordinates of the i th grid point. X_{\max} , Y_{\max} , and Z_{\max} denotes the maximum values of the X , Y , Z coordinates of the design domain boundary and X_{\min} , Y_{\min} , and Z_{\min} denotes the minimum values of the X , Y , Z coordinates of the design domain boundary.

3.3.2 Objective and constraint functions

As shown in Fig. 3.1, we consider four types of analyses - one kinematic analysis, and three types of compliance analyses - to perform for considering K&C characteristics of a vehicle suspension in this research. In order to synthesize a vehicle suspension using a topology optimization considering K&C characteristics simultaneously, the following formulation is proposed.

$$\begin{aligned} &\text{Find } \xi^T, \xi^X, \text{ and } \xi^B \\ &\text{to minimize } 1 - \bar{\eta} \end{aligned} \quad (3.33a)$$

Subject to 1) Kinematic condition under a given input motion

$$g_t^{k(i)}(\mathbf{v}_t^*) \leq \varepsilon^{k(i)} \quad (t^* = 1, 2, 3, \dots, t_{\max}) \quad (3.33b)$$

2) Compliance constraints for given lateral load

$$g_{\text{lat}}^{c(j)}(\Delta \mathbf{v}_{\text{lat}}) \leq \varepsilon_{\text{lat}}^{c(j)} \quad (3.33c)$$

3) Compliance constraints for given longitudinal load

$$g_{\text{longi}}^{c(k)}(\Delta \mathbf{v}_{\text{longi}}) \leq \varepsilon_{\text{longi}}^{c(k)} \quad (3.33d)$$

4) Compliance constraints for given aligning moment

$$g_{\text{align}}^{c(l)}(\Delta \mathbf{v}_{\text{align}}) \leq \varepsilon_{\text{align}}^{c(l)} \quad (3.33e)$$

5) Constraints on the maximum number of bushings

$$\sum_{m=1}^{N_a} \xi_{a_m}^T \leq 6 \quad (3.33f)$$

6) Nodal distance

$$\text{Dist}(i, j) \geq 10 \text{ mm} \quad (i, j = 1, 2, \dots, N_n, i \neq j) \quad (3.33g)$$

where

$$\bar{\eta} = \frac{1}{t_{\max}} \sum_{t=1}^{t_{\max}} \eta_t \quad (\eta_t : \text{Work transmittance efficiency at time } t) \quad (3.34)$$

In Eq. (3.33), the mean value of work transmittance efficiency function ($\bar{\eta}$) is used as an objective here. The explanation and calculation of the work transmittance efficiency function are not given here as they are already given in Chapter 2.3. The constraint functions through Eq. (3.33b) to (3.33e) are related to the K&C characteristics. The symbol $g_t^{k(i)}$ represents the i th kinematic constraint, $g_{\text{lat}}^{c(j)}$ is the j th compliance constraint when a lateral force is applied, $g_{\text{longi}}^{c(k)}$ is the k th compliance constraint when a longitudinal force is applied, and $g_{\text{align}}^{c(l)}$ is the l th compliance constraint when an aligning moment is applied. The all compliance characteristics are defined at the initial position and the detailed forms about the K&C constraint functions are given in the next chapter with the each problem definition. The constraint function in Eq. (3.33f) is employed to restrict the total number of bushings at the convergence. Since there are no vehicle suspensions with more than six bushings, we set to six as the maximum number of bushings when synthesizing a vehicle suspension. The last constraint function in Eq. (3.33g) is used for numerical stability. A flow chart of the topology optimization process for synthesizing vehicle suspensions simultaneously considering K&C characteristics is presented in Fig. 3.8.

3.3.3 Sensitivity analysis

For an efficient mechanism synthesis, the method of moving asymptotes (MMA) [50], a gradient-based optimizer, is used in this research. To use a gradient-based optimizer, the sensitivities of the objective and constraint functions with respect to the design variables are required. The calculation process for sensitivities of the objective and kinematic constraint functions are identical to the 2D SBM. Thus, only sensitivities of the compliance constraints are given here. In addition, as the calculation of the sensitivities for each compliance constraints are not different, only the sensitivity of the compliance constraints when a lateral load is applied ($g_{\text{lat}}^{c(j)}$) is only given, and it is as below.

$$\frac{dg_{\text{lat}}^{c(j)}}{d\xi} = \begin{bmatrix} \frac{dg_{\text{lat}}^{c(j)}}{d\xi^T} \\ \frac{dg_{\text{lat}}^{c(j)}}{d\xi^X} \\ \frac{dg_{\text{lat}}^{c(j)}}{d\xi^B} \end{bmatrix} = \begin{bmatrix} \frac{d\mathbf{k}^c}{d\xi^T} \left(\frac{\partial g_{\text{lat}}^{c(j)}}{\partial \mathbf{k}^c} + \frac{d\Delta \mathbf{v}_{\text{lat}}}{d\mathbf{k}^c} \frac{\partial g_{\text{lat}}^{c(j)}}{\partial \Delta \mathbf{v}_{\text{lat}}} \right) \\ \frac{d\mathbf{X}}{d\xi^X} \left(\frac{\partial g_{\text{lat}}^{c(j)}}{\partial \mathbf{X}} + \frac{d\Delta \mathbf{v}_{\text{lat}}}{d\mathbf{X}} \frac{\partial g_{\text{lat}}^{c(j)}}{\partial \Delta \mathbf{v}_{\text{lat}}} \right) \\ \frac{d\mathbf{k}_a^c}{d\xi^B} \left(\frac{\partial g_{\text{lat}}^{c(j)}}{\partial \mathbf{k}_a^c} + \frac{d\Delta \mathbf{v}_{\text{lat}}}{d\mathbf{k}_a^c} \frac{\partial g_{\text{lat}}^{c(j)}}{\partial \Delta \mathbf{v}_{\text{lat}}} \right) \end{bmatrix} \quad (3.35)$$

Because the compliance constraint function is derived from the compliance analysis, \mathbf{k}^c is used here. The partial derivatives $\partial g_{\text{lat}}^{c(j)} / \partial \mathbf{k}^c$, $\partial g_{\text{lat}}^{c(j)} / \partial \mathbf{X}$, and $\partial g_{\text{lat}}^{c(j)} / \partial \mathbf{k}_a^c$ are all zero because $g_{\text{lat}}^{c(j)}$ is an explicit function of state variables in this study. To obtain the sensitivity related to the topology controlling design variables, $d\mathbf{k}^c / d\xi^T$ is calculated as

$$\frac{d\mathbf{k}^c}{d\xi^T} = \left\{ \frac{d\mathbf{k}_b^c}{d\xi^T}, \frac{d\mathbf{k}_a^c}{d\xi^T} \right\} \quad (3.36)$$

$$\frac{d\mathbf{k}_b^c}{d\xi^T} = \left\{ \frac{d\mathbf{k}_{b_1}^c}{d\xi^T}, \frac{d\mathbf{k}_{b_2}^c}{d\xi^T}, \dots, \frac{d\mathbf{k}_{b_l}^c}{d\xi^T}, \dots, \frac{d\mathbf{k}_{b_{N_b}}^c}{d\xi^T} \right\} \quad (3.37a)$$

$$\frac{d\mathbf{k}_{b_l}^c}{d\xi^T} = \left\{ 0 \quad \dots \quad \left(\frac{d\mathbf{k}_{b_l}^c}{d\xi_{b_l}^T} \right)^t \quad \dots \quad 0 \right\}^t \quad (3.37b)$$

$$\frac{d\mathbf{k}_{b_l}^c}{d\xi_{b_l}^T} = 3 \left(\xi_{b_l}^T \right)^2 \mathbf{k}_{\text{rigid}} \quad (3.37c)$$

$$\frac{d\mathbf{k}_a^c}{d\xi^T} = \left\{ \frac{d\mathbf{k}_{a_1}^c}{d\xi^T}, \frac{d\mathbf{k}_{a_2}^c}{d\xi^T}, \dots, \frac{d\mathbf{k}_{a_j}^c}{d\xi^T}, \dots, \frac{d\mathbf{k}_{a_{N_a}}^c}{d\xi^T} \right\} \quad (3.38a)$$

$$\frac{d\mathbf{k}_{a_j}^c}{d\xi^T} = \left\{ 0 \quad \dots \quad \left(\frac{d\mathbf{k}_{a_j}^c}{d\xi_{a_j}^T} \right)^t \quad \dots \quad 0 \right\}^t \quad (3.38b)$$

$$\frac{d\mathbf{k}_{a_j}^c}{d\xi_{a_j}^T} = 3 \left(\xi_{a_j}^T \right)^2 \times \left\{ (1 - \xi_j^B) \mathbf{k}_{\text{bushing,min}} + \xi_j^B \mathbf{k}_{\text{bushing,max}} \right\} \quad (3.38c)$$

Next, $d\Delta\mathbf{v}_{\text{lat}}/d\mathbf{k}^c$ can be derived from Eq. (3.18) as

$$\frac{d \left(\mathbf{K}^c \Delta\mathbf{v}_{\text{lat}} - \mathbf{F}^{\text{ext}} \right)}{d\mathbf{k}^c} = \frac{d\mathbf{K}^c \Delta\mathbf{v}_{\text{lat}}}{d\mathbf{k}^c} = \frac{d}{d\mathbf{k}^c} \left(\frac{\partial \mathbf{K}^c \Delta\mathbf{v}_{\text{lat}}}{\partial \mathbf{k}^c} + \frac{d\Delta\mathbf{v}_{\text{lat}}}{d\mathbf{k}^c} \frac{\partial \mathbf{K}^c \Delta\mathbf{v}_{\text{lat}}}{\partial \Delta\mathbf{v}_{\text{lat}}} \right) = 0 \quad (3.39a)$$

$$\frac{d\Delta\mathbf{v}_{\text{lat}}}{d\mathbf{k}^c} = - \left(\frac{\partial \mathbf{K}^c \Delta\mathbf{v}_{\text{lat}}}{\partial \mathbf{k}^c} \right)^{-1} \frac{\partial \mathbf{K}^c \Delta\mathbf{v}_{\text{lat}}}{\partial \Delta\mathbf{v}_{\text{lat}}} = - \left(\frac{\partial \mathbf{K}^c}{\partial \mathbf{k}^c} \Delta\mathbf{v}_{\text{lat}} \right)^{-1} \mathbf{K}^c \quad (3.39b)$$

As \mathbf{K}^c is made by assembling the local stiffness matrices $\mathbf{K}_{b_i}^c$ and $\mathbf{K}_{a_j}^c$, the partial derivative $\partial \mathbf{K}^c / \partial \mathbf{k}^c$ in Eq. (3.39b) can be also obtained by assembling the partial derivative of the local stiffness matrices $\partial \mathbf{K}_{b_i}^c / \partial \mathbf{k}^c$ and $\partial \mathbf{K}_{a_j}^c / \partial \mathbf{k}^c$. In addition, $\partial \mathbf{K}_{b_i}^c / \partial \mathbf{k}^c$ ($\partial \mathbf{K}_{a_j}^c / \partial \mathbf{k}^c$) can be calculated easily because $\mathbf{K}_{b_i}^c$ ($\mathbf{K}_{a_j}^c$) is composed of $\mathbf{K}_{b_i,Tr}^c$ and $\mathbf{K}_{b_i,Ro}^c$ ($\mathbf{K}_{a_j,Tr}^c$ and $\mathbf{K}_{a_j,Ro}^c$), and the components of $\partial \mathbf{K}_{b_i}^c / \partial \mathbf{k}^c$ ($\partial \mathbf{K}_{a_j}^c / \partial \mathbf{k}^c$) are either 0 or 1 according to the order of spring stiffness. As more details can be found in [47], the detailed explicit formula for them will not be given here.

To calculate the sensitivity related to the dimension controlling design variables, $d\mathbf{X} / d\boldsymbol{\xi}^X$ is calculated as

$$\frac{d\mathbf{X}}{d\boldsymbol{\xi}^X} = \text{diag}(X_{\max} - X_{\min}, Y_{\max} - Y_{\min}, Z_{\max} - Z_{\min}, \dots, X_{\max} - X_{\min}, Y_{\max} - Y_{\min}, Z_{\max} - Z_{\min}) \quad (3.40)$$

In addition, $d\mathbf{v}_0 / d\mathbf{X}$ can be derived from Eq. (3.18) as

$$\frac{d(\mathbf{K}^c \Delta \mathbf{v}_{\text{lat}} - \mathbf{F}^{\text{ext}})}{d\mathbf{X}} = \frac{d\mathbf{K}^c \Delta \mathbf{v}_{\text{lat}}}{d\mathbf{X}} = \frac{d}{d\mathbf{X}} \left(\frac{\partial \mathbf{K}^c \Delta \mathbf{v}_{\text{lat}}}{\partial \mathbf{X}} + \frac{d\Delta \mathbf{v}_{\text{lat}}}{d\mathbf{X}} \frac{\partial \mathbf{K}^c \Delta \mathbf{v}_{\text{lat}}}{\partial \Delta \mathbf{v}_{\text{lat}}} \right) = 0 \quad (3.41a)$$

$$\frac{d\Delta \mathbf{v}_{\text{lat}}}{d\mathbf{X}} = - \left(\frac{\partial \mathbf{K}^c \Delta \mathbf{v}_{\text{lat}}}{\partial \mathbf{X}} \right)^{-1} \frac{\partial \mathbf{K}^c \Delta \mathbf{v}_{\text{lat}}}{\partial \Delta \mathbf{v}_{\text{lat}}} = - \left(\frac{\partial \mathbf{K}^c}{\partial \mathbf{X}} \Delta \mathbf{v}_{\text{lat}} \right)^{-1} \mathbf{K}^c \quad (3.41b)$$

The partial derivative $\partial \mathbf{K}^c / \partial \mathbf{X}$ can be calculated easily because $\tilde{\mathbf{s}}$ is explicitly

used in \mathbf{K}^c .

At last, the sensitivity related to the design variables for bushing stiffness can be calculated as below. (The other terms already calculated in Eq. (3.39).)

$$\frac{d\mathbf{k}_a^c}{d\xi^B} = \left\{ \frac{d\mathbf{k}_{a_1}^c}{d\xi^B}, \frac{d\mathbf{k}_{a_2}^c}{d\xi^B}, \dots, \frac{d\mathbf{k}_{a_j}^c}{d\xi^B}, \dots, \frac{d\mathbf{k}_{a_{N_a}}^c}{d\xi^B} \right\} \quad (3.42a)$$

$$\frac{d\mathbf{k}_{a_j}^c}{d\xi^B} = \left\{ 0 \quad \dots \quad \left(\frac{d\mathbf{k}_{a_j}^c}{d\xi_j^B} \right)^t \quad \dots \quad 0 \right\}^t \quad (3.42b)$$

$$\frac{d\mathbf{k}_{a_j}^c}{d\xi_j^B} = (\xi_{a_j}^T)^3 \times (\mathbf{k}_{\text{bushing,max}} - \mathbf{k}_{\text{bushing,min}}) \quad (3.42c)$$

3.4 Design of vehicle suspensions for rear using the proposed method

3.4.1 Definition of problem

Problem definition for synthesizing a vehicle suspension using a 3D SBM is shown in Fig. 3.9. As shown in Fig. 3.9(a), $3 \times 3 \times 3$ blocks are employed for designing a vehicle suspension. The left $3 \times 2 \times 3$ blocks are employed to synthesis a suspension linkage mechanism because they are enough to represent the various types of suspension linkage mechanisms such as a double wishbone type or an integral link type. The rightmost $3 \times 1 \times 3$ rigid blocks (darkly shaded) represent a wheel carrier as a whole and they are rigidly connected to each other by their block-connecting springs. (The stiffnesses of block-connecting springs used to connect the wheel carrier blocks are set to the maximum and they are not designed during optimization process.) The wheel center is located at the center of the middle block among the wheel carrier blocks. The suspension mechanism to be synthesized in the design domain should be connected not only to the wheel carrier but also to the vehicle chassis lying next to the chassis-side of the design domain (it is not explicitly shown in Fig. 3.9). Therefore, as the use of bushings must be considered in connecting the chassis and the vehicle suspension, all corners in the red-shaded zone are connected to the chassis (ground) by anchoring springs. The radius of the tire is 0.273 m and design domain is given as $D_x \times D_y \times D_z = 0.42 \text{ m} \times 0.5 \text{ m} \times 0.4 \text{ m}$. The numbers of the block-connecting springs (N_b) and anchoring springs (N_a) are 168 and 36,

respectively, and the number of grid points to design (N_n) is 48.

The way to perform K&C analyses shown in Fig. 3.1 using the 3D SBM is given through Fig. 3.9(b) to Fig. 3.9(e). As shown in Fig. 3.9(b), the wheel center motion is determined according to the given input motion which is prescribed z-coordinate of the wheel center. Lateral and longitudinal force applied at the contact patch for compliance characteristics are changed to the equivalent force and moments at the wheel center, respectively since it is more convenient to perform compliance analysis using the 3D SBM. The force and moment vectors applied to the system for compliance characteristics are as below.

$$\begin{aligned} \mathbf{F}_{\text{lat}}^c &= -1000\mathbf{e}_y \text{ N}; \quad \mathbf{M}_{\text{lat}}^c = -273\mathbf{e}_y \times \mathbf{e}_z \text{ Nm}; \\ \mathbf{F}_{\text{long}}^c &= 1000\mathbf{e}_x \text{ N}; \quad \mathbf{M}_{\text{long}}^c = -273\mathbf{e}_x \times \mathbf{e}_z \text{ Nm}; \quad \mathbf{M}_{\text{Align}}^c = 1000\mathbf{e}_x \times \mathbf{e}_y \text{ Nm}; \\ (\mathbf{e}_x, \mathbf{e}_y, \mathbf{e}_z : \text{unit vectors in the } X, Y, \text{ and } Z \text{ directions in the global coordinates}) \end{aligned}$$

The values of spring stiffness for kinematic and compliance analysis is as below.

$$\begin{aligned} k_{\text{max}}^k &= 1 \times 10^6 \text{ N/m}; & k_{\text{rigid}} &= 2 \times 10^{11} \text{ N/m}; \\ k_{x,\text{min}}^c &= 5 \times 10^2 \text{ N/m}; & k_{x,\text{max}}^c &= 5 \times 10^6 \text{ N/m}; \\ k_{y,\text{min}}^c &= k_{z,\text{min}}^c = 1 \times 10^4 \text{ N/m}; & k_{y,\text{max}}^c &= k_{z,\text{max}}^c = 1 \times 10^8 \text{ N/m}; \end{aligned}$$

As for the design cases of suspension mechanism synthesis, we will solve two types of problems. First, by recovering the reference suspension linkage, the proposed method will be validated. (The reference suspension is derived from the target cascading method explained in Appendix A.) Second, a suspension linkage

mechanism which can improve R&H performances compared to the reference suspension will be synthesized. For both design problems, kinematic requirements is given as to generate the target wheel center motion which is obtained from the reference suspension linkage. By recovering the reference suspension linkage using the proposed method in the first design case, compliance constraint functions are given so as to have the similar compliance characteristics of the reference suspension linkage. By the way, in the second design problem, the compliance constraint functions are given in order to improve R&H performances. The more details will be explained in the following chapters.

3.4.2 Design Case 1 - Recovery of a double wishbone suspension

In Appendix A, a double-wishbone suspension which has a good R&H performances is designed. In this chapter, the double-wishbone suspension is recovered using the proposed methodology. The optimization formulation used for synthesis is as shown in Eq. (3.33) and the detailed constraint functions are as

$$\begin{aligned} g_t^{k(1)}(\mathbf{v}_t^*) &= |x_t^Q - \hat{x}_t^Q|; \quad g_t^{k(2)}(\mathbf{v}_t^*) = |y_t^Q - \hat{y}_t^Q|; \\ g_t^{k(3)}(\mathbf{v}_t^*) &= |\phi_t^Q - \hat{\phi}_t^Q|; \quad g_t^{k(4)}(\mathbf{v}_t^*) = |\theta_t^Q - \hat{\theta}_t^Q|; \quad g_t^{k(5)}(\mathbf{v}_t^*) = |\psi_t^Q - \hat{\psi}_t^Q| \quad (3.43a) \\ (t^* &= 1, 2, \dots, 20) \end{aligned}$$

$$\begin{aligned} g_{\text{lat}}^{c(1)}(\Delta \mathbf{v}_{\text{lat}}) &= |\Delta y_{\text{lat}}^Q - \Delta \hat{y}_{\text{lat}}^Q|; \\ g_{\text{lat}}^{c(2)}(\Delta \mathbf{v}_{\text{lat}}) &= |\Delta \phi_{\text{lat}}^Q - \Delta \hat{\phi}_{\text{lat}}^Q|; \quad g_{\text{lat}}^{c(3)}(\Delta \mathbf{v}_{\text{lat}}) = |\Delta \psi_{\text{lat}}^Q - \Delta \hat{\psi}_{\text{lat}}^Q| \quad (3.43b) \end{aligned}$$

$$\begin{aligned} g_{\text{longi}}^{c(1)}(\Delta \mathbf{v}_{\text{longi}}) &= \left| \Delta x_{\text{longi}}^Q - \Delta \hat{x}_{\text{longi}}^Q \right|; \\ g_{\text{longi}}^{c(2)}(\Delta \mathbf{v}_{\text{longi}}) &= \left| \Delta \phi_{\text{longi}}^Q - \Delta \hat{\phi}_{\text{longi}}^Q \right|; \quad g_{\text{longi}}^{c(3)}(\Delta \mathbf{v}_{\text{longi}}) = \left| \Delta \psi_{\text{longi}}^Q - \Delta \hat{\psi}_{\text{longi}}^Q \right| \end{aligned} \quad (3.43c)$$

$$g_{\text{align}}^{c(1)}(\Delta \mathbf{v}_{\text{align}}) = \left| \Delta \phi_{\text{align}}^Q - \Delta \hat{\phi}_{\text{align}}^Q \right|; \quad g_{\text{align}}^{c(2)}(\Delta \mathbf{v}_{\text{align}}) = \left| \Delta \psi_{\text{align}}^Q - \Delta \hat{\psi}_{\text{align}}^Q \right| \quad (3.43d)$$

The error bounds used are set as below.

$$\varepsilon^{k(1)} = \varepsilon^{k(2)} = 5 \times 10^{-3} \text{ m}; \quad \varepsilon^{k(3)} = \varepsilon^{k(4)} = 0.05^\circ; \quad \varepsilon^{k(5)} = 0.015^\circ \quad (3.44a)$$

$$\varepsilon_{\text{lat}}^{c(1)} = 1.05 \times 10^{-4} \text{ m}; \quad \varepsilon_{\text{lat}}^{c(2)} = 0.0417^\circ; \quad \varepsilon_{\text{lat}}^{c(3)} = 0.0655^\circ \quad (3.44b)$$

$$\varepsilon_{\text{longi}}^{c(1)} = 4.15 \times 10^{-4} \text{ m}; \quad \varepsilon_{\text{longi}}^{c(2)} = 0.0859^\circ; \quad \varepsilon_{\text{longi}}^{c(3)} = 0.159^\circ \quad (3.44c)$$

$$\varepsilon_{\text{align}}^{c(1)} = 0.129^\circ; \quad \varepsilon_{\text{align}}^{c(2)} = 0.313^\circ \quad (3.44d)$$

As shown in Eq. (3.43a), the differences between the generated wheel center motion and the target wheel center motion when the wheel goes up and down are given as the kinematic constraint functions for generating target wheel center motion obtained from the reference suspension linkage. For the compliance constraint functions, eight characteristics obtained from the three kinds of compliance analyses which are used to define compliance characteristics of vehicle suspension in CARSIM software are used. The differences between the values from the mechanism synthesis and the target values in Table A.3 are given to the compliance constraint functions so that the resulting mechanism has the similar compliance characteristics with the reference suspension at the convergence.

The results related to this design case are presented in Fig. 3.10 to Fig. 3.12. In Fig. 3.10, it is showed that the final optimized layout represented by the SBM and its

equivalent linkage mechanism. We found that the result suspension is a double wishbone type. Fig. 3.11 illustrates the converged values of the design variables. In Fig. 3.11(a), the converged values of the topology controlling design variables related to the block-connecting springs are shown. Fig. 3.11(b) shows the converged values of the topology controlling design variables related to the anchoring springs and it can be found that only five pivot points to the chassis are generated after the optimization. Fig. 3.11(c) indicates that the bushing stiffness of the anchoring springs used in mounting points to the chassis are well adjusted to satisfy the compliance characteristics by the design variables for bushing stiffness. Note that the red bars in Fig. 3.11(c) indicates the design variables for bushing stiffness related to the mounting points to the chassis. (The black bars which are not converged to the minimum in Fig. 3.11(c) does not affect the system stiffness because the topology controlling design variables matched with them are converged to the minimum.) Fig. 3.11(d) indicates the converged design variables for grid points.

Fig. 3.12 shows the convergence histories of the objective and constraint functions. As shown in Fig. 3.12(a), the mean value of the work transmittance efficiency function goes to 1, and it indicates the result suspension mechanism has a one degree-of-freedom. Fig. 3.12(b) and Fig. 3.12(c) shows the maximum values of the kinematic constraint functions related to the displacement error and angular error, respectively. Fig. 3.12(d) to Fig. 3.12(f) shows the values of compliance constraint functions at the convergences. The detailed values are shown in Table 3.1 and Table

3.2, in which all constraint values at the convergence satisfy the given design conditions. Through the results presented through Fig. 3.10 to Fig. 3.12, it is proved that the proposed method can synthesize the suspension linkage but also the bushing stiffnesses which can satisfy the target K&C characteristics obtained from the reference suspension.

At last, for verifying the validation of the K&C characteristics obtained from the 3D SBM, Fig. 3.13 is prepared. In Fig. 3.13(a), the result suspension model built by ADAMS software is shown. The kinematics curves at the wheel center obtained from the SBM and ADAMS model is shown in Fig. 3.13(b), and it can be found that two curves are exactly the same. In addition, the comparison of the compliance characteristic values from the three types of compliance analyses is shown in Fig. 3.13(c), and it indicates that the compliance characteristic values obtained by using the 3D SBM is almost the same as the values from ADAMS. Therefore, it is verified that the modeling and formulation proposed for topology optimization of suspension linkages simultaneously considering kinematic and compliance characteristics are valid from these results.

3.4.3 Design Case 2 - Suspension synthesis for improving ride and handling (R&H) performances

The aim of Design Case 2 is to design a suspension mechanism which can improve R&H performances compared to the reference suspension linkage. Although R&H

performances of a vehicle can be defined by various components in a vehicle, there is a certain guideline for K&C characteristics of a suspension to improve the R&H performances. In Design Case 2, while kinematic constraints for suspension linkage synthesis are kept as the same as Design Case 1, compliance constraints are changed to help to improve R&H performances of a vehicle. The followings are mainly required for compliance characteristics to improve the R&H performances:

- High lateral and spin stiffnesses
- High compliance in longitudinal direction
- Toe-in during braking and cornering

It is easy to know that if the stiffness of a vehicle suspension becomes higher, the handling performance related the response onto a steering input will be improved. Therefore, the first requirement is needed for compliance characteristics of a vehicle suspension. Second, the stiffness of a vehicle suspension in longitudinal direction needs high compliance because the impact coming from the ground should be absorbed well for a good ride performance. The last requirement is needed to ensure the stability of a vehicle when cornering or braking [45, 47, 49, 58]. Like these conditions, as the requirements for compliance characteristics of a vehicle suspension to improve R&H performances are complicated, it is difficult to satisfy all requirements by simply increasing or decreasing the stiffness of the bushing. Therefore, these compliance characteristics should be considered in determining the topology of a suspension as we insisted.

As mentioned above, the kinematic conditions are set to be the same as Design Case 1, we will only explain about the compliance constraint functions here. The compliance constraint functions for improving R&H performances are as follows:

$$\begin{aligned} g_{\text{lat}}^{c(1)}(\Delta \mathbf{v}_{\text{lat}}) &= \Delta y_{\text{lat}}^{\mathcal{O}} - \Delta \hat{y}_{\text{lat}}^{\mathcal{O}}; \\ g_{\text{lat}}^{c(2)}(\Delta \mathbf{v}_{\text{lat}}) &= \Delta \phi_{\text{lat}}^{\mathcal{O}} - \Delta \hat{\phi}_{\text{lat}}^{\mathcal{O}}; g_{\text{lat}}^{c(3)}(\Delta \mathbf{v}_{\text{lat}}) = \Delta \psi_{\text{lat}}^{\mathcal{O}} \end{aligned} \quad (3.45a)$$

$$\begin{aligned} g_{\text{longi}}^{c(1)}(\Delta \mathbf{v}_{\text{longi}}) &= -(\Delta x_{\text{longi}}^{\mathcal{O}} - \Delta \hat{x}_{\text{longi}}^{\mathcal{O}}); \\ g_{\text{longi}}^{c(2)}(\Delta \mathbf{v}_{\text{longi}}) &= -(\Delta \theta_{\text{longi}}^{\mathcal{O}} - \Delta \hat{\theta}_{\text{longi}}^{\mathcal{O}}); g_{\text{longi}}^{c(3)}(\Delta \mathbf{v}_{\text{longi}}) = \Delta \psi_{\text{longi}}^{\mathcal{O}} \end{aligned} \quad (3.45b)$$

For compliance constraints in Design Case 2, only 2 types of compliance analyses are considered because the requirements mentioned to improve R&H performances are obtained from the two types of compliance analyses. In compliance constraints by a lateral force, the displacements of y -coordinate of the wheel center ($\Delta y_{\text{lat}}^{\mathcal{O}}$) and the angular displacement related to the camber angle ($\Delta \phi_{\text{lat}}^{\mathcal{O}}$) are set to be less than the values obtained from the reference suspension linkage. In compliance constraints by a longitudinal force, the displacement of x -coordinate of the wheel center ($\Delta x_{\text{longi}}^{\mathcal{O}}$) is set to be larger than the target value as to secure high compliance in longitudinal direction, by the way, the angular displacement related to the spin ($\Delta \theta_{\text{longi}}^{\mathcal{O}}$) is set to be stiffer than the reference suspension linkage. In addition, the angular displacements of the wheel in rotation along the z axis are set such that toe-in can be achieved in both types of compliance analyses. All error bounds for compliance constraint functions are set to zero and the other parameters mainly used for optimization are the same as in Design Case 1.

The optimization results are shown in Fig. 3.14 to Fig. 3.16 and Table 3.3 and 3.4. Fig. 3.14 shows that the final optimized layout represented by the SBM and its equivalent linkage mechanism. The converged values of the design variables are found in Fig. 3.15. In Fig. 3.15(a), the converged values of the topology controlling design variables is illustrated. The green bars in Fig. 3.15(a) indicated design variables for block-connecting springs used to connect the wheel carrier blocks. Fig. 3.15(b) shows the converged values of the topology controlling design variables for anchoring springs, and it can be found that four mounting points are generated to connect the result mechanism to the chassis. Fig. 3.15(c) illustrated the converged values of design variables for bushing stiffness and the design variables related to the mounting points (red bars) are well adjusted to satisfy the compliance constraints. Fig. 3.15(d) shows the converged values of the design variables for grid points. The kinematic constraint values at the convergence are in Table 3.3 and it shows that all the values are below the kinematic error bounds. The comparison of compliance characteristics between the result suspension and the reference suspension is presented in Table 3.4. As intended, the comparison result shows that lateral and spin stiffnesses are higher than the target values, compliance in a longitudinal direction is higher than the target values, and making toe-in when a cornering or a braking force is applied.

For identifying the topology of the result suspension defined by the springs, Fig. 3.16 is prepared. The left side of Fig. 3.16 illustrated the final state of the SBM. (The

shape of the blocks is illustrated as the initial shape for easy identification.) In the figure, blocks of the same color form a single rigid body or link as a whole. The figure shows that the result suspension is consisted with three rigid bodies (2 rigid arms and one rigid link). In detail, Blocks 1 to 6, the green blocks located in the bottom floor, are connected rigidly to each other by block-connecting springs 1 to 16 and 49 to 60. Block-connecting springs 64 and 67 connects the green block group to the wheel carrier by a spherical joint. Although two block-connecting springs are used to connect, the block-connecting springs can represent just one spherical joint because the location of them is the same. In addition, the green block group is connected to the chassis (ground) by bushings represented by anchoring springs 4 and 10. Note that these springs serve to connect these blocks to the chassis by a spherical joints in a kinematic analysis. All the blocks on the middle floor are floating blocks that do not make a kinematic chain of the result mechanism.

About the blocks on the top floor, there are two groups of rigid blocks. One is consisted of Blocks 20 and 23 and the other is consisted of Blocks 21 and 24. Blocks 20 and 23 are connected to each other by block-connecting springs 101 to 104 and Blocks 21 and 24 are connected to each other by block-connecting springs 105 to 108. The orange block group is connected to the wheel carrier by the block-connecting spring 115, and it is also connected to the purple block group by a spherical joint represented by the block-connecting spring 43. The purple block group is connected to the wheel charrier by the block-connecting spring 119. In

addition, the purple block group is connected to the chassis (ground) by bushings represented by anchoring springs 33 and 34.

The final layout of the SBM in Design Case 2 shows that there are two arms and one link between the wheel carrier and the chassis as the same as the result suspension in Design Case1 and the reference suspension, but the connectivity is different from them. In detail, the topology of the result suspension in Design Case 1 and the reference suspension is identical to a double wishbone suspension, but the result suspension in Design Case 2 is more like an integral link suspension [58]. Fig. 3.17 is prepared to help to understand of suspension topology. A cylinder and a circle denote a revolute joint and a spherical joint, respectively, and a link with a revolute joint and a spherical joint means a rigid arm. In Fig. 3.17(a) and Fig. 3.17(b), topologies of a double wishbone suspension and an integral link suspension are shown, respectively. The key feature of an integral link suspension compared to a double wishbone suspension is that there is an integral link that connects a wheel carrier to a link, not a chassis. In Design Case 2, the result suspension is composed of two rigid arms and one link as a double wishbone suspension, but the connectivity of it is more like an integral link suspension as one link connects the rigid arm to a wheel carrier as shown in Fig. 3.17(c). Through these results, it is found that the topology of a suspension can be different depending on the target compliance characteristics, and the proposed method can find the right design for the suspension linkage which can satisfy the given K&C conditions.

3.5 Summary

In this chapter, we applied the topology optimization method of linkage mechanisms simultaneously considering K&C characteristics to design a vehicle suspension. In the design of a vehicle suspension, compliance characteristics are important features as well as kinematic characteristics in that R&H performances of a vehicle are determined by K&C characteristics.

For the topology optimization of suspension linkages simultaneously considering K&C characteristics, there are two issues to be addressed. First, the model adapt to apply the topology optimization method for linkage mechanisms considering K&C characteristics was needed to develop. Second, the bushing stiffness can be adjusted for applying the realistic design problem, in this case a vehicle suspension design. For resolving the first issue, we develop a spatial spring-connected rigid block model (SBM) and use the Tait-Bryan angles to define the posture of rigid blocks in 3D space. The 3D nonlinear bar based model was already used for topology optimization of suspension linkages, but it is found that the nonlinear bar based model is not suitable to represent bushing stiffness because the nonlinear bars share the one anchoring spring which should be used to represent bushings. However, in the 3D SBM, an anchoring spring is not shared many rigid blocks, and thus it is useful to represent bushing stiffness in three-dimensional space at the convergence of topology optimization of suspension linkages.

The second issue is solved by employing design variables for adjusting bushing stiffness. As there is no need to represent bushings in a kinematic analysis, the design variables are only used in a compliance analysis. In addition, as bushings are usually used to connect to suspension linkages and the chassis, only the stiffness values of anchoring springs are adjusted by the design variables. At last, optimization formulation to implement the topology optimization of suspension linkages simultaneously considering K&C characteristics is also proposed.

With two design cases, the validation and effectiveness are shown. In Design Case 1, a double wishbone suspension is generated when the K&C constraints are given as to recover the reference suspension linkage of which topology is a double wishbone suspension. Unlike this, in Design Case 2, when the compliance characteristics are given as to help to improve the R&H performances of a vehicle, a suspension linkage having the different topology is generated. Although the composition of the result suspension in Design Case 2 is the same as that of a double wishbone suspension, the connectivity of two suspensions is different because the link of the result suspension in Design Case 2 connects the upper arm and the wheel carrier. This kind of connectivity is more like an integral link suspension and thus it is found that the topology of a result suspension linkage is changed as compliance characteristics changes. Through these results, it is proven that the proposed method can design a suspension linkage but also bushing stiffness as to satisfy the desired K&C characteristics.

Table 3.1 Values of the kinematic constraint functions at convergence for Design Case 1

$\max(g_{t^*}^{k(1)})$ (m)	$\max(g_{t^*}^{k(2)})$ (m)	$\max(g_{t^*}^{k(3)})$ (deg)	$\max(g_{t^*}^{k(4)})$ (deg)	$\max(g_{t^*}^{k(5)})$ (deg)
2.5×10^{-3}	2.5×10^{-3}	0.021	0.040	0.0076

Table 3.2 Values of the compliance constraint functions at convergence for Design Case 1

$g_{\text{lat}}^{c(1)}$ (m)	$g_{\text{lat}}^{c(2)}$ (deg)	$g_{\text{lat}}^{c(3)}$ (deg)	$g_{\text{longi}}^{c(1)}$ (m)	$g_{\text{longi}}^{c(2)}$ (deg)	$g_{\text{longi}}^{c(3)}$ (deg)	$g_{\text{align}}^{c(1)}$ (deg)	$g_{\text{align}}^{c(2)}$ (deg)
2.5×10^{-5}	0.029	0.026	5.1×10^{-5}	0.048	0.14	0.0022	0.19

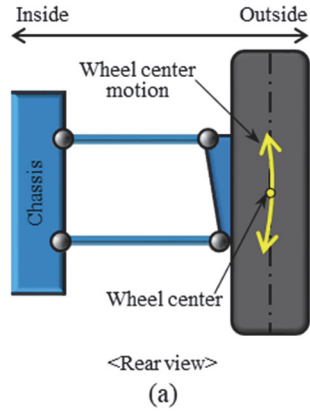
Table 3.3 Values of the kinematic constraint functions at convergence for Design Case 2

$\max(g_i^{k(1)})$ (m)	$\max(g_i^{k(2)})$ (m)	$\max(g_i^{k(3)})$ (deg)	$\max(g_i^{k(4)})$ (deg)	$\max(g_i^{k(5)})$ (deg)
5.0×10^{-3}	5.0×10^{-3}	0.028	0.050	0.014

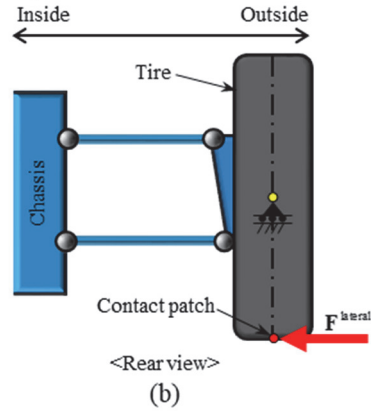
Table 3.4 Comparison between compliance characteristic values of the result suspension in Design Case 2 and the target values

	Δy_{lat} (m)	$\Delta \phi_{\text{lat}}$ (deg)	$\Delta \psi_{\text{lat}}$ (deg)	Δx_{longi} (m)	$\Delta \theta_{\text{longi}}$ (deg)	$\Delta \psi_{\text{longi}}$ (deg)
Result	-5.7×10^{-5}	-0.020	0.0027	4.4×10^{-4}	-0.17	0.0085
Target	-1.1×10^{-4}	-0.042	0.066	4.2×10^{-4}	-0.21	-0.16

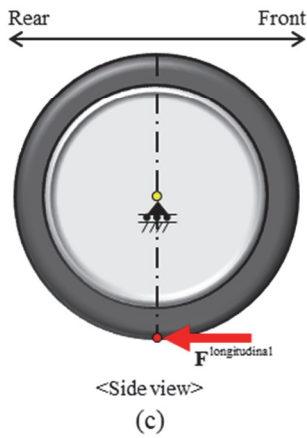
1) Kinematic characteristics



2) Compliance characteristics by a lateral force



3) Compliance characteristics by a longitudinal force



4) Compliance characteristics by an Aligning moment

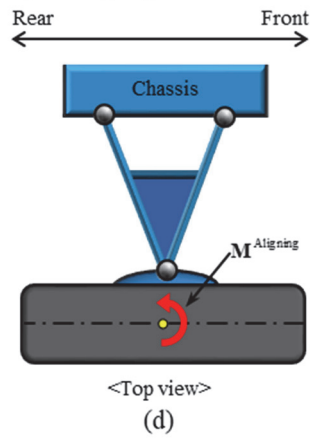


Fig. 3.1 Analysis conditions to define K&C characteristics of a vehicle suspension. (a) Wheel bump/rebound motion for kinematic characteristics, (b) lateral force for compliance characteristics, (c) longitudinal force for compliance characteristics, and (d) aligning moment for compliance characteristics

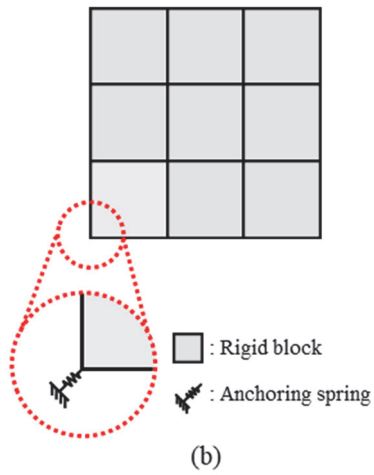
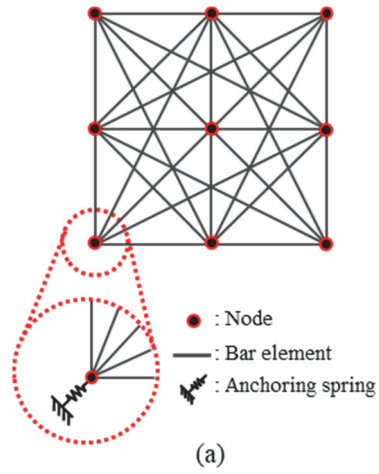


Fig. 3.2 Illustrations of the models used for topology optimization of linkage mechanisms. (a) The nonlinear bar based model and (b) the SBM

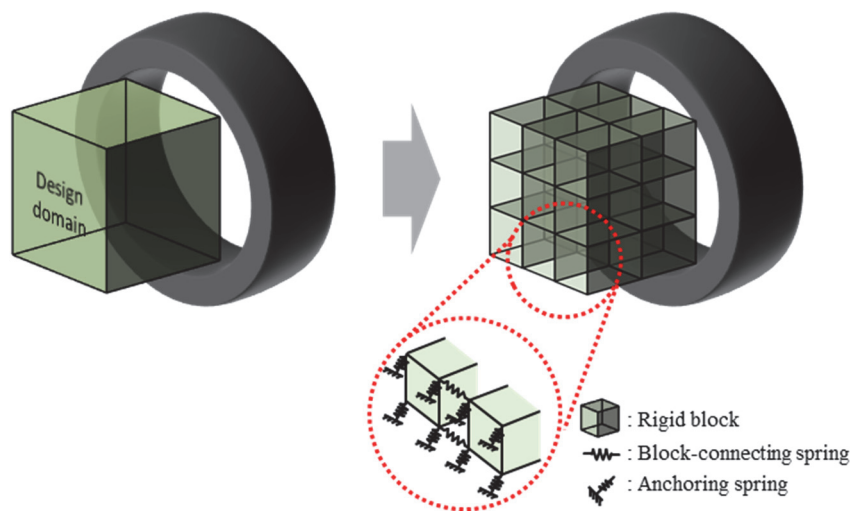


Fig. 3.3 Modeling with the spatial SBM for designing a vehicle suspension

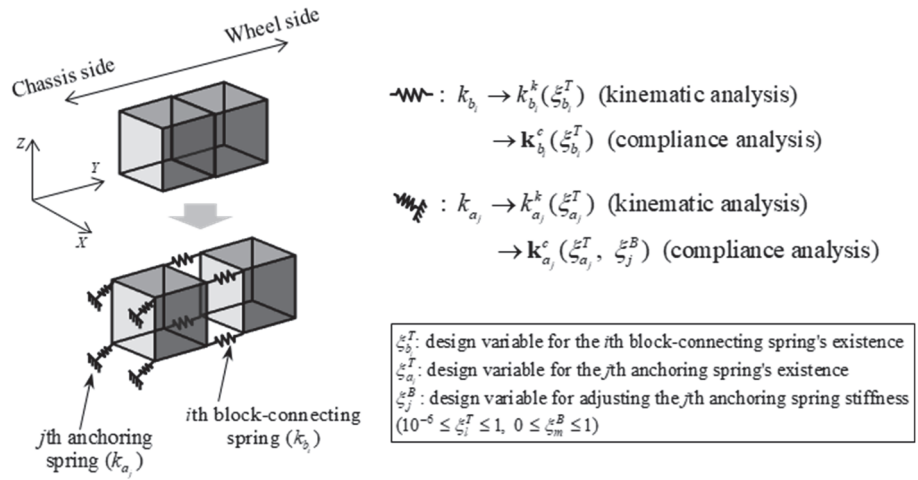
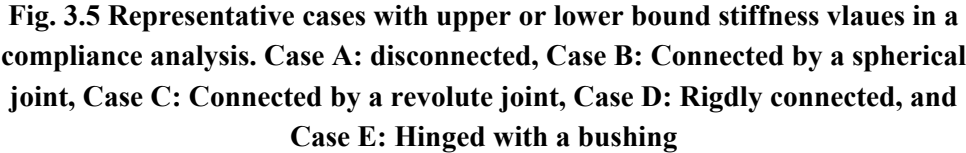


Fig. 3.4 Explanation about spring connection of the two blocks connecting between chassis and wheel carrier



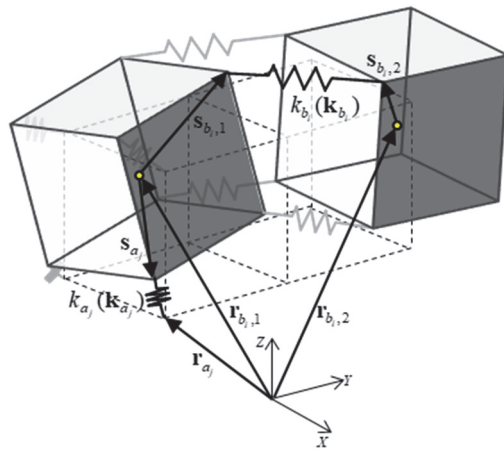


Fig. 3.6 A snapshot of two rigid blocks in a moved position by a given input motion or an external force

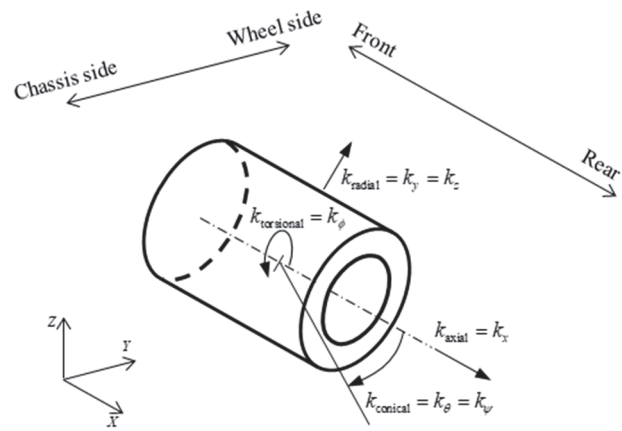


Fig. 3.7 Spring stiffness for a cylindrical bushing

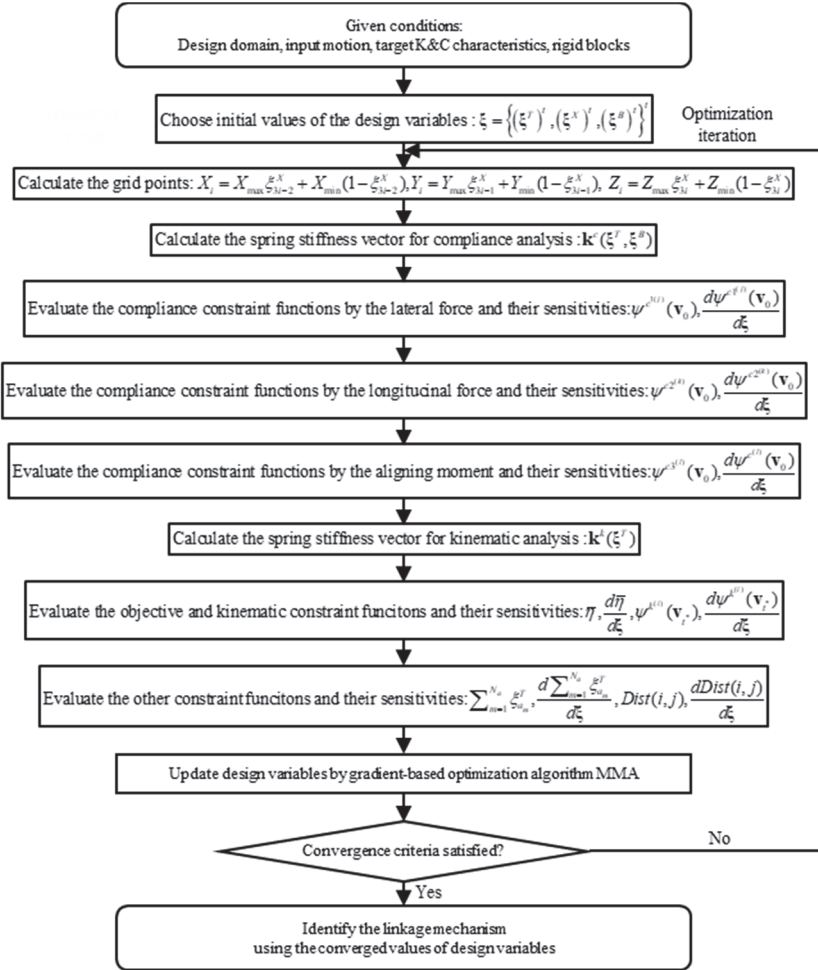


Fig. 3.8 Flow chart for topology optimization of vehicle suspensions considering both kinematic and compliance characteristics

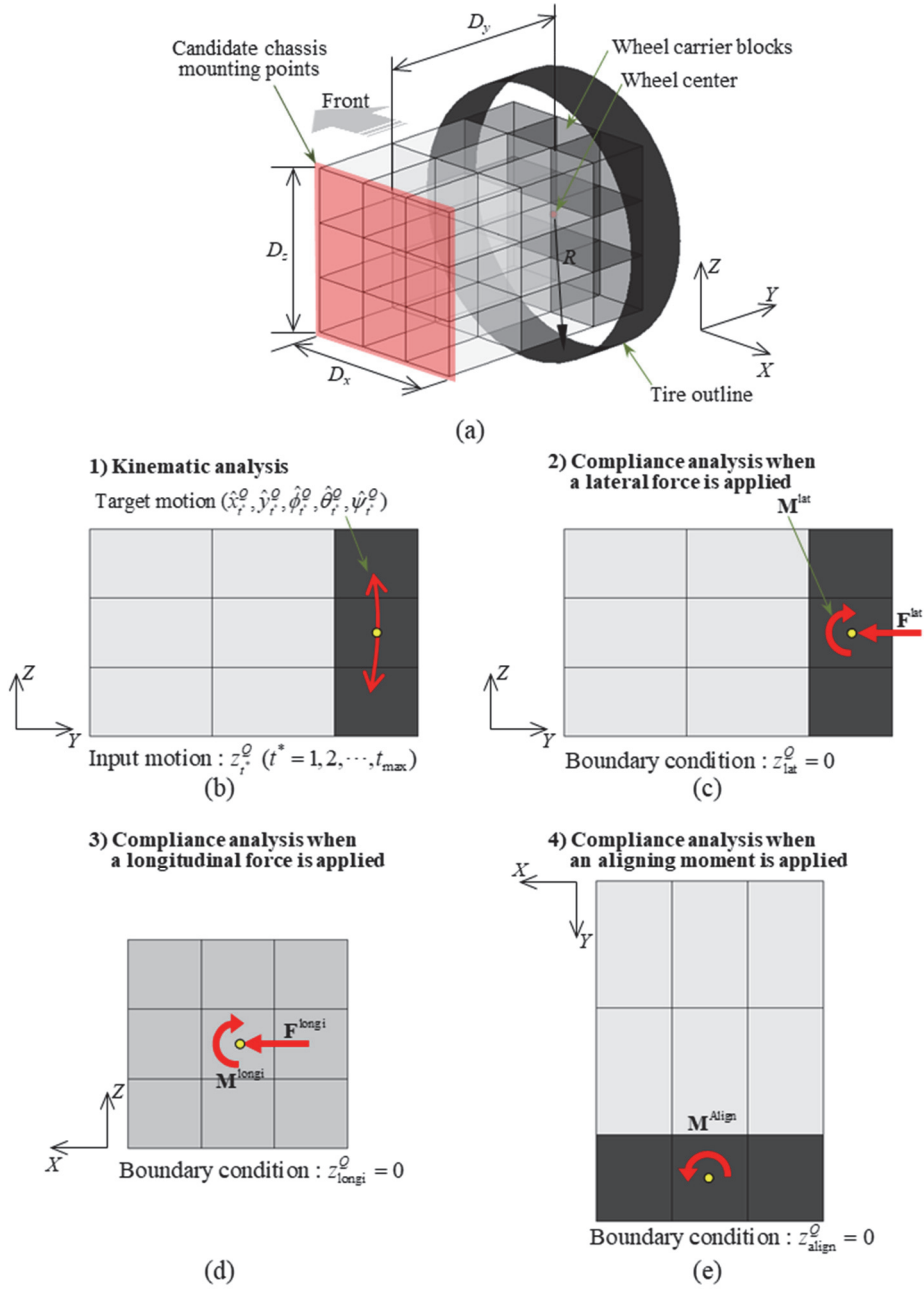


Fig. 3.9 Problem definition for suspension linkage synthesis. (a) Design domain and the employed SBM, (b) analysis conditions for kinematic characteristic, and analysis conditions for compliance characteristics by (c) a lateral force, (d) a longitudinal force, and (e) an aligning moment

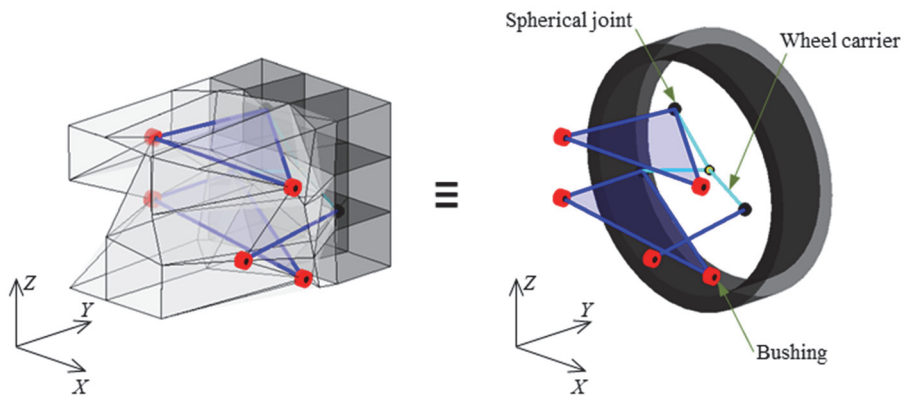


Fig. 3.10 Final optimization layout of the spatial SBM (left) and its equivalent linkage mechanism (right) for Design Case 1

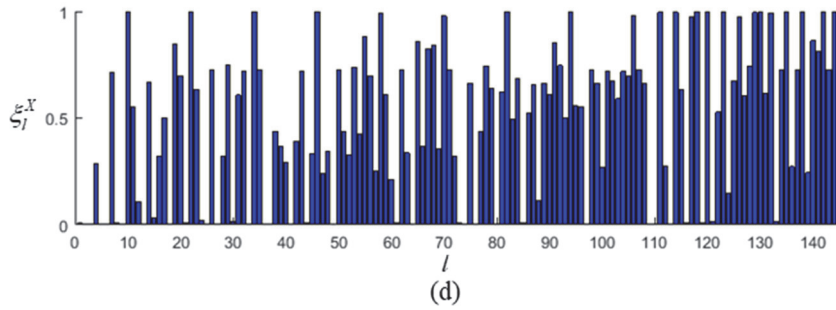
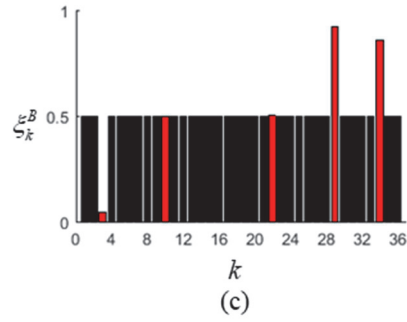
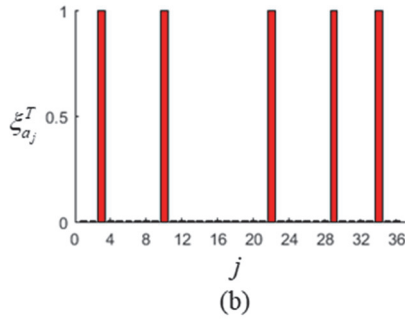
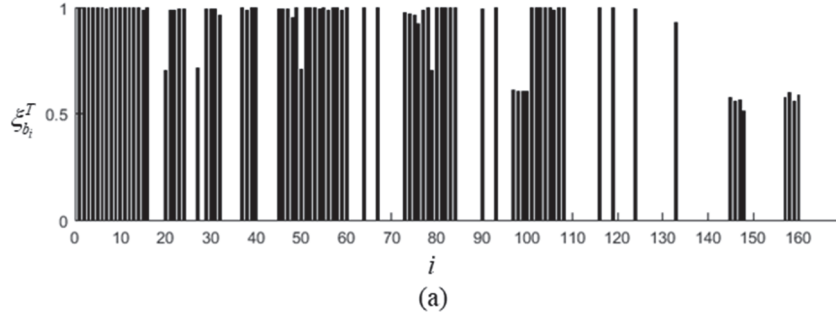


Fig. 3.11 Design variables at convergence for Design Case 1: (a) topology controlling design variables related to the block-connecting springs, (b) topology controlling design variables related to the anchoring springs, (c) bushing stiffness design variables (the red bars indicates the design variables for bushing stiffness related to the mounting points to the chassis), and (d) shape design variables

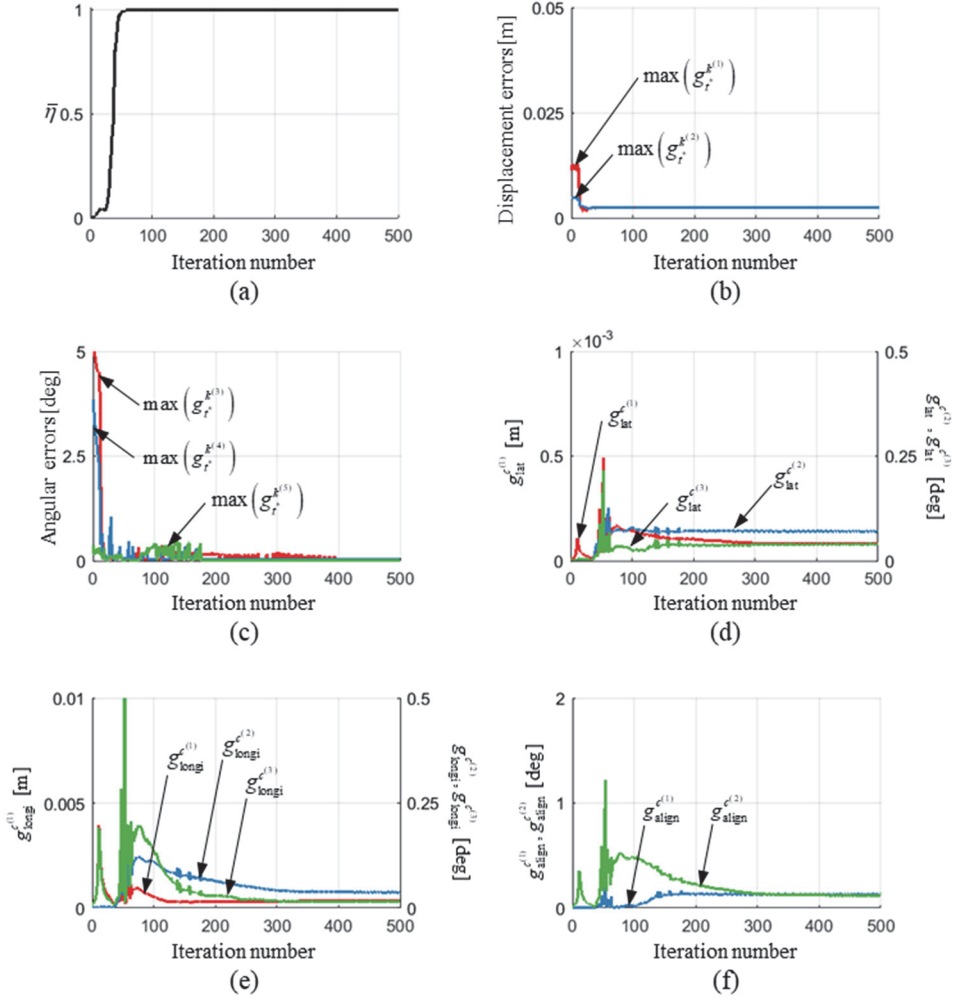
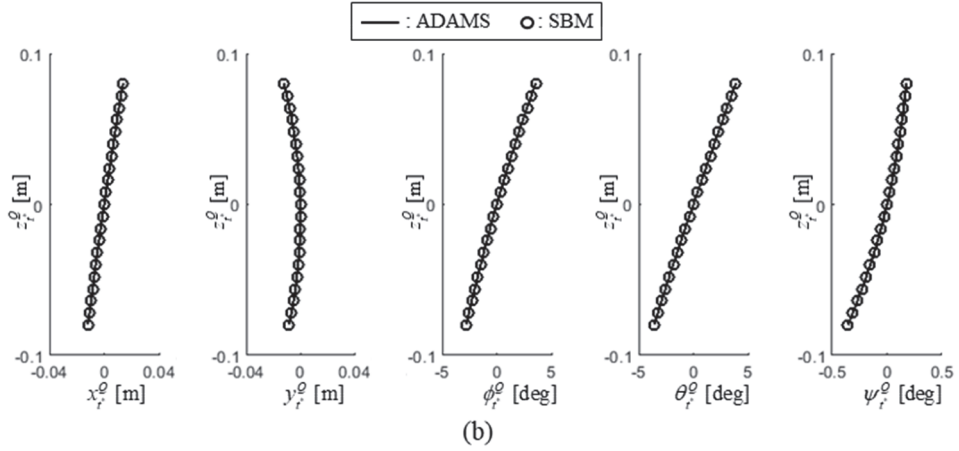
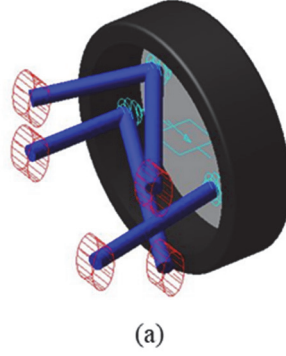


Fig. 3.12 Convergence histories of Design Case 1: (a) objective, (b) kinematic constraints related to the displacement error, (c) kinematic constraints related to the angular error, (d) compliance constraints by a lateral force, (e) compliance constraints by a longitudinal force, and (f) compliance constraints by an aligning moment



	$\Delta y_{\text{lat}}^{\phi}$ (mm)	$\Delta \phi_{\text{lat}}^{\phi}$ (deg)	$\Delta \psi_{\text{lat}}^{\phi}$ (deg)	$\Delta x_{\text{longi}}^{\phi}$ (mm)	$\Delta \phi_{\text{longi}}^{\phi}$ (deg)	$\Delta \psi_{\text{longi}}^{\phi}$ (deg)	$\Delta \phi_{\text{align}}^{\phi}$ (deg)	$\Delta \psi_{\text{align}}^{\phi}$ (deg)
SBM	-0.0807	-0.0708	0.0399	0.3550	0.0376	-0.0160	-0.1313	0.1200
ADAMS	-0.0808	-0.0708	0.0399	0.3540	0.0373	-0.0159	-0.1310	0.1200
Error	0.12 %	0 %	0 %	0.28 %	0.8 %	0.63 %	0.23 %	0 %

(c)

Fig. 3.13 Comparison the K&C characteristics obtained from the SBM and ADAMS software to verify the validity of the proposed method using the result of Design Case 1. (a) The result suspension model using ADAMS software, (b) the comparison of kinematic curves, and (c) the comparison of compliance characteristic values

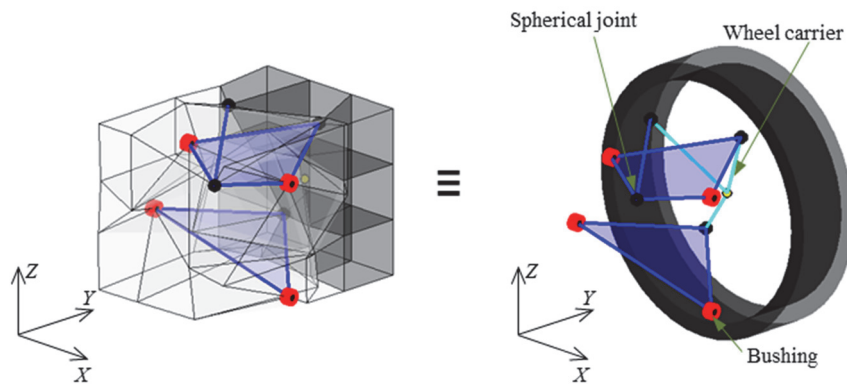


Fig. 3.14 Final optimization layout of the spatial SBM (left) and its equivalent linkage mechanism (right) for Design Case 2

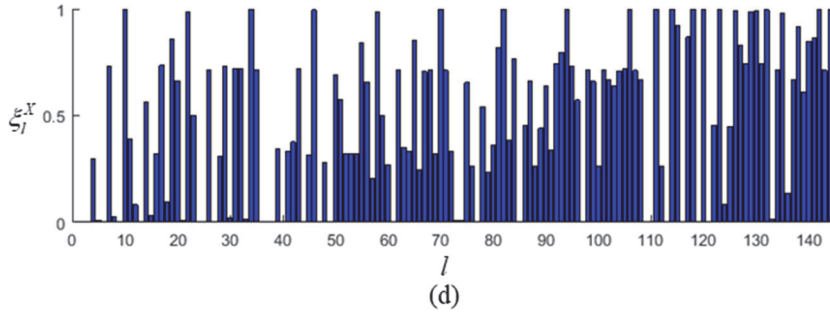
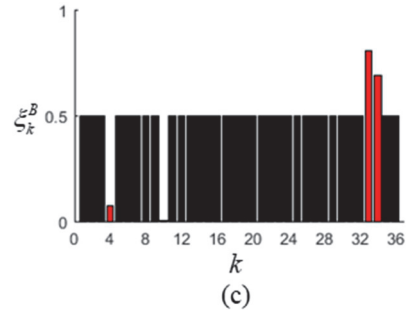
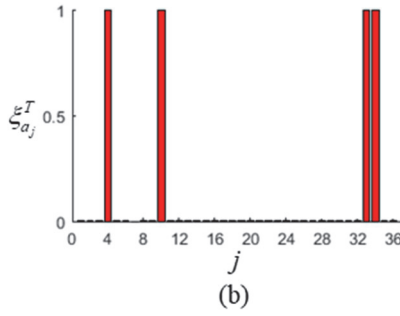
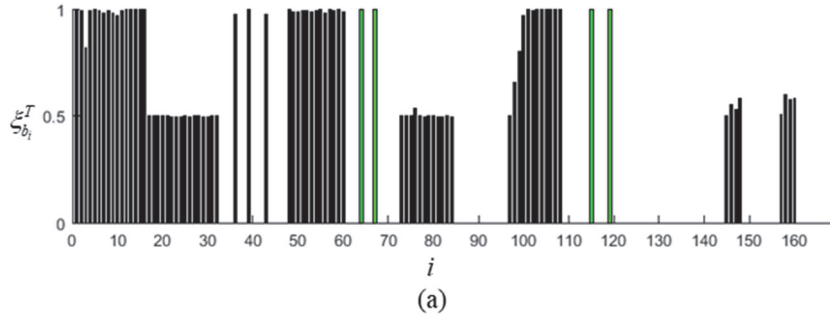


Fig. 3.15 Design variables at convergence for Design Case 2: (a) topology controlling design variables related to the block-connecting springs, (b) topology controlling design variables related to the anchoring springs, (c) bushing stiffness design variables (the red bars indicates the design variables for bushing stiffness related to the mounting points to the chassis), and (d) shape design variables

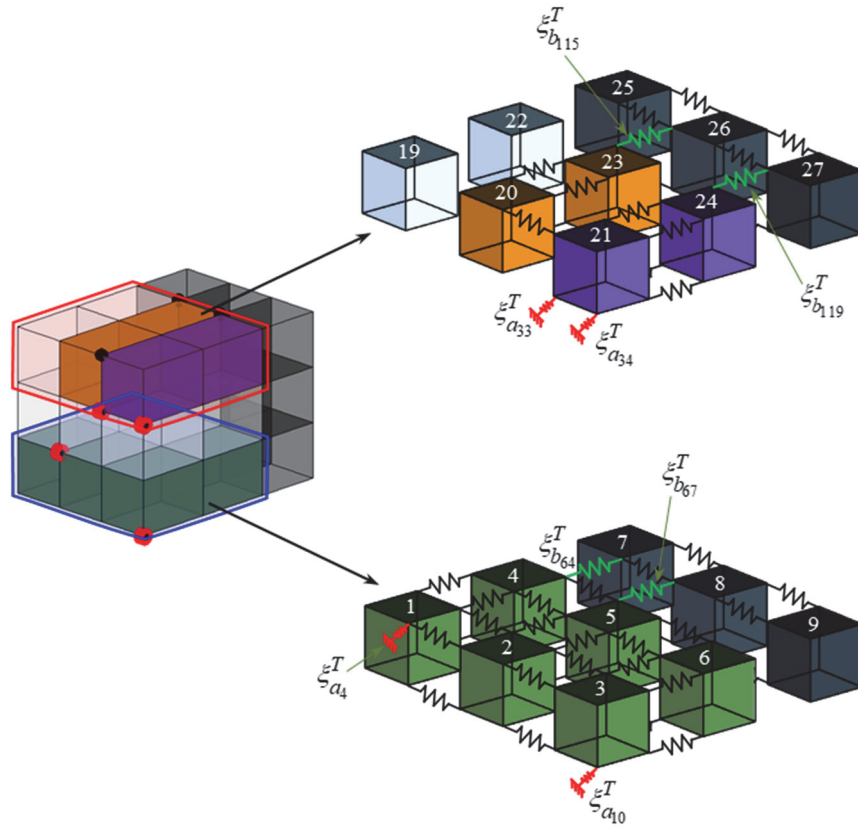
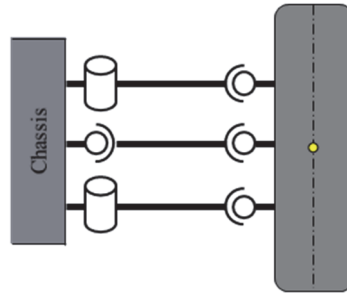
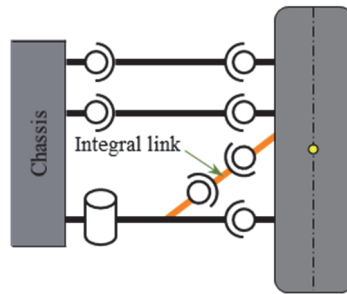


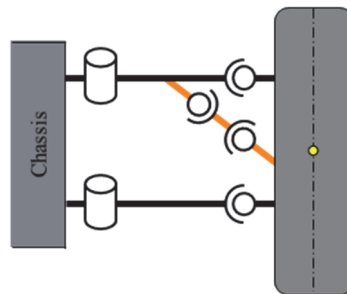
Fig. 3.16 Identified the topology of the result linkage mechanism for Design Case 2 (left) from the optimized layout expressed by rigid blocks connected by the block-connecting and anchoring springs having the maximum stiffness value (right). (In this figure, the block is illustrated as the initial shape of them to decern easily.)



(a)



(b)



(c)

Fig. 3.17 Illustrations of suspension topology. (a) Double wishbone suspension, (b) integral link suspension, (c) the result suspension of Design Case 2

CHAPTER 4.

Conclusions

In this dissertation, we proposed a new topology optimization method for linkage mechanism synthesis simultaneously considering kinematic and compliance characteristics. The proposed method is presented in the way that kinematic and compliance analyses are performed in a streamlined optimization process. It was shown that various linkages from planar mechanisms to spatial mechanisms such as vehicle suspensions can be designed by the proposed method.

There were two main issues to be resolved for the topology optimization of linkage mechanisms considering kinematic and compliance characteristics simultaneously. First, a new ground model that can allow both kinematic and compliance analyses was needed. Second, elastic elements such as bushings should be represented within the model. To address these issues, we used the spring-connected rigid block model (SBM) developed earlier for mechanism synthesis considering only kinematic characteristics, but we made it suitable for the simultaneous consideration of K&C characteristics during mechanism synthesis by making its zero-length springs

multifunctional. Variable-stiffness springs were used to identify the mechanism kinematic configuration only in the existing methods, but in the proposed approach, they serve to determine not only the mechanism kinematic configuration but also the compliance element distribution. In particular, the ground-anchoring springs used to anchor a linkage mechanism to the ground were functionalized to simulate actual bushings as well as to identify the desired linkage kinematic chain.

In Chapter 2, the proposed approach was implemented for synthesizing planar linkage mechanisms. Through an example to validate compliance analysis using the SBM, the feasibility of compliance analysis using the SBM was shown. The effectiveness and validation of the proposed method were demonstrated with three case studies. Also, the limitation of the optimization methodology for mechanism synthesis for considering K&C characteristics based on the existing method was presented. Thereby, an additional design process to consider K&C characteristics is needed because the existing topology optimization method can consider only kinematic characteristics. It was found that the existing method was difficult to apply for the present design problems or required repeated optimization runs using different initial guesses. However, the proposed simultaneous optimization approach yielded successfully synthesized mechanisms satisfying all of the required K&C characteristics even when the two-step sequential formulation could not. In addition, we succeeded in synthesizing a 2D vehicle suspension which can be interpreted as a six-bar linkage. The synthesized linkage mechanism indeed exhibited improved

lateral stiffness compared to the 2D version of a double wishbone suspension, which is a four-bar linkage.

In Chapter 3, the methodology for synthesizing a linkage mechanism considering both kinematic and compliance characteristics simultaneously was applied to design a spatial vehicle suspension. Although a spatial suspension linkage has already been synthesized using a mechanism topology optimization method [8], but only kinematic constraints were considered. Because the nonlinear bar model used in [8] was not suitable for the simultaneous consideration, we developed a spatial SBM for which the Tait-bryan angles which match well the camber, spin, and toe angles defining the posture of a vehicle wheel were employed to define the posture of rigid blocks. Bushing elements were represented by anchoring springs as in the 2D space, but six values were given to anchoring springs as stiffnesses of a cylindrical bushing are different depending on the direction in a compliance analysis. In addition, for realistic design of vehicle suspensions, we added design variables to adjust the stiffness values of anchoring springs unlike in 2D problems, and thus the suitable bushing stiffnesses were obtained when the topology optimization was completed.

To design vehicle suspensions, we considered two design cases. First, we aimed to recover a known (reference) suspension linkage layout by using its kinematic and compliance properties in the constraint equations. The topology of the reference suspension linkage was a double wishbone and the result of Design Case 1 was found

to be exactly the same. For Design Case 2, we changed the compliance characteristics to improve the R&H performances of a vehicle while keeping the same kinematic characteristics as those of the reference suspension. Specifically, the compliance characteristics were so given as 1) to improve lateral and spin stiffnesses which in turn help improve the vehicle response to a steering input, 2) to improve the longitudinal compliance related to impact harshness, and 3) to do toe-in when a braking or a cornering force is applied. The suspension mechanism synthesized in Design Case 2 had two rigid arms and one link same as in a double wishbone suspension, but we found that their connectivity was different. Because one rigid link in the synthesized suspension was connected to the upper arm, not to a wheel carrier; the suspension designed in Design Case 2 is found to be similar to an integral link suspension.

To sum up, a new topology optimization methodology for mechanism synthesis simultaneously considering kinematic and compliance (K&C) characteristics was developed based on the spring-connected rigid block model (SBM) in this thesis, and the effectiveness and validation was verified by three case studies. Furthermore, the developed method was applied to design a vehicle suspension, and in the process of applying, a spatial SBM was developed and also design variables for adjusting bushing stiffness were added. By using the developed synthesis method, two types of suspension linkages were successfully obtained. In that this study is the first attempt to carry out the topology optimization of linkage mechanisms considering

kinematic characteristics and also the other characteristics, it is expected that the developed method can be further expanded to synthesize mechanisms in which system stiffness or joint forces need to be considered.

APPENDIX A.

Target cascading process for deriving K&C characteristics of a suspension to improve vehicle's R&H performances

A.1 Overview

Target cascading means to the process of deriving the requirements from the whole vehicle to each subsystems such as suspensions or dampers [49]. In this Appendix, the explanation of the target cascading process to derive K&C requirements for a vehicle suspension to help to improve R&H performances of a vehicle is given. For generating data of a variety of K&C characteristics, we used a double wishbone suspension. By changing the geometry of the suspension, we can make a reliable data of K&C characteristics. The K&C characteristics are used to define a vehicle suspension in CARSIM, and thus we can investigate the relationship between the K&C characteristics and R&H performances. Finally, through design optimization of a double wishbone suspension for improving R&H performances, we can obtain the K&C characteristics to improve R&H performances. The more details are in the following chapters.

A.2 Ride and handling (R&H) performances

For evaluating R&H performances of a vehicle, we use the thirteen performance indices listed in Table A.1. The handling performances related with ISO 4318, ISO 7401, and ISO 3888 is obtained from the four types of full-car simulation using CARSIM.

- 1) Step steer (SS)
- 2) Double lane change (DLC)
- 3) Steady-state circle simulation (SSC)
- 4) Rough road simulation (RRS)

The full-car model used is built based on DANIGO, an ultra-compact electric car, and the steering input angle in SS is set so that the lateral acceleration equals 0.7 g (g : gravity) and the velocity for DLC is kept in 70 km/h. In SSC, the radius of the circle is 50 m and the velocity for RRS is set to 10 km/h. The some representative graphs of the four simulations are shown in Fig. A.1. The ride performances is evaluated by the kinematic and compliance characteristics which are well known to be related with ride performances [49].

A.3 Analysis procedure to evaluate R&H performances using a double wishbone suspension

The overall analysis procedure to evaluate R&H performance from a configuration of a double wishbone suspension is that K&C characteristics are obtained from a double wishbone suspension using MATLAB, and the K&C characteristics are used to be applied to CARSIM software to evaluate R&H performances. Through this process, we can build an integrated analysis procedure to evaluate R&H performances of a vehicle from the design of the suspension. The overall procedure is as shown in Fig. A.2.

A.4 Design optimization of a double wishbone suspension for deriving K&C characteristics to improve R&H performances

A.4.1 Design variable and interpolation

The initial configuration of a double wishbone suspension is shown in Fig. A.3, and the layout is changed by design variables. The design variables to be used in this research are the position of the hard points and bushing stiffness as follow:

$$\xi = \left\{ \left(\xi^X \right)^t, \left(\xi^B \right)^t \right\} \quad (\text{A.1})$$

where

$$\xi^X = \left\{ \xi_1^X, \xi_2^X, \dots, \xi_{24}^X \right\}^t \quad (0 \leq \xi_i^X \leq 1) \quad (\text{A.2})$$

$$\xi^B = \left\{ \xi_1^B, \xi_2^B, \xi_3^B, \xi_4^B \right\}^t \quad (0 \leq \xi_j^B \leq 1) \quad (\text{A.3})$$

In Eq. (A.1), ξ^X and ξ^B denote the design variable for position of hard points and design variable for bushing stiffness. The position of hard points is interpolated by the design variables as follow:

$$\mathbf{X} = \{X_1, Y_1, Z_1, X_2, Y_2, Z_2, \dots, X_8, Y_8, Z_8\}^t \quad (\text{A.4a})$$

$$X_i = X_{i,\text{initial}} + 10 \times (\xi_{3i-2}^X - 0.5) \quad (i=1, 2, \dots, 8) \quad (\text{A.4b})$$

$$Y_j = Y_{j,\text{initial}} + 50 \times (\xi_{3j-1}^X - 0.5) \quad (j=1, 2, \dots, 8) \quad (\text{A.4c})$$

$$\begin{aligned} Z_l &= Z_{l,\text{initial}} + 10 \times (\xi_{3l}^X - 0.5) \quad (l=1, 2, 6); \\ Z_k &= Z_{k,\text{initial}} + 1 \times (\xi_{3k}^X - 0.5) \quad (k=2, 3, 4, 7, 8) \end{aligned} \quad (\text{A.4d})$$

The units in Eq. (A.4) is millimeter (mm), and the range where the hard points can

be moved is set to be different by the directions as considering the change of kinematic curves according to the position changes. Especially, as the kinematic curves are sensitive to the z -coordinates, the range where the z -coordinates can be moved are limited in 1 mm as in Eq. (A.4d).

As in Fig. A.3, as bushings are used to connect the upper and lower arm to the chassis, four design variables are employed to interpolate the bushing stiffness. The rotation axis of each bushings are fixed parallel to the line connecting the front and rear hard points of each arm, and the bushing stiffnesses are interpolated by the design variables as below.

$$\mathbf{k} = \{k_{1,P}, k_{1,Q}, k_{2,P}, k_{2,Q}, k_{4,P}, k_{4,Q}, k_{5,P}, k_{5,Q}\}^t \quad (\text{A.5a})$$

$$\begin{Bmatrix} k_{i,P} \\ k_{i,Q} \end{Bmatrix} = 0.7 \times \begin{Bmatrix} (k_{i,P})_{\text{initial}} \\ (k_{i,Q})_{\text{initial}} \end{Bmatrix} + 0.6 \times \begin{Bmatrix} \xi_i \\ \xi_i \end{Bmatrix} \quad (i = 1, 2, 4, 5) \quad (\text{A.5b})$$

The bushing stiffness is set to be able to be $\pm 30\%$ from the initial value, and the stiffness ratio by the direction in one bushing is kept as one design variable controls two stiffness values in one bushing.

A.4.2 Metamodeling

As the purpose of this optimization problem is to design a double wishbone suspension which can improve the R&H performances, multi-objective optimization is suitable to use. For a multi-objective optimization, a multi-objective genetic algorithm (MOGA) is generally used, but it requires a high computational cost

because of population based optimization method. To resolve this, we build a metamodel which mimic the behavior of simulation models with analytical expressions and reduce the computational costs for the efficient optimization [59-61].

Design of experiments (DoE) denotes the planning method for the experiment, and the importance of it is increasing as the number of design variables is increasing. For building a metamodel, choosing an adequate sampling technique is important, and we use optimal Latin hypercube design (OLHD) technique which is a modified Latin hypercube design technique to improve space-filling [62]. PIANO software is used for the sampling based on OLHD. The number of sample points is generated as 1000 which is more than the square of the number of design variables (n_d^2 , n_d : the number of design variables), and R&H performance values for the sample points are calculated using CARSIM software. (Note that a metamodel is built for only the R&H performance indices from CARSIM because the computational costs to run the MATLAB code for K&C analysis is low.)

PIANO is also used to build a metamodel. A kriging metamodel in PIANO is used, and it is verified with using an additional 100 sample points which are chosen by augmented Latin hypercube design (ALHD) method [63]. The comparison between the index values obtained from the metamodel and simulation model is shown in Fig. A.4. In Fig. A.4, the x -axis means the sample points from the ALHD, and y -axis

denotes the performance index values from the two models. The blue line denotes the index values from the metamodel and the red-dashed line denotes the index values from the simulation model. As shown in Fig. A.4, the index values obtained from the metamodel and CARSIM are almost identical, and thus it can be said that the metamodel has a good accuracy.

A.4.3 Optimization formulation

If all R&H performance index values are used to be objectives, optimization formulation can be written as below.

$$\begin{aligned} &\text{Find } \xi^X \text{ and } \xi^B \\ &\text{to minimize } f_m \quad (m=1, 2, \dots, 13) \end{aligned} \tag{A.6}$$

In Eq. (A.6), f_1 to f_{13} denote the performance index values listed in Table A.2.

For using multi-objective global optimizer more efficiently, reducing the number of functions to use as an objective is needed. To do this, we conduct a correlation analysis between the handling performance indices because some of them may have the similar trends. The result of the correlation analysis is as shown in Fig. A.5. In Fig. A.5(a), it seems that some indices have the similar trends to other indices, and the result after grouping the indices with the similar trends is as in Fig. A.5(b). Therefore, they can be grouped in four as below.

Group A : f_7, f_9 , Group B : f_1, f_3, f_6 , Group C : f_8, f_{10} , Group D : f_2, f_4, f_5 ,

We choose one in each group as objectives, and also add two which are interested.

As a result, for the design optimization nine objectives are used and optimization formulation is as below.

$$\begin{aligned} &\text{Find } \xi^X \text{ and } \xi^B \\ &\text{to minimize } f_n \quad (n=1, 2, 5, 6, 7, 8, 11, 12, 13) \end{aligned} \tag{A.7}$$

A.4.4 Optimization result

Using MOGA in PIA_{NO}, we can obtain a Pareto-optimal set and it is illustrated in Fig. A.6. As shown in Fig. A.6, the global optimal cannot find through the optimization process, but a Pareto-optimal set is obtained. Because the number of objectives is more than three, the results are illustrated as each subplot comparing one by one for each objective function. All the values are normalized by their maximum and minimum values, and thus if the value has the minimum, it will be zero, and if the value has the maximum, it will be one. For example, the top-left subplot denotes a plot of the normalized values of the Pareto-optimal set of f_9 and f_9 , and the one next to it is an illustration of f_9 and f_7 .

To derive one design solution for a double wishbone suspension improving R&H performances, a guideline is needed and we choose a data set that could improve f_2 at the most while the other handling performances are better than the initial. The comparison of the R&H performances is shown in Fig. A.7. As in Fig. A.7, f_2 is improved about 5 % compared when the initial layout while the other performances are maintained at a similar level as the initial layout. The K&C characteristics of the

optimal layout are presented in Fig. A.8 and Table A.3. Through these results, it is found that the K&C characteristics which can improve R&H performances can be derived using the presented process.

Table A.1 R&H performance index used in this research

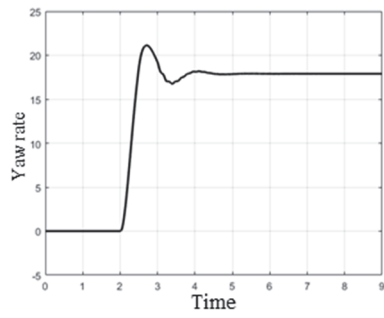
No	Analysis	Index	Category
1	Step steer	Overshoot value of yaw rate	Handling
2		90% response time of yaw rate	Handling
3	Double lane change	The second peak to peak interval value in yaw rate	Handling
4		Root mean square value of slip angles	Handling
5		Root mean square value of steering wheel angles	Handling
6	Steady-state circle simulation	Linearity of lateral acceralation	Handling
7		Roll gradient value	Handling
8		Steering wheel angle gradient	Handling
9		Limit value of lateral acceralation	Handling
10	Rough road simulation	Root mean square value of the steering wheel angles	Handling
11	Kinematic	Anti-squat at 50 mm bump	Ride
12		Anti-lift at 50 mm bump	Ride
13	Compliance	Longitudinal stiffness under impact load	Ride

Table A.2 Explanation of objectives used for the optimization

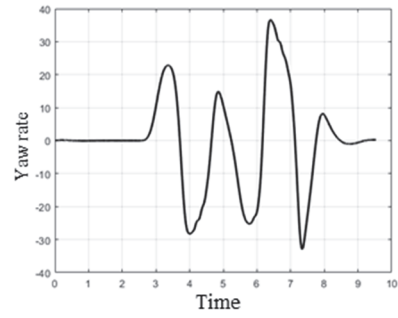
No	Index
f_1	Overshoot value of yaw rate
f_2	90% response time of yaw rate
f_3	The second peak to peak interval value in yaw rate
f_4	Root mean square value of slip angles
f_5	Root mean square value of steering wheel angles
f_6	Linearity of lateral acceralation
f_7	Roll gradient value
f_8	Steering wheel angle gradient
f_9	Limit value of lateral acceralation
f_{10}	Root mean square value of the steering wheel angles
f_{11}	Anti-squat at 50 mm bump
f_{12}	Anti-lift at 50 mm bump
f_{13}	Longitudinal stiffness under impact load

Table A.3 Compliance characteristics of the initial and optimized layout

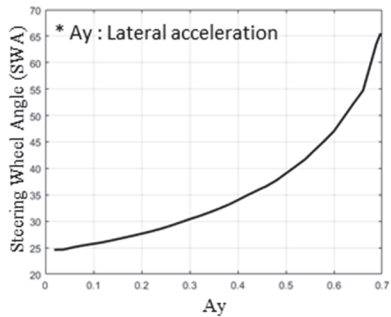
Type	Displacement	Optimized	Initial	Unit
Cornering force	Contact patch	0.273	0.235	mm/kN
	Toe	0.066	0.043	deg/kN
	Camber	0.042	0.033	deg/kN
Braking force	Contact patch	-3.024	-2.091	mm/kN
	Toe	-0.159	-0.088	deg/kN
	Camber	0.859	0.329	deg/kN
Aligning moment	Toe	0.313	0.183	deg/kN
	Camber	0.129	0.087	deg/kN



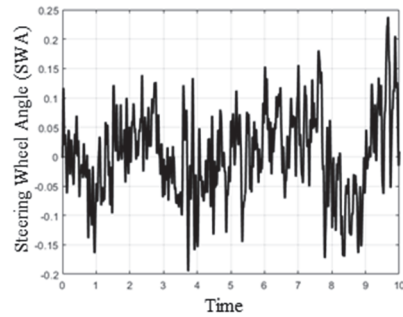
(a)



(b)



(c)



(d)

Fig. A.1 Sample graphs of full-car simulations considering in this research: (a) step steer, (b) double-lane change, (c) steady-circle simulation, and (d) rough road simulation

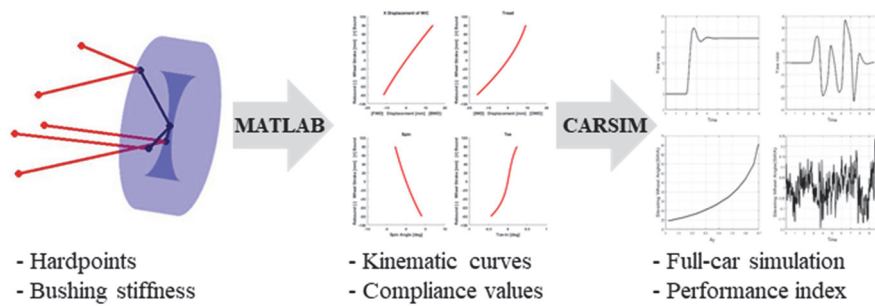
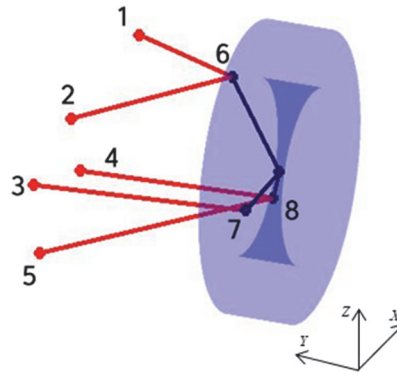


Fig. A.2 The overall analysis procedure automatically evaluating R&H performances from a configuration of a double wishbone suspension



Names of hard points	Index	X	Y	Z	P	Q
Upper Arm Front Mount	1	189.0	370.0	136.0	1200	52.5
Upper Arm Rear Mount	2	-188.0	369.0	126.0	1200	52.5
Assist Arm Mount	3	-142.0	468.0	-42.0	-	-
Lower Arm Front Mount	4	37.0	436.0	-83.0	800	300
Lower Arm Rear Mount	5	-215.0	427.0	-141.5	1200	300
Upper Arm Knuckle Joint	6	0.0	101.0	174.0	-	-
Assist Arm Knuckle Joint	7	-105.0	31.0	-39.0	-	-
Lower Arm Knuckle Joint	8	75.0	42.0	-90.0	-	-

* Units of X, Y, Z : mm, Units of P, Q : kgf/mm

Fig. A.3 The information for initial configuration of a double wishbone suspension to be used (P: bushing stiffness for radial direction, Q: bushing stiffness for the axial direction)

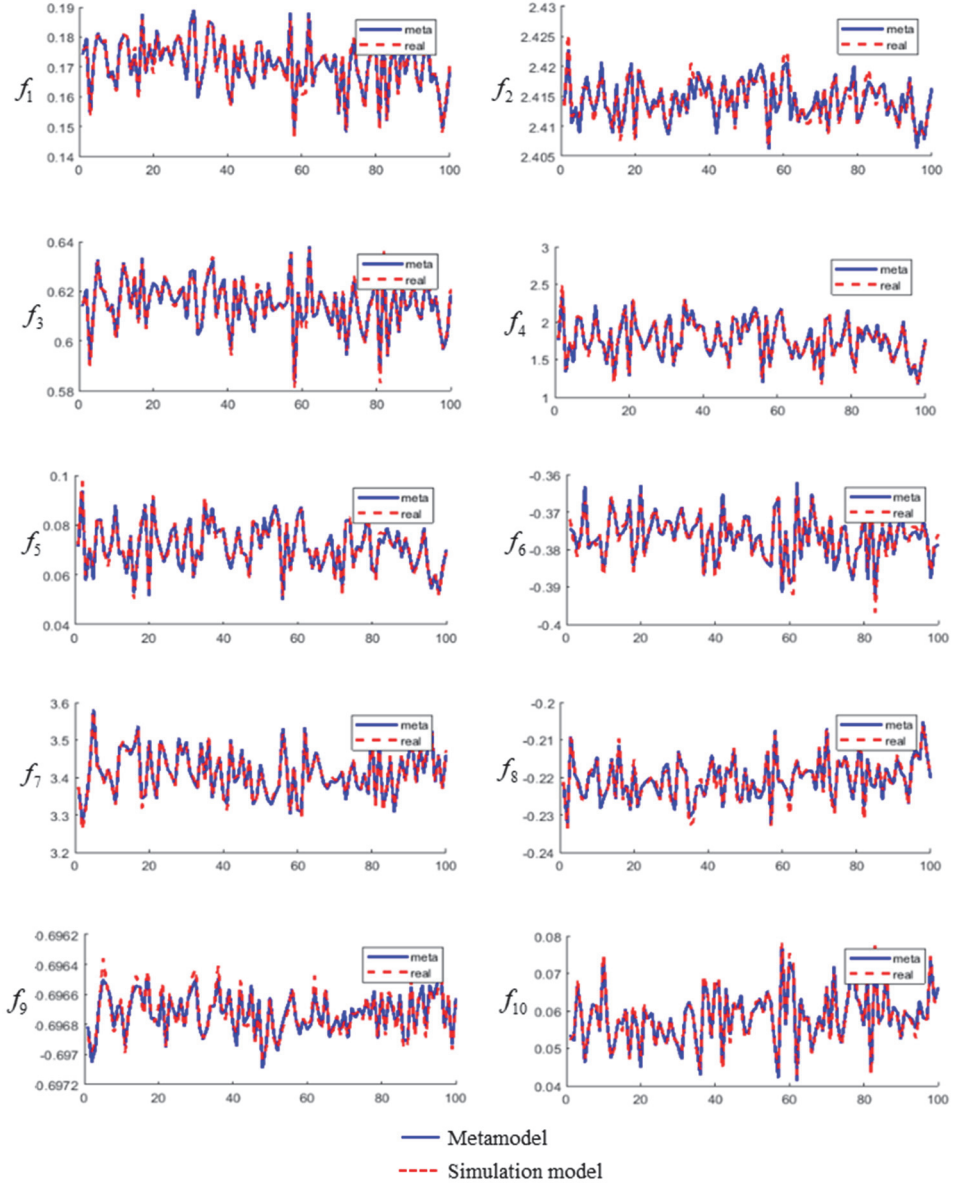


Fig. A.4 The comparison of analysis results when using a metamodel and using a simulation model (The function numbers denote the performance indices from 1 to 10 in Table A.1, respectively)

	f_1	f_2	f_3	f_4	f_5	f_6	f_7	f_8	f_9	f_{10}
f_1	1.00	-0.20	-0.01	-0.13	0.89	0.64	0.74	0.92	-0.86	-0.89
f_2	-0.20	1.00	0.86	0.82	-0.10	-0.52	-0.59	-0.13	-0.23	-0.09
f_3	-0.01	0.86	1.00	0.99	-0.14	-0.51	-0.62	-0.11	-0.24	-0.10
f_4	-0.13	0.82	0.99	1.00	-0.29	-0.58	-0.71	-0.26	-0.09	0.05
f_5	0.89	-0.10	-0.14	-0.29	1.00	0.60	0.79	0.98	-0.91	-0.94
f_6	0.64	-0.52	-0.51	-0.58	0.60	1.00	0.90	0.58	-0.40	-0.46
f_7	0.74	-0.59	-0.62	-0.71	0.79	0.90	1.00	0.77	-0.54	-0.62
f_8	0.92	-0.13	-0.11	-0.26	0.98	0.58	0.77	1.00	-0.92	-0.96
f_9	-0.86	-0.23	-0.24	-0.09	-0.91	-0.40	-0.54	-0.92	1.00	0.98
f_{10}	-0.89	-0.09	-0.10	0.05	-0.94	-0.46	-0.62	-0.96	0.98	1.00

(a)

	f_9	f_7	f_1	f_3	f_6	f_8	f_{10}	f_2	f_5	f_4
f_9	1.00	0.90	0.64	0.60	0.58	-0.40	-0.46	-0.52	-0.51	-0.58
f_7	0.90	1.00	0.74	0.79	0.77	-0.54	-0.62	-0.59	-0.62	-0.71
f_1	0.64	0.74	1.00	0.89	0.92	-0.86	-0.89	-0.20	-0.01	-0.13
f_3	0.60	0.79	0.89	1.00	0.98	-0.91	-0.94	-0.10	-0.14	-0.29
f_6	0.58	0.77	0.92	0.98	1.00	-0.92	-0.96	-0.13	-0.11	-0.26
f_8	-0.40	-0.54	-0.86	-0.91	-0.92	1.00	0.98	-0.23	-0.24	-0.09
f_{10}	-0.46	-0.62	-0.89	-0.94	-0.96	0.98	1.00	-0.09	-0.10	0.05
f_2	-0.52	-0.59	-0.20	-0.10	-0.13	-0.23	-0.09	1.00	0.86	0.82
f_5	-0.51	-0.62	-0.01	-0.14	-0.11	-0.24	-0.10	0.86	1.00	0.99
f_4	-0.58	-0.71	-0.13	-0.29	-0.26	-0.09	0.05	0.82	0.99	1.00

(b)

0.7~1.0	Strong positive correlation	-1.0~-0.7	Strong negative correlation
0.3~0.7	Weak positive correlation	-0.7~-0.3	Weak negative correlation
-0.3~-0.3	No correlation		

Fig. A.5 The result of correlation analysis between handling performance index values using the data points obtained from OLHD: (a) The result sorting by the function number and (b) the result after rearranging with similar correlations

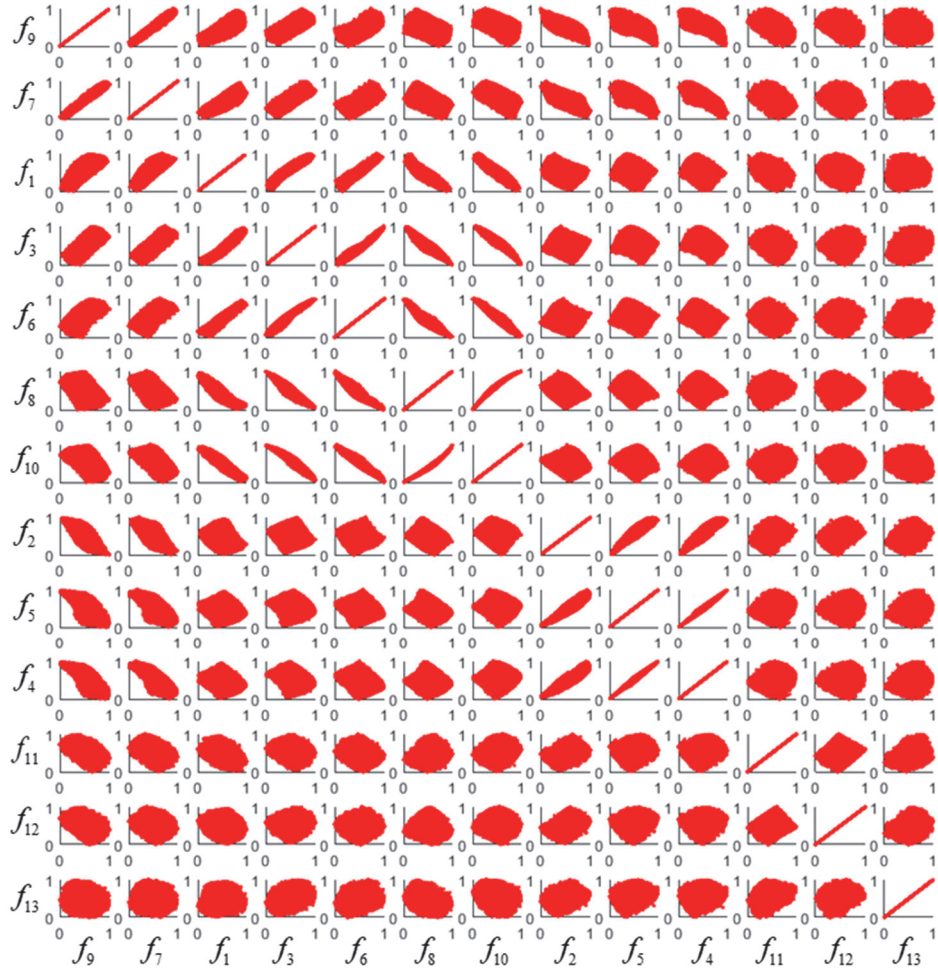


Fig. A.6 Pareto-optimal set obtained from the optimization problem in Appendix A. The Pareto-optimal set is plotted by two objective domain.

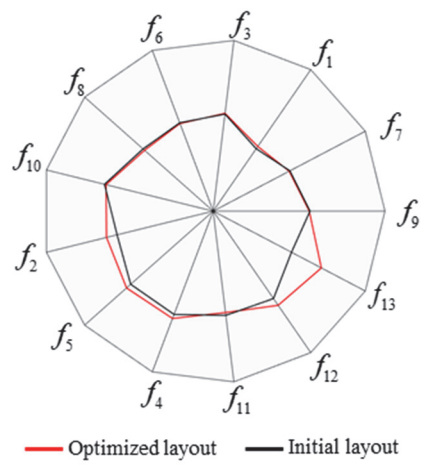


Fig. A.7 Rador chart for comparing the values of R&H performance index from the initial layout and optimized layout

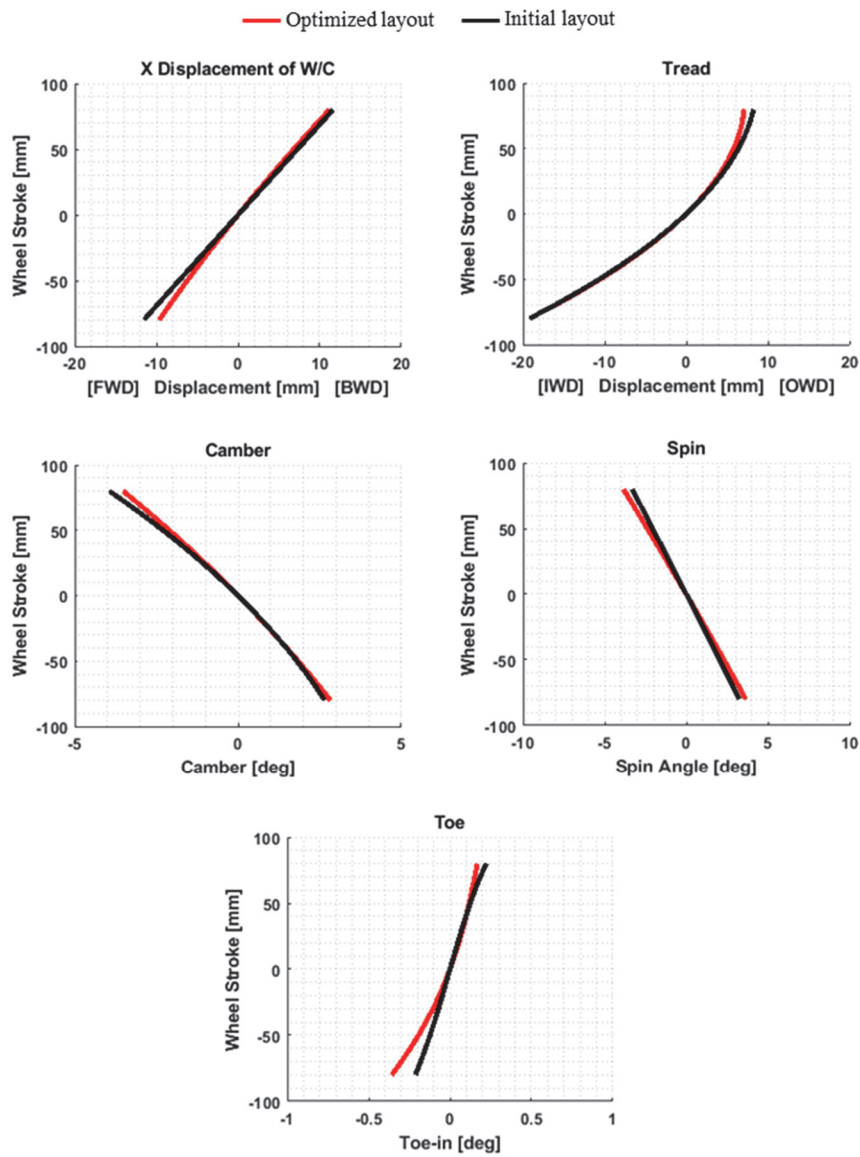


Fig. A.8 Comparison of knematic curves obtained from the initial layout and optimized layout

APPENDIX B.

Technique to suppress floating blocks

B.1 Overview

Floating blocks in a SBM denote the blocks connected with only weak springs and do not be used to transfer motion [10]. In other words, floating blocks do not participate in composing any kinematic chain. Like these, the existence of floating blocks do not make changes of the topology of linkage mechanisms, but if floating blocks appear during the optimization process, they may cause numerical problems like singularity [10]. For this reason, some techniques were proposed to resolve the floating block issues [10, 64].

In this Appendix, the techniques to alleviate numerical singularity by anchoring the floating blocks during the optimization will be explained and Case study 3 in Chapter 2.4 will be revisited with the technique. In addition, by comparing the results when using and not using the technique, the effects of floating blocks will be discussed.

B.2 Explanation of techniques to suppress floating blocks

For preventing to being made floating blocks during topology optimization of linkage mechanisms, it is important to detect which blocks are being floated and there are two types of techniques to detect floating blocks [10, 64]. The first presented in [10] is to use the spring stiffness connected to a block. In the first technique, the number of springs connected to one block whose stiffness is above a certain small value is counted during the optimization process. If the number is 0 or 1, the block is determined to be floated, and it will be anchored to the ground by the four anchoring springs connected to the block. This method seems somewhat reasonable because if zero or only one corner is connected to the other part, the block cannot compose a kinematic chain. However, if two or more blocks are connected to each other by block-connecting springs but they are all floating blocks, the number of springs with stiffness greater than a certain small value is not 0 or 1. (They are called a grouping dummy).

The second technique is presented in [64] and the key idea is to use the Jacobian matrix of the total strain energy as

$$\mathbf{J} = \frac{d}{d\mathbf{q}} \left(\frac{dU(\mathbf{q})}{d\mathbf{q}} \right) = \frac{d\mathbf{F}^{\text{int}}}{d\mathbf{q}} \quad (\text{B.1})$$

where $U(\mathbf{q})$ denotes the total strain energy in Eq. (2.5). As in Eq. (B.1), the Jacobian matrix means the change of the internal forces by the springs when each block is perturbed to its DOF's direction because the Jacobian is obtained from the derivative

by the state variable vector of the blocks. As the eigenvalues of the Jacobian matrix denote the change of internal force when a block is perturbed following the DOF, and thus if a block is being floated, the eigenvalues corresponding to the block will be nearly zero [64]. Therefore, by evaluating eigenvalues of the Jacobian matrix, it is determined which blocks are floating even if there is a grouping dummy which is not possible in the first technique. If detecting a floating block, it will be anchored to the ground by the anchoring springs connected to the floating block as in the first technique.

B.3 Revisit Case study 3 for applying the technique to suppress floating blocks

In the result of Case study 3, it can be found that some blocks were redundantly attached to the skeletal blocks which are used to transfer motion at the convergence as shown in Fig. B.1, and the springs attached to the blocks were not converged at their maximum or minimum. As these blocks and springs do not affect the kinematic and compliance characteristics of the result mechanism, the result mechanism is determined as a six-bar linkage mechanism, but it is meaningful to investigate the optimization result of Case study 3 with the technique of suppressing floating blocks as it could help stable convergence by resolving numerical instability.

The technique to be applied is the methodology using the eigenvalues of the Jacobian matrix because it can detect a grouping dummy. However, it is difficult to apply the method right away to the proposed method. Because if a block is determined to float, it will be grounded by the anchoring springs, and this causes a violation of the constraint function related to the maximum number of bushings presented in Eq. (2.21d). Therefore, the stiffness values of the anchoring springs to be used to ground the floating block will be decreased by that constraint, and thus the optimization may not converge until there is no floating block. To resolve this, the technique is applied to help to perform kinematic analysis. Specifically, as floating blocks can occur numerical singularity while do not affect the kinematic motion, they are anchored to the ground during kinematic analysis. Although the state of the SBM system is not

the same as the state represented by the design variables, it would not matter because the kinematic motion needed to use for the objective and constraint functions does not change by the state of the floating blocks. The optimization results the technique of suppressing floating blocks are as in Fig. B.2 and Fig. B.3.

As shown in Fig. B.2(a), the result mechanism with the technique is a six-bar linkage mechanism as the same as the result in Case study 3 in Chapter 2.4 and the connectivity of the skeletal blocks determined by the springs at the convergence shown in Fig. B.2(c) and (d) is also the same as in the result of Case study 3 in Chapter 2.4. The difference between the result mechanisms using and not using the technique is the connectivity with the floating blocks. In the result when not using the technique, Blocks 7 and 8 are connected to the Blocks 5 and 6 by the spring not converged at their minimum, but in the result when using the technique, Blocks 7 and 8 are clearly disconnected to the Blocks 5 and 6. However, as floating blocks do not affect to compose a result mechanism, this difference does not matter to compose a result mechanism using the SBM at the convergence.

The convergence histories of the objective and constraint functions are shown in Fig. B.3, and they are almost the same as those of Case study 3 in Chapter 2.4. Especially, the convergence histories of the constraint functions for both results are almost identical. By the way, after when the value of the work transmittance function goes to nearly 1, the convergence history of the objective when using the technique seems

more stable than when not using the technique. Therefore, it can be said that this technique does not make it change of the optimization results, but it can be helpful for a stable convergence of optimization.

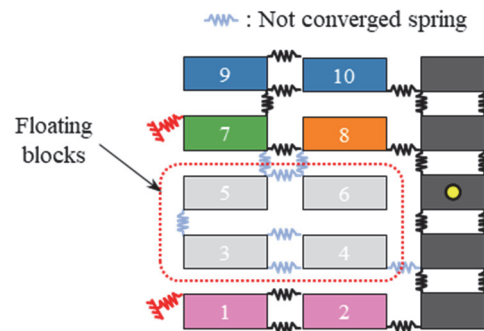


Fig. B.1 Illustration of floating blocks existing in the result of Case study 3.

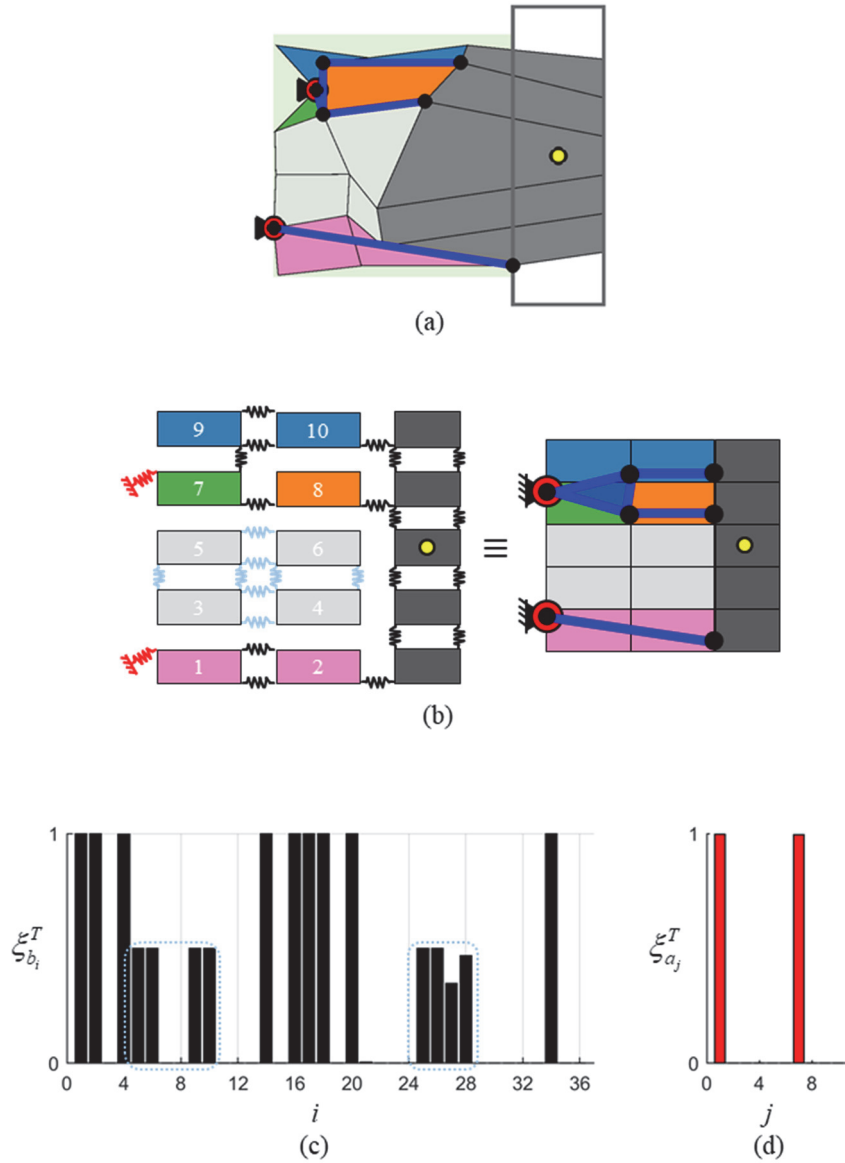


Fig. B.2 Optimization results for the 2D vehicle suspension design problem with the technique of suppressing floating blocks: (a) final optimized layout (thick lines represent the synthesized links), (b) identified linkage mechanism (right) from the optimized layout expressed by rigid blocks connected by block-connecting and anchoring springs having a lower bound stiffness value, (c) converged values of the design variables for block-connecting springs, and (d) converged values of design variables of the anchoring springs

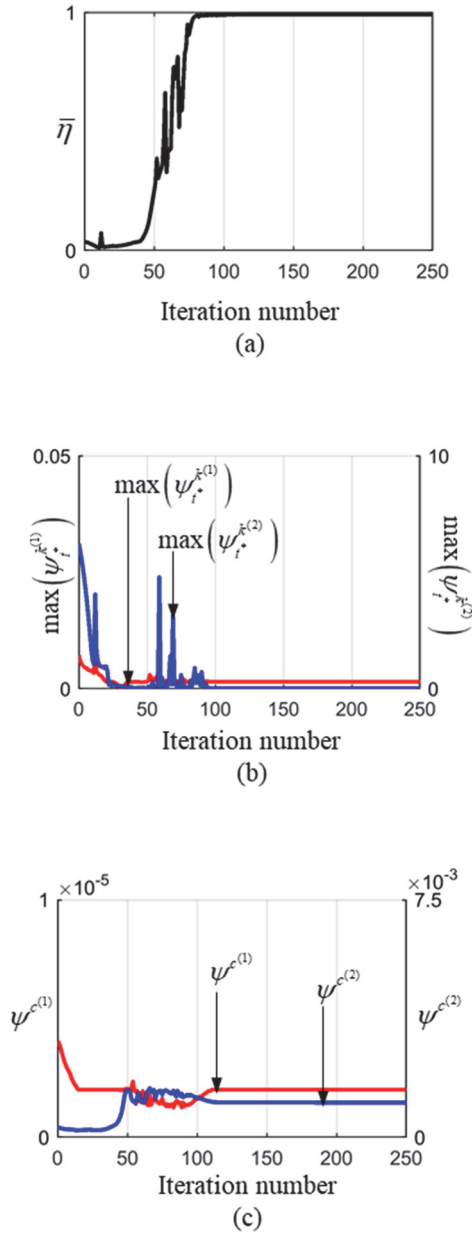


Fig. B.3 Iteration histories for Case study 3 with the technique of suppressing floating blocks: (a) the mean value of the work transmittance efficiency function, (b) kinematic constraint functions, and (c) compliance constraint functions

APPENDIX C.

Investigation of mesh dependency issue

C.1 Overview

In a SBM based topology optimization of linkage mechanisms, as the topology of a linkage mechanism possible to be synthesized at convergence is dependent on the number of blocks, the number of rigid blocks used to synthesize a linkage mechanism is an important factor. To resolve the mesh dependency issue, two remedies are presented in [65], and the simultaneous topology and shape optimization approach is used in this research.

While the remedy to resolve the mesh dependency issue has been used and the number of blocks to be used for mechanism synthesis in this thesis is suitable for representing the required mechanism topology, it is worthwhile to investigate that a linkage mechanism can be synthesized when using more blocks for being more general methodology. For the investigation, Case study 1 in Chapter 2.4 is re-considered in this Appendix.

C.2 Re-consideration of Case study 1 with the more number of rigid blocks

In Chapter 2.4, a four-bar linkage mechanism which can generate a banana path is recovered using the proposed method in Case study 1, and 3 by 3 rigid blocks are used for the SBM. The target K&C characteristics used to synthesize the mechanism are described in Fig. 2.7(b), and the problem definition is shown in Fig. C.1. First, as shown in Fig. C.1(a), we employ a 5 by 5 rigid blocks with which more than eight-bar mechanism can be represented to recover the reference linkage mechanism. Second, 11 by 11 rigid blocks is employed to test the capability of the proposed methodology as shown in Fig. C.1(b), and this is the first attempt in topology optimization of linkage mechanism based on the SBM. The optimization formulation used for the testing is set to be the same as Case study 1 in Chapter 2.4, and for the stable convergence, the technique to suppress floating blocks using the Jacobian matrix is applied.

The optimization results are shown in Fig. C.2. As shown in the left of Fig. C.2(a), the reference linkage mechanism is recovered when using 5 by 5 rigid blocks, and the layout of the mechanism is similar with the result mechanism of Case study 1 in Chapter 2.4. As shown in the right of Fig. C.2(a), the mean value of the work transmittance efficiency function goes to 1 which means that one degree-of-freedom mechanism is synthesized, and it is shown that the values of the constraint functions are within the error bounds shaded green. The optimization results using the 11 by

11 rigid blocks are shown in Fig. C.2(b). Even though, the employed rigid blocks can represent a variety of topologies of the linkage mechanism, a four-bar linkage mechanism which can generate the target K&C characteristics is synthesized as shown in the left of Fig. C.2(b). The right of Fig. C.2(b) illustrates the convergence histories of the objective and constraint functions, and it shows that there is a convergence after 100th iteration. Although the convergence rate is slower than when using 3 by 3 rigid blocks and 5 by 5 rigid blocks, that is natural phenomenon because the number of design variables is 1212 when using 11 by 11 rigid blocks. An important thing is that we succeed to synthesize a linkage mechanism using more than 100 blocks using the proposed methodology. To solve the more general problem, it can be needed to test the maximum number of rigid blocks able to be used, but since more than 100 blocks are enough to represent most of linkage mechanisms to be used, it is expected that the proposed methodology can be applied to various applications.

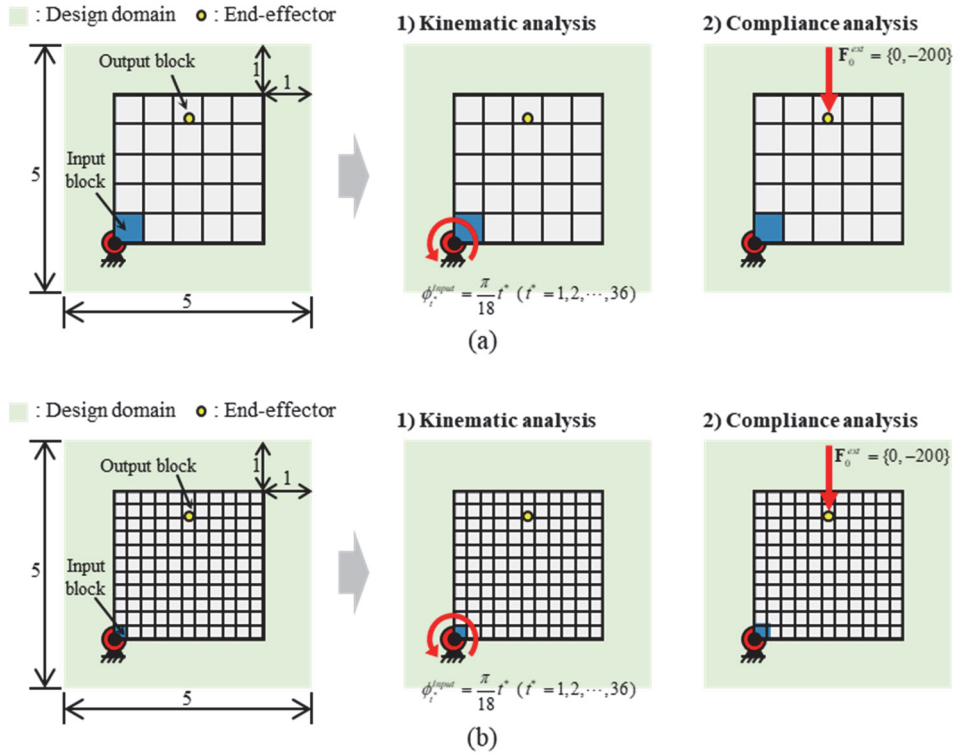


Fig. C.1 Problem definition for re-considering Case study 1 with (a) 5 by 5 rigid blocks and (b) 11 by 11 rigid blocks

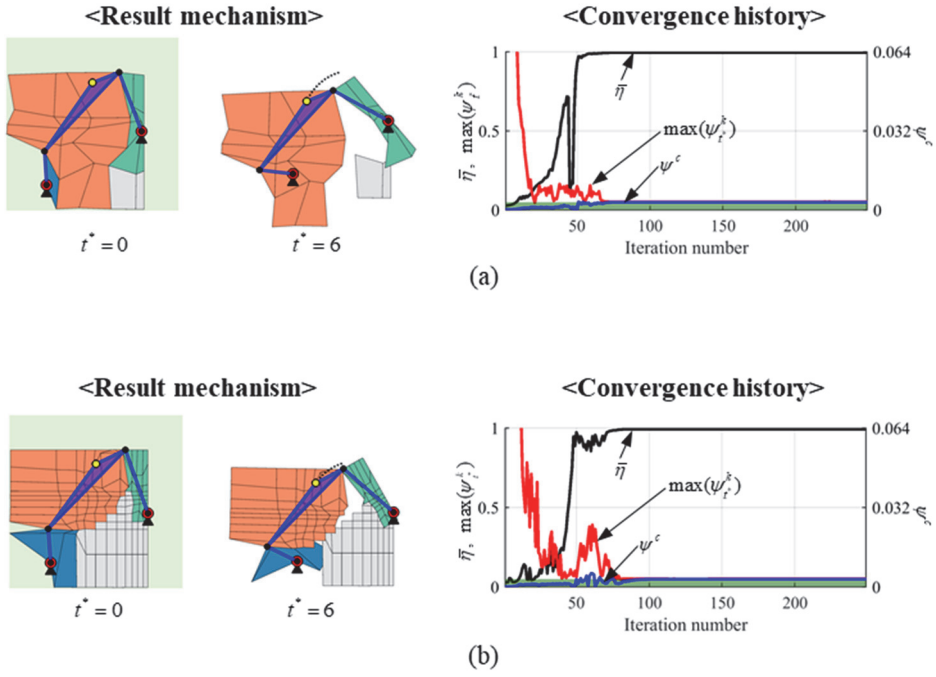


Fig. C.2 Optimization results for re-considering Case study 1 with (a) 5 by 5 rigid blocks and (b) 11 by 11 rigid blocks

REFERENCES

- [1] Felter, C., and Sigmund, O., 2003, "Topology optimization of rigid body mechanisms," Technical University of Denmark, Lyngby, Denmark.
- [2] Kawamoto, A., Bendsøe, M. P., and Sigmund, O., 2004, "Planar articulated mechanism design by graph theoretical enumeration," *Structural and Multidisciplinary Optimization*, 27(4), pp. 295-299.
- [3] Kawamoto, A., Bendsøe, M. P., and Sigmund, O., 2004, "Articulated mechanism design with a degree of freedom constraint," *International Journal for Numerical Methods in Engineering*, 61(9), pp. 1520-1545.
- [4] Kawamoto, A., 2005, "Path generation of articulated mechanisms by shape and topology variations in non-linear truss representation," *International journal for numerical methods in engineering*, 64(12), pp. 1557-1574.
- [5] Sedlacek, K., and Eberhard, P., 2009, "Topology optimization of large motion rigid body mechanisms with nonlinear kinematics," *Journal of Computational and Nonlinear Dynamics*, 4(2), p. 021011.
- [6] Ohsaki, M., and Nishiwaki, S., 2009, "Generation of link mechanism by shape-topology optimization of trusses considering geometrical nonlinearity," *Journal of Computational Science and Technology*, 3(1), pp. 46-53.
- [7] Kim, S. I., and Kim, Y. Y., 2014, "Topology optimization of planar linkage mechanisms," *International Journal for Numerical Methods in Engineering*, 98(4),

pp. 265-286.

[8] Kim, S. I., Kang, S. W., Yi, Y.-S., Park, J., and Kim, Y. Y., 2018, "Topology optimization of vehicle rear suspension mechanisms," *International Journal for Numerical Methods in Engineering*, 113(8), pp. 1412-1433.

[9] Kim, Y. Y., Jang, G.-W., Park, J. H., Hyun, J. S., and Nam, S. J., 2007, "Automatic synthesis of a planar linkage mechanism with revolute joints by using spring-connected rigid block models," *Journal of Mechanical Design*, 129(9), pp. 930-940.

[10] Nam, S. J., Jang, G.-W., and Kim, Y. Y., 2012, "The spring-connected rigid block model based automatic synthesis of planar linkage mechanisms: numerical issues and remedies," *Journal of Mechanical Design*, 134(5), p. 051002.

[11] Kang, S. W., Kim, S. I., and Kim, Y. Y., 2016, "Topology optimization of planar linkage systems involving general joint types," *Mechanism and Machine Theory*, 104, pp. 130-160.

[12] Kang, S. W., and Kim, Y. Y., 2018, "Unified topology and joint types optimization of general planar linkage mechanisms," *Structural and Multidisciplinary Optimization*, 57(5), pp. 1955-1983.

[13] Yim, N. H., Kang, S. W., and Kim, Y. Y., 2019, "Topology Optimization of Planar Gear-Linkage Mechanisms," *Journal of Mechanical Design*, 141(3), p. 032301.

[14] Han, S. M., In Kim, S., and Kim, Y. Y., 2017, "Topology optimization of planar linkage mechanisms for path generation without prescribed timing," *Structural and Multidisciplinary Optimization*, 56(3), pp. 501-517.

- [15] Yu, J., Han, S. M., and Kim, Y. Y., 2020, "Simultaneous Shape and Topology Optimization of Planar Linkage Mechanisms Based on the Spring-Connected Rigid Block Model," *Journal of Mechanical Design*, 142(1), p. 011401.
- [16] Kim, B. S., and Yoo, H. H., 2012, "Unified synthesis of a planar four-bar mechanism for function generation using a spring-connected arbitrarily sized block model," *Mechanism and Machine Theory*, 49, pp. 141-156.
- [17] Kim, B. S., and Yoo, H. H., 2014, "Unified mechanism synthesis method of a planar four-bar linkage for path generation employing a spring-connected arbitrarily sized rectangular block model," *Multibody System Dynamics*, 31(3), pp. 241-256.
- [18] Kim, B. S., and Yoo, H. H., 2015, "Body guidance syntheses of four-bar linkage systems employing a spring-connected block model," *Mechanism and Machine Theory*, 85, pp. 147-160.
- [19] Ohsaki, M., Kanno, Y., and Tsuda, S., 2014, "Linear programming approach to design of spatial link mechanism with partially rigid joints," *Structural and Multidisciplinary Optimization*, 50(6), pp. 945-956.
- [20] Ohsaki, M., Kanno, Y., and Yamaoka, Y., 2018, "Second-Order Cone Programming Approach to Design of Linkage Mechanisms With Arbitrarily Inclined Hinges," *Journal of Mechanical Design*, 140(10), p. 102301.
- [21] Ohsaki, M., Tsuda, S., and Miyazu, Y., 2016, "Design of linkage mechanisms of partially rigid frames using limit analysis with quadratic yield functions," *International Journal of Solids and Structures*, 88-89, pp. 68-78.
- [22] Rai, A. K., Saxena, A., and Mankame, N. D., 2010, "Unified synthesis of

- compact planar path-generating linkages with rigid and deformable members," *Structural and Multidisciplinary Optimization*, 41(6), pp. 863-879.
- [23] Yoon, G. H., and Heo, J. C., 2012, "Constraint force design method for topology optimization of planar rigid-body mechanisms," *Computer-Aided Design*, 44, pp. 1277-1296.
- [24] Erdman, A. G., and Sandor, G. N., 1997, *Mechanism design: Analysis and synthesis. Vol. I*, Prentice Hall, New Jersey.
- [25] Rattan, S. S., 2009, *Theory of Machines*, McGraw-Hill Higher Education, New Delhi.
- [26] Norton, R. L., 2011, *Kinematics and Dynamics of Machinery*, McGraw-Hill, New York.
- [27] Olson, D. G., Erdman, A. G., and Riley, D. R., 1985, "A systematic procedure for type synthesis of mechanisms with literature review," *Mechanism and Machine Theory*, 20(4), pp. 285-295.
- [28] Vinogradov, O., 2000, *Fundamentals of kinematics and dynamics of machines and mechanisms*, CRC press.
- [29] Myszka, D. H., 2004, *Machines and mechanisms*, Prentice Hall.
- [30] Stolpe, M., and Kawamoto, A., 2005, "Design of planar articulated mechanisms using branch and bound," *Mathematical programming*, 103(2), pp. 357-397.
- [31] Currey, N. S., 1988, *Aircraft landing gear design: principles and practices*, American Institute of Aeronautics and Astronautics, Washington, DC.
- [32] Rice, J. J., Schimmels, J. M., and Huang, S., 2015, "Design and Evaluation of a

Passive Ankle Prosthesis With Powered Push-Off," *Journal of Mechanisms and Robotics*, 8(2), p. 021012.

[33] Sun, Y., Ge, W., Zheng, J., and Dong, D., 2015, "Design and Evaluation of a Prosthetic Knee Joint Using the Geared Five-Bar Mechanism," *IEEE Transactions on Neural Systems and Rehabilitation Engineering*, 23(6), pp. 1031-1038.

[34] Jiang, H., Xu, G., Zeng, W., and Gao, F., 2019, "Design and kinematic modeling of a passively-actively transformable mobile robot," *Mechanism and Machine Theory*, 142, p. 103591.

[35] Kong, K., and Tomizuka, M., 2012, "Design of a Rehabilitation Device Based on a Mechanical Link System," *Journal of Mechanisms and Robotics*, 4(3), p. 035001.

[36] Park, S., Bae, J., Jeon, Y., Chu, K., Bak, J., Seo, T., and Kim, J., 2018, "Optimal design of toggle-linkage mechanism for clamping applications," *Mechanism and Machine Theory*, 120, pp. 203-212.

[37] Chin, Y.-W., Ang, Z., Luo, Y., Chan, W.-L., Chahl, J. S., and Lau, G.-K., 2018, "Spring-Assisted Motorized Transmission for Efficient Hover by Four Flapping Wings," *Journal of Mechanisms and Robotics*, 10(6), p. 061014.

[38] Gosselin, C., 1990, "Stiffness mapping for parallel manipulators," *IEEE Transactions on Robotics and Automation*, 6(3), pp. 377-382.

[39] Knapczyk, J., and Maniowski, M., 2006, "Stiffness Synthesis of a Five-Rod Suspension for Given Load-Displacement Characteristics," *Proceedings of the Institution of Mechanical Engineers, Part D: Journal of Automobile Engineering*,

220(7), pp. 879-889.

[40] Birglen, L., Laliberté, T., and Gosselin, C. M., 2007, *Underactuated robotic hands*, Springer, Berlin.

[41] Dong, D., Ge, W., Liu, S., Xia, F., and Sun, Y., 2017, "Design and optimization of a powered ankle-foot prosthesis using a geared five-bar spring mechanism," *International Journal of Advanced Robotic Systems*, 14(3), p. 172988141770454.

[42] Liu, J., Xiong, C., and Fu, C., 2019, "An Ankle Exoskeleton Using a Lightweight Motor to Create High Power Assistance for Push-Off," *Journal of Mechanisms and Robotics*, 11(4), p. 041001.

[43] Luo, H.-T., and Zhao, J.-S., 2018, "Synthesis and kinematics of a double-lock overconstrained landing gear mechanism," *Mechanism and Machine Theory*, 121, pp. 245-258.

[44] Milliken, W. F., and Milliken, D. L., 1995, *Race car vehicle dynamics*, Warrendale: Society of Automotive Engineers, PA.

[45] Yi, Y.-S., Park, J., and Hong, K.-J., 2014, "Design optimization of suspension kinematic and compliance characteristics," *SAE Technical Paper No. 0148-7191*.

[46] Jin, G., and Xiujian, Y., 2013, "Sensitivity Study of Bushing Stiffness Affecting Suspension Compliance Characteristics and Transient Handling Stability [J]," *Automobile Technology*, 11.

[47] Kang, J. S., Yun, J. R., Lee, J. M., and Tak, T. O., 1997, "Elastokinematic analysis and optimization of suspension compliance characteristics," *SAE Technical Paper No. 0096-736X*.

- [48] Wang, M., Beeh, E., Krüger, D., and Friedrich, H. E., 2018, "Topological optimization of a suspension concept considering the kinematics and compliance performance and the geometric nonlinearity," *Proceedings of the Institution of Mechanical Engineers, Part D: Journal of Automobile Engineering*, 232(3), pp. 318-329.
- [49] HeiBing, B., and Ersoy, M., 2010, *Chassis handbook: fundamentals, driving dynamics, components, mechatronics, perspectives*, Springer, New York.
- [50] Svanberg, K., 1987, "The method of moving asymptotes—a new method for structural optimization," *International journal for numerical methods in engineering*, 24(2), pp. 359-373.
- [51] Raghavan, M., 1996, "Number and dimensional synthesis of independent suspension mechanisms," *Mechanism and Machine Theory*, 31(8), pp. 1141-1153.
- [52] Jing, L., Wu, L., Li, X., and Zhang, Y., "Study on kinematic and compliance test of suspension," *Proc. IOP Conference Series: Materials Science and Engineering*, IOP Publishing, p. 012186.
- [53] Liao, S., Cao, K., Wei, H., Liu, J., and Xie, C., "Robust Optimization of Multi-link Suspension Compliance Characteristics Based on Taguchi Method," Atlantis Press.
- [54] Arikere, A., Saravana Kumar, G., and Bandyopadhyay, S., 2010, "Optimisation of Double Wishbone Suspension System Using Multi-Objective Genetic Algorithm," *Springer Berlin Heidelberg*, pp. 445-454.
- [55] Simionescu, P. A., and Beale, D., 2002, "Synthesis and analysis of the five-link

rear suspension system used in automobiles," *Mechanism and Machine Theory*, 37(9), pp. 815-832.

[56] Suh, K., and Yoon, H., 2018, "Design Optimization of a Rear Independent Suspension for the Korean Light Tactical Vehicle," *International Journal of Automotive Technology*, 19(2), pp. 245-252.

[57] Wang, W., and Chen, X., 2019, "Design methodology for wheel corner module topology based on position and orientation characteristics," *Mechanism and Machine Theory*, 136, pp. 122-140.

[58] Zandbergen, P., and Girelli Consolaro, A., 2013, "Ford Motor Company's New Rear Suspension Architecture for the Global CD Platform," Springer Berlin Heidelberg, pp. 9-20.

[59] Deb, K., 2001, *Multi-objective optimization using evolutionary algorithms*, John Wiley & Sons.

[60] Li, M., Li, G., and Azarm, S., 2008, "A Kriging Metamodel Assisted Multi-Objective Genetic Algorithm for Design Optimization," *Journal of Mechanical Design*, 130(3), p. 031401.

[61] Liu, H., Ong, Y.-S., and Cai, J., 2018, "A survey of adaptive sampling for global metamodeling in support of simulation-based complex engineering design," *Structural and Multidisciplinary Optimization*, 57(1), pp. 393-416.

[62] Park, J.-S., 1994, "Optimal Latin-hypercube designs for computer experiments," 39(1), pp. 95-111.

[63] McKay, M. D., Beckman, R. J., and Conover, W. J., 1979, "Comparison of Three

Methods for Selecting Values of Input Variables in the Analysis of Output from a Computer Code," 21(2), pp. 239-245.

[64] Jeon, B., 2016, "Research on numerical stability of spring-connected rigid block model with Jacobian-based anchoring method," Bachelor, Seoul National University.

[65] Kim, S. I., 2017, "Development of Unified Topology and Dimension Synthesis Methodology for Linkage Mechanisms and its Application to Conceptual Design of Automobile Suspensions," Doctoral, Seoul National University.

ABSTRACT (KOREAN)

기구학적 특성과 컴플라이언스 특성을 동시에 고려한 기구 위상 및 형상 통합 최적설계

한 상 민

서울대학교 대학원

기계항공공학부

위상 최적화(topology optimization) 기법을 이용한 한 기구 합성(mechanism synthesis)은 그 효율성으로 인해 최근 많은 주목을 받고 있다. 이러한 추세
의 주 원인은 기구 위상 최적화 기법으로 인해 기구의 위상(topology)
과 치수(dimension)를 자동으로 합성할 수 있기 때문이다. 이러한 방향성
을 가지고 지금까지 많은 연구들이 진행되어 왔지만, 지금까지 진행된
연구들은 모두 경로 합성이나 운동 합성과 같이 기구학적 특성을 고려하
는 데에만 관심이 집중되었다.

본 연구에서는 기구의 기구학적 특성(kinematic characteristics)과 컴플라이
언스 특성(compliance characteristics)을 동시에 고려할 수 있는 새로운 기

구 위상 최적화 기법을 제안한다. 기구학적 특성은 기구 설계에 있어 매우 중요한 특성이지만, 외력이 작용하였을 때 자동차 서스펜션(vehicle suspension)의 부싱(bushing)과 같은 탄성 요소들의 변형으로 인해 나타나는 컴플라이언스 특성 또한 기구 설계 시 고려해야 할 중요한 특성이기 때문이다. 새로운 기구 위상 최적화 기법을 위해 우리는 기구학적 특성만을 고려하기 위해 개발되었던 스프링-연결 블록 모델(spring-connected block model)을 기구학적 특성과 컴플라이언스 특성을 동시에 고려할 수 있도록 고안하였다. 기존의 스프링-연결 블록 모델에서는 기구학적 연결 관계만을 표현하는데 사용되던 가변 강성 스프링을 본 연구에서는 기구학적 연결 관계뿐 아니라 실제 부싱을 표현하도록 다목적으로 활용하여 기구학적 특성과 컴플라이언스 특성을 하나의 모델링을 통해 성공적으로 표현하였다.

개발한 방법론의 효과를 입증하기 위해 평면 기구 합성을 목표로 한 세 종류의 사례 연구(case study)를 진행하였고, 이러한 사례 연구를 통해 우리는 제안한 방법이 기존의 방법으로는 해결할 수 없는 문제 상황을 해결할 수 있음을 확인하였다. 개발한 방법론을 보다 실용적인 문제에 적용하기 위해 3차원 자동차 서스펜션(vehicle suspension) 설계 하고자 하였으며, 이를 위해 스프링-연결 블록 모델을 3차원으로 확장하였다. 또한, 보다 실용적인 설계 결과 도출을 위해 2차원 사례 연구에서는 사용하지

않았던 부싱 강성 조절 설계 변수를 추가적으로 도입하여, 부싱 강성도 동시에 설계를 진행하였다. 3차원 서스펜션 설계는 기구학적 조건은 동일하지만, 컴플라이언스 특성은 다른 두 가지 조건에 대해 진행되었으며, 두 설계 조건에서 모두 서스펜션 합성에 성공하였다. 특히, 두 서스펜션의 결과 위상이 서로 다른 것을 확인할 수 있었는데, 이를 통해 기구학적 조건은 동일하되 컴플라이언스 조건이 달라지면 결과 위상이 달라질 수 있음을 확인하였고, 개발한 방법론을 통해 설계 조건에 맞는 기구의 위상과 치수 그리고 필요한 부싱 강성까지도 성공적으로 설계할 수 있음을 증명하였다.

본 연구는 컴플라이언스 조건이 특히 중요시 되는 자동차 서스펜션을 설계하는데 집중하였지만, 개발한 방법론은 기구학적 특성과 컴플라이언스 특성이 모두 요구되는 다른 설계 문제에도 적용될 수 있을 것으로 기대된다. 또한, 이 연구는 기구학적 특성뿐만 아니라 힘과 관련된 다른 특성을 고려한 일반적인 기구 위상 최적화 기법으로의 발전에 기여할 것으로 기대된다.

주요어: 위상 최적화, 강체 기구, 기구학적 특성, 컴플라이언스 특성

학 번 : 2013-23838

ACKNOWLEDTEMENTS

This research was supported by the National Research Foundation of Korea (NRF) Grant No. 2016R1A2B3010231 funded by the Ministry of Science and ICT (MSIT), Korea, contracted through Institute of Advanced Machines and Design (IAMD) at Seoul National University in Korea. Also, this research was supported by the SNU-Hyundai NGV cooperative research project Grant No. 0420-20180064 funded by Hyundai Motor Company and the Samsung Research Funding Center of Samsung Electronics under Project No. SRFC-IT1901-02.